KU Leuven
Biomedical Sciences Group
Faculty of Medicine
Department of Imaging & Pathology
OMFS-IMPATH Research Group
Kapucijnenvoer 7 block a- box 7001
B-3000 LEUVEN, BELGIUM
tel. + 32 16 32 00800
yifei.gu@kuleuven.be

OMFS IMPATH

Yifei Gu

3D-PRINTED POROUS METALLIC SCAFFOLD FOR MAXILLOFACIAL BONE RECONSTRUCTION

2022

The author

Yifei Gu achieved her Bachelor of Medicine and Master of Dental Medicine degrees from West China College of Stomatology, Sichuan University, Chengdu, Sichuan, China (2010 - 2018). She started working as a Ph.D. candidate (OMFS-IMPATH, KU Leuven) in 2018, with Prof. Constantinus Politis, Prof. Reinhilde Jacobs, and Dr. Yi Sun as her (co-)promotors. The research topic for her Ph.D. is related to bone tissue engineering with biomimetic calcium phosphate/BMP-2 coated 3D printed titanium scaffold and biodegradable WE43 alloy scaffold.
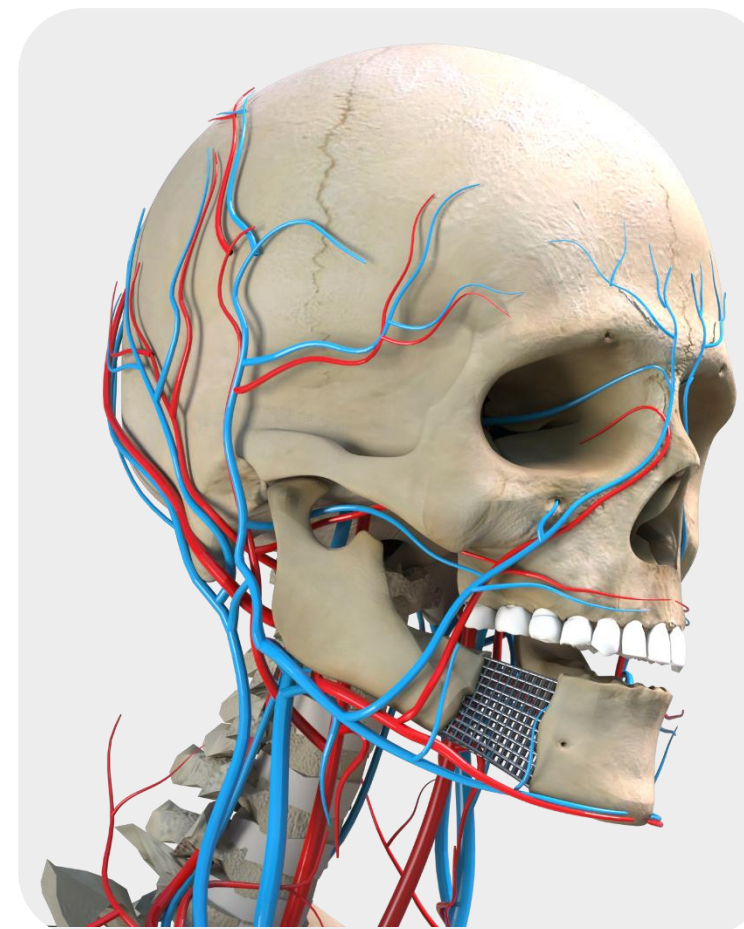
Abstract

Bone tissue engineering is a potentially effective treatment for maxillofacial bone defects. This doctoral thesis aims to fabricate metal scaffolds that are suitable for bone tissue engineering and evaluate the scaffolds' osteogenic ability in animal models. Both the BMP-2 integrated biomimetic CaP-coated Ti-based porous scaffold and the biodegradable WE43 porous scaffold exhibited good osteogenic properties. Translating lab-made methods into clinically relevant products will require a joint effort of clinicians and engineers.

KU LEUVEN

DOCTORAL SCHOOL OF BIOMEDICAL SCIENCES

3D-PRINTED POROUS METALLIC SCAFFOLD FOR MAXILLOFACIAL BONE RECONSTRUCTION

YIFEI GU
2022

KU Leuven
Biomedical Sciences Group
Faculty of Medicine
Department of Imaging and Pathology

OMFS
IMPATH

KU LEUVEN

DOCTORAL SCHOOL
BIOMEDICAL SCIENCES

3D-PRINTED POROUS METALLIC SCAFFOLD FOR MAXILLOFACIAL BONE RECONSTRUCTION

Yifei Gu

Dissertation presented in partial
fulfilment of the requirements for
the degree of
Doctor in Biomedical Sciences

<u>Jury</u>:

Supervisor: Prof. dr. Constantinus Politis
Co-supervisor: Prof. dr. Reinhilde Jacobs
                Dr. Yi Sun
Chair examining committee: Prof. dr. Steven Dymarkowski
Jury members: Prof. dr. Antoon De Laat
                Prof. dr. Joke Duyck
                Prof. dr. Ivo Lambrichts
                Prof. dr. Michael Bornstein

August 2022

Preface

This doctoral thesis consists of 5 research articles, preceded with a general introduction, and concluded with a general discussion. The research articles followed the standard scientific IMRAD structure (Introduction, Materials and Methods, Results and Discussion) and were based on the following peer-reviewed publications:

Article 1

Gu Y, Ma H, Shujaat S, Orhan K, Coucke W, Amoli MS, Bila M, Politis C, Jacobs R. Donor-and recipient-site morbidity of vascularized fibular and iliac flaps for mandibular reconstruction: A systematic review and meta-analysis. Journal of Plastic, Reconstructive & Aesthetic Surgery. 2021 Jul;74(7):1470-9. Doi: 10.1016/j.bjps.2021.03.055.

Article 2

Gu Y, Sun Y, Shujaat S, Braem A, Politis C, Jacobs R. 3D-printed porous Ti64 scaffolds for long bone repair in animal models: a systematic review. Journal of orthopaedic surgery and research. 2022 Dec;17(1):1-7. Doi: 10.1186/s13018-022-02960-6.

Article 3

Gu Y, Wei L, Zhang Z, Van Dessel J, Driesen RB, Lambrichts I, Jacobs R, Tian L, Sun Y, Liu Y, Politis C. BMP-2 integrated biomimetic CaP coating functionalized 3D-printed Ti64 scaffold induces ectopic bone formation in a dog model. Materials & Design. 2022 Feb;110443. Doi: 10.1016/j.matdes.2022.110443.

Article 4

Gu Y, Liu Y, Van Dessel J, Jacobs R, Tian L, Sun Y, Liu Y, Politis C. BMP-2 integrated biomimetic CaP coating functionalized Ti scaffolds promotes bone formation in a dog model with bicortical bone defects. Manuscript in preparation for submission.

Article 5

Gu Y, Liu Y, Jacobs R, Tian L, Sun Y, Jahr H, Politis C. Biocompatibility and osteogenic capability of additively manufactured biodegradable porous WE43 scaffolds: an in vivo study in beagle dogs. Manuscript in preparation for submission.

Personal Acknowledgements

First and foremost, I'd like to convey my gratitude to my supervisor, **Prof. Constantinus Politis**. I am very grateful for his help, encouragement, and patience throughout my Ph.D. years. I could not have completed my Ph.D. without his support.

Second, I'd like to sincerely thank **Prof. Reinhilde Jacobs**, my co-promoter. Throughout my Ph.D., she has provided me with unwavering care and support in both my academics and life. She has been an excellent spiritual role model for me to learn from.

In particular, I wish to express my deep gratitude to **Dr. Yi Sun**, my external co-promoter, for his support and guidance throughout my Ph.D. journey. Only with his help and encouragement can I complete my Ph.D. research. He is both a good friend and a great teacher.

Further, I would also like to thank all the other Professors who also helped me in my Ph.D. life, including **Prof. Antoon De Laat** and **Prof. Joke Duyck** from KU Leuven, **Prof. Yuelian Liu** from ACTA, **Prof. Lei Tian** from the FMMU, **Prof. Ivo Lambrichts** from Hasselt University, as well as **Prof. Holger Jahr** from RWTH Aachen University. My academic work has been completed bit by bit thanks to your help, and I am very grateful to you.

In addition, I'd like to show my thankfulness to the entire **OMFS-IMPATH research group**. I have lovely memories of the welcoming and helpful work environment. Thanks to my Chinese colleagues: **Dandan**, **Jiqing**, **Hongyang**, **Xiaotong**, **Lianyi**, **Qimin**, and **Shengping**. My friendship with you helped me cope with the loneliness of studying abroad.

Most of all, I would like to thank my parents (**Hehe & Zhongying**) and husband (**Gen**). Without your love and support, I would never be able to finish my Ph.D. study alone abroad. I sincerely hope that I can make you proud. Also, thanks to **my motherland and China Scholarship Council (CSC)**. In the most challenging years of fighting against the COVID, they still support me in completing my study. I hope that I can dedicate my strength to my motherland's development.

Finally, I would like to end up my acknowledgement part with a motto that I cherish: "Studies progress through diligence and are slowed by indolence; success comes through forethought, while thoughtlessness leads to failure." (Hanyu,768-824 AD)

业精于勤而荒于嬉，行成于思而毁于随。**(韩愈，768-824 AD)**

Table of Contents

List of Abbreviations

2D	Two-demensional
3D	Three-dimensional
ALB	Albumin
ALP	Alkaline phosphate
ALT	Alanine aminotransferase
AM	Additive manufacturing
AST	Aspartate aminotransferase
BA	Bone area
BA/TA	Bone area fraction
BGS	Bone graft substitutes
BIC	Bone-implant-contact
BMP	Bone morphogenic protein
BSE	Backscattered electron
BTE	Bone tissue engineering
BU	Blood urea
BV	Bone volume
BV/TV	Bone volume fraction
Ca	Calcium
CAD/CAM	Computer-Aided Design and Manufacturing
CaP	Calcium Phosphate
CR	Serum creatinine
Cu	Copper
EBM	Electron Beam Melting
ECM	Extracellular matrix
EDS	Energy-dispersive X-ray spectroscopy
ELISA	Enzyme-linked immunosorbent assay
Fe	Iron
ICP-OES	Inductively coupled plasma-optical emission spectrometry
Mg	Magnesium
OCP	Octacalcium phosphate
P	Phosphate
PEEK	Polyetheretherketone
PLT	Platelets
PMMA	Polymethylmethacrylaat
RBC	Red blood cell

ROI	Region of interest
SE	Secondary electrons
SEM	Scanning electron microscope
SLM	Selective laser melting
STL	Standard triangulation language
TA	Tissue area
Tb.N	Trabecular number
Tb.Sp	Trabecular Separation
Tb.Th	Trabecular thickness
Ti	Titanium
Ti64	Titanium-6aluminum-4vanadium
TPMS	Triply periodic minimal surface
VEGF	Vascular endothelial growth factor
VFF	Vascularized fibular flap
VIF	Vascularized iliac flap
WBC	White blood cell
Zn	Zinc

General Introduction

Aims & Hypotheses

0.1 Bone and maxillofacial bone defects

Bone is a mineralized tissue that is highly vascularized and innervated and is involved in a variety of critical functions in the human body. The bone tissue is made up of cells, minerals, and the extracellular matrix, which is made up of collagen fibers and hydroxyapatite [1]. **Table 0.1** shows the composition of natural bone. Bones have properties such as strength, stiffness, as well as the resistance to compression, tension, and torsion. They give the body the mechanical stability it needs to support weight and can help protect the interior organs [2]. Bone also plays a significant role in the production and preservation of blood cells and is the body's Ca and P store [3].

Table 0.1 The chemical composition of bone (wt%)

Inorganic Phase	Organic Phase
$H_2O \approx 9$	Non-collagenous proteins ≈ 3
Hydroxyapatite ≈ 60	Collagen ≈ 20
Citrate ≈ 0.9	Traces: cytokines, lipids, and polysaccharides
Carbonate ≈ 4	Primary bone cell: osteoblasts, osteoclasts, and osteocytes
$Mg^{2+} \approx 0.5$	
$Na^+ \approx 0.7$	
Cl^-	
Others: $Fe^{2+}, Cu^{2+}, Sr^{2+}, K^+, F^-, Zn^{2+}$, and Pb^{2+}	

The structure of mature bone tissue is complicated. There are at least five different hierarchical levels of bone tissue, as shown in **Figure 0.1**. These five levels include macro-level (cortical bone and cancellous bone), micro-level, sub-micro-level (canals of Havers, osteons, and lamellae), nano-level (collagen fibers), and sub-nano-level (collagen and minerals, etc.) [4].

The bone is made up of two types of tissue: cancellous bone (about 20%) and cortical bone (about 80%) [5]. The cancellous bone is a comparatively soft bone comprising a high-porosity trabecular bone network (50%-90%). It has a sponge-like structure with many honeycomb-like branches throughout the inner side of the bone [5, 6]. Furthermore, bone trabeculae grow naturally following stress distributions, allowing bones to resist the maximum load with the least amount of bone mass [7]. The cancellous bone contains a variety of organic components, such as blood vessels and bone marrow, and it transports metabolic wastes and nutrients [7]. The cortical bone has a higher stiffness and lower flexibility because of its greater mineralized structure and lack of organic components. The porosity of the cortical bone is normally less than 10% [8]. The harder and denser structure of cortical bone serves as a protective shell for the spongy-like structure inside. The combination of cortical and cancellous bone makes bone a unique mechanical structure capable of withstanding higher levels of loading and deformation than its components alone can

achieve [9]. In addition, natural bone has a high porosity and stiffness, which enables bone matrix cells to diffuse and adhere to the bone tissue, allowing the formation of new bone matrix.
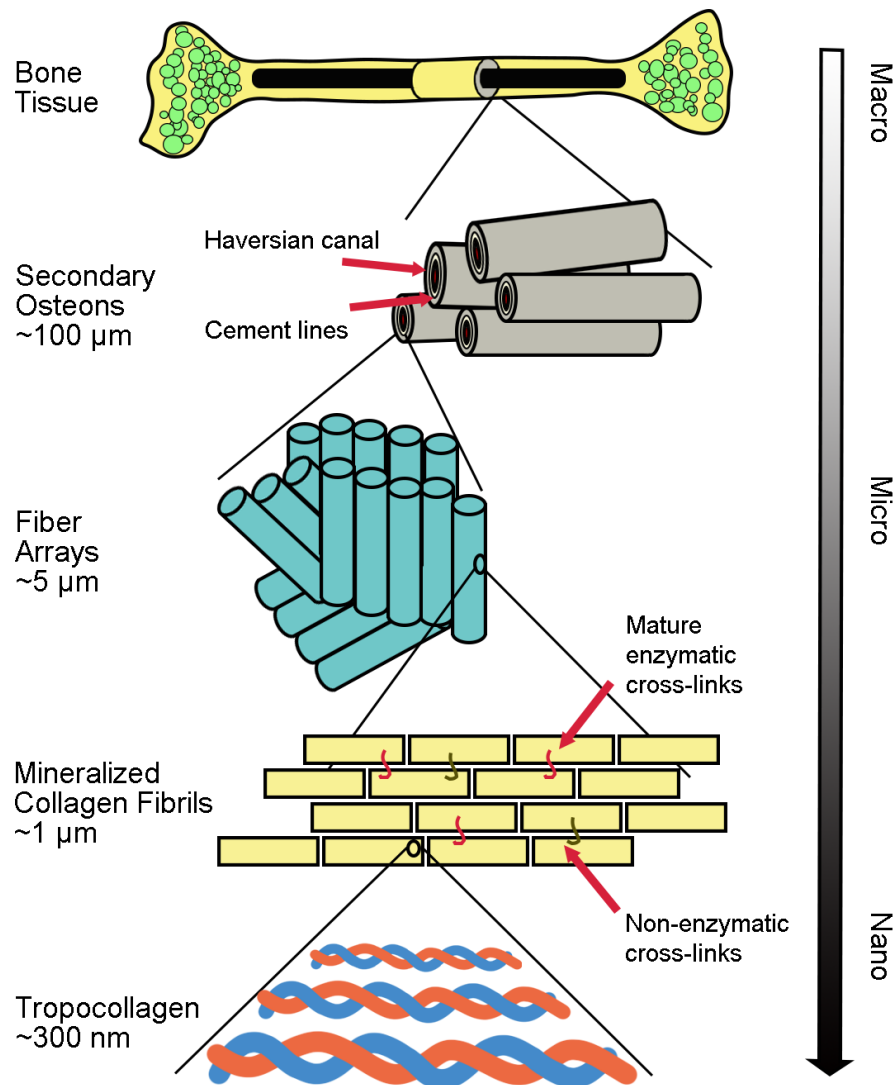

Figure 0.1. Different levels of the bone tissue

Maxillofacial bones are among the most functional bones in the human body because they are vital for chewing, speaking, and swallowing. In addition, the maxillofacial bones provide support for internal structures such as the eye sockets, nose, cheeks, and lips to maintain aesthetics. Therefore, due to the complex structure of bone and soft tissue, resection of tumors, trauma, or deformities in the maxilla and mandible presents considerable aesthetic and functional problems. In the maxillofacial area, some tiny fractures can heal on their own without the need for surgery due to the great regenerating ability of bone tissue, especially in young people [7]. Through its dynamic properties, bone tissue can remain healthy over time, undergo adaptive structural

3

changes in response to mechanical loading changes, and repair harmed parts of itself through an uninterrupted remodeling mechanism throughout the lifespan [10]. Osteoblasts and osteoclasts are two types of cells involved in the physiological process of repairing bone fractures [7]. Typically, bone healing begins with inflammation, and blood clots form a stable framework for developing new bone tissue. The blood clot is replaced by fibrous and collagenous tissue, the soft callus. The callus will harden several weeks after the fracture. Bone remodeling occurs in the months following the fracture [11, 12].

However, if severe bone tissue injury occurs, such as a result of an accident, autologous remodeling processes alone may not be adequate to restore maxillofacial bone integrity. Furthermore, accidents, tumor excision, congenital abnormalities, pathological damage, infection, and other factors can result in bone abnormalities, osteoarthritis, and other disorders that affect the human body's normal musculoskeletal system [13, 14]. Currently, there are almost 1.5 million people who receive bone graft surgery worldwide each year, generating about 1.5 billion US dollars in market turnover [15]. After blood, bone has become the second most widely used human transplant tissue. The demand for bone grafts is predicted to increase as the world's population ages [16].

Although considerable progress has been made in the field of maxillofacial bone repair over the past few decades, the actual reconstruction of the shape and function of bone defects still poses a significant challenge since maxillofacial bone repair is technically complex. Different cells, proteins, and signaling molecules work together to repair bone defects. For adequate fracture healing, four precise prerequisites must be met: the supply of osteoblasts, the construction of an osteoconductive scaffold, the addition of appropriate growth factors, and the supply of a stable environment, which together constitute the necessary conditions for fracture healing [16].

0.2   Clinical procedures for repairing bone defects

At present, autologous bone transplantation remains the gold standard for repairing large-scale bone defects. During this procedure, donor bone is harvested from a non-weight-bearing part of the patient. Such bone grafts allow for faster and more complete osseointegration. In addition, autologous bone has a 3D and porous structure, and also combines all the characteristics necessary for bone regeneration: including non-immunogenicity, histocompatibility, osteoconductivity and osteoinductivity [17]. However, autologous bone grafting also has some disadvantages that cannot be ignored, such as blood loss, longer operative time, infection at the donor site, and a limited amount of graft material, etc. [18]. The cancellous bone, cortical bone,

bone marrow, and vascularized bone tissue are the most commonly used autologous bone grafts [19].

Alternatives to vascularized autologous bone grafting include methods such as xenografting and allogeneic bone grafting. Allogeneic bone grafts (cadaveric or living sources) are the second higher option for orthopedic surgeons, which is appropriate for cases where the patient cannot provide their own bone tissue. There are many types of bone grafts that are available, such as cancellous, cortical, and demineralized bone grafts, and they are widely accessible. They are mainly osteoconductive and lack osteoinductive properties [20]. Allografts, on the other hand, have a higher chance of transmitting illness and producing an immune response than autografts. Besides, because this graft lacks biological components that help tissue regeneration, it does not heal as well as autologous bone grafts [16, 18].

Synthetic BGS is an alternative to the two procedures mentioned above. The use of BGS in autologous transplantation minimizes the need for extra surgical sites and reduces operative time. Simultaneously, it eliminates the risk of disease transmission and immunological issues associated with allogeneic transplantation [16]. BGS must be biocompatible, bioabsorbable, and have acceptable mechanical qualities (strength, flexibility, ductility, etc.) to suit clinical needs in clinical applications. Furthermore, BGS must have an appropriate cost-benefit ratio.

In addition, BGS should meet the following requirements: osteoconductivity, osteoinductivity and osseointegration ability [21]. The mechanism by which bone and vasculature migrate in-growth through the surface of the graft is referred to as osteoconductivity, and the ability to induce cells from various lineages to become bone-forming cells is referred to as osteoinductivity [22]. Osseointegration occurs when bone and implant directly contact each other. Osteointegration rates are affected by several factors, including bone graft type and implant location, etc. [23].

0.3   BTE: objectives and methods

There has been an enormous amount of research in the area of BTE, focusing on using the combination of cells, biomaterials, and signals to promote repair and regeneration of tissue. Porous 3D scaffolds of various biomaterials are carriers of cells and signals, and are able to be manufactured in a wide variety of ways [24]. The BTE strategy is shown in **Figure 0.2**.
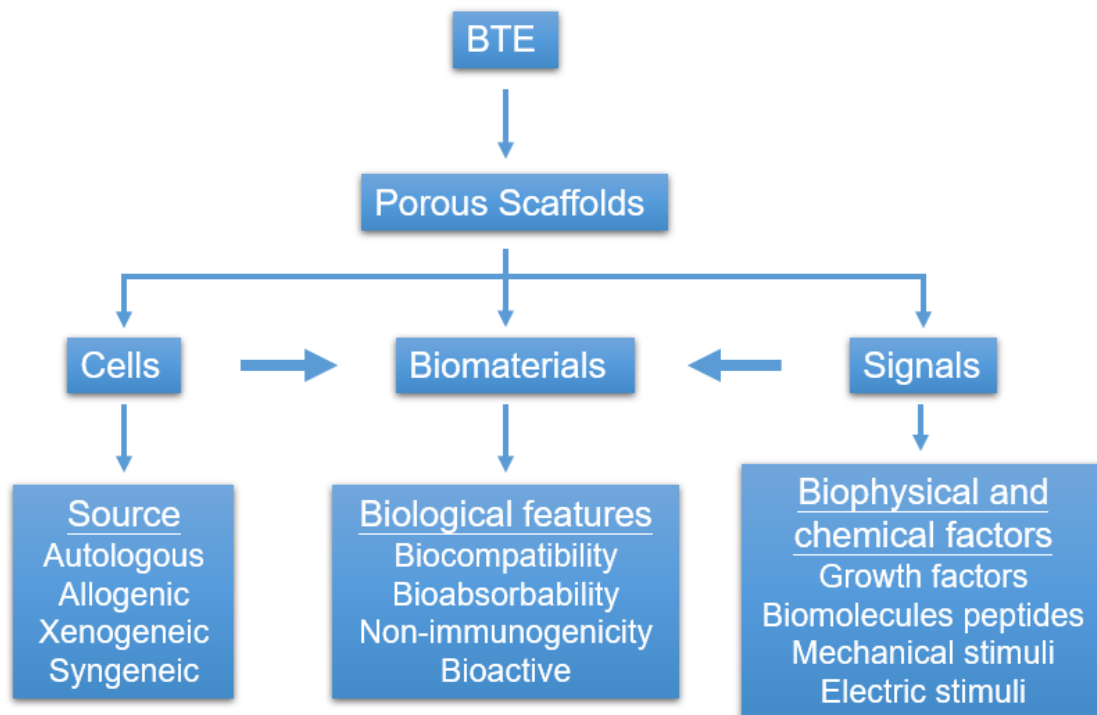
Figure 0.2. The strategy of BTE

0.4 The role of porous scaffold in bone defect repairing

Porous scaffolds are a core element of BTE [25]. A bone scaffold is a 3D matrix that allows osteoinductive cells to attach and proliferate on its surface and has sufficient physical properties to support bone repair. In the scaffolds, the pore network facilitates cell migration as well as nutrient and oxygen transport. In addition, these pores facilitate the growth of blood vessels and tissues, promote angiogenesis, and prevent new tissue necrosis due to inadequate vascularization [26]. Compared with solid metal implants, porous metal implants can achieve more physiological load transfer, which can avoid the stress shielding effect after implantation [27].

0.5 The basic requirements for porous scaffold

The following issues must be considered when designing bone scaffolds: 1) The scaffold must be biocompatible for cell attachment and proliferation, and it must be non-toxic and non-inflammatory; 2) The scaffold must be biodegradable, with degradation products that are not hazardous or poisonous to humans; 3) The scaffold should possess specific mechanical characteristics and be comparable to the adjacent bones; 4) The scaffold should have an appropriate pore structure (pore size and porosity) for cell infiltration, nutrient and waste transportation, and blood vessel ingrowth; 5) The scaffold should imitate the physiological structure of bone as closely as possible (the orderly arrangement of hydroxyapatite and collagen), and facilitate mesenchymal stem cell proliferation

and differentiation; 6) The scaffold must maintain sterility while maintaining biological activity; 7) The scaffold must be capable of delivering biologically active molecules or medications in a controlled manner [11, 28, 29].

0.6 Material selection for porous scaffold

According to archeological finds, a variety of materials, including coral, shells, animal bones, and many different metals, have all been used to replace human bones and teeth [30]. Similarly, over the years, many synthetic and natural, biodegradable, and non-biodegradable materials have been used to create bone scaffolds using diverse methods [11]. An ideal biomaterial should be biocompatible, biodegradable, and easy to manufacture and process. In general, there are two types of preclinical investigations on scaffold materials: in vitro studies, including culture experiments with human or animal cells (bone marrow stromal cells, mesenchymal stem cells, etc.) as well as in vivo experiments using animal models (for example, restoring the integrity of animal bones).

Biomaterials have been divided into three generations since their appearance during the 1960s [24]: First-generation biomaterials aim to obtain biomaterial qualities that are similar to those of the replaced tissue, and they are generally physiologically inert. The first generation of biomaterials include metals (for example, stainless steel), synthetic polymers (for example, PEEK), and ceramics (for example, zirconia).

One of the most prominent properties of second-generation biomaterials (including natural and synthetic materials such as collagen, CaP, calcium carbonate, bioactive glass, etc.) is their biological activity, as well as the fact that some materials can degrade in vivo. A third-generation biomaterial consists of the addition of guiding substances (such as biochemical factors and external physical stimuli) to second-generation biomaterials and/or new biomaterials with enhanced properties in order to promote a specific biological reaction. .

0.6.1 Scaffold composed of a single biomaterial

The choice of matrix material has a huge effect on how well bone scaffolds work. As a result, we will describe various biomaterials, discussing their benefits, drawbacks and features.

0.6.1.1 Metals

Common metal biomaterials, including Ti and Ti alloys, nickel-Ti alloys, Mg alloys, and tantalum, are characterized by excellent biocompatibility and mechanical properties. Under suitable designing parameters, the elastic modulus of porous metal scaffolds can be similar to that of

human bones.

The most widely utilized metal materials in biomedicine are Ti and Ti alloys. When formed into porous structures, it is durable, biocompatible, and corrosion resistant, and its elastic modulus is remarkably comparable to that of trabecular bone [31].

Ti and Ti alloy-printed porous scaffolds have been employed clinically, primarily as artificial spinal cages or artificial acetabular joints (**Figure 0.3**). For example, products including Zimmer Biomet's TrellOss®-TC Porous Ti Interbody System [32] and OsseoTi® Porous Metal Technology [33], Nuvasive Inc.'s Modulus Ti Technology [34] as well as Spineart's Juliet Ti® TL [35]. These porous scaffolds have a high mechanical strength and an elastic modulus similar to that of bone, and are additionally resistant to scratches, cracks, and spalling [36]. However, these implants lack osteoinductive properties.

Figure 0.3. Artificial spinal cage (left) and acetabular joint (right) from Zimmer Biomet.

0.6.1.2 Natural polymers

Chitosan, hyaluronic acid, collagen, alginate, silk, glycosaminoglycans, elastin, and peptides are some of the most commonly studied natural polymers for BTE applications. [37]. Natural polymers have properties that are similar to ECM, such as particular breakdown rates and biocompatibility. They are, however, difficult to sterilize and handle, and there are concerns about immunogenicity and supply. In addition, the low mechanical strength makes it difficult for them to be widely used in BTE [38].

0.6.1.3 Synthetic polymers

Polycaprolactone, Poly(D-lactide), Poly(L-lactic acid), and Poly(L-lactic-co-glycolide) are synthetic polymers commonly used in BTE [19]. Synthetic polymers degrade at different rates depending on their chemical structure and crystallinity, and they have a variety of mechanical and physical properties. On the other hand, their bioactivity and osteoconductivity are reduced if compared to natural polymers [39].

0.6.1.4 Bioceramics

The range of bioceramics has expanded from amorphous bioactive glass, crystalline ceramics, and tricalcium phosphate to calcium silicate. Bioceramics have an inorganic composition similar to bone. These materials share characteristics with bone, including osteoinductivity, osteoconductivity, acceptable biocompatibility, favorable bioactivity, high stiffness, and hydrophilicity [40]. On the other hand, bioceramics' limited ductility is a significant drawback, limiting their use in load-bearing areas, filling bone deformities, and covering metal implants [10].

In the field of BTE, CaP is among the most widely studied and used bioceramics. They were first incorporated into dental and orthopedic applications in the 1980s [41]. CaP is biocompatible, similar in structure and composition to that of mineralized bone, osteoconductive, and biologically active. Although strength is one of the limiting considerations for using CaP in load-bearing applications, the ultimate limiting factor for CaP may be the material's intrinsic brittleness [42]. Therefore, the brittleness problem of CaP materials remains to be solved.

0.6.2 Scaffolds composed of composite biomaterials

Composite biomaterials are made up of two or more different components. The primary goal of employing composite materials in manufacturing scaffolds is to increase the scaffolds' processing, printing, mechanical properties, and biological activities [1]. In addition, the composite scaffolds containing additives have excellent bone regeneration ability. Composite biomaterials include ceramic matrix composites, polymer matrix composites, metallic matrix composites, and functional composites, etc. [1]. Among them, bioactive metal matrix composite materials are widely used in clinical medical environments due to their corrosion resistance, outstanding biocompatibility, thermal resistance, and superior mechanical characteristics. Ti alloys are the preferred metal biomaterial for scaffolds, and Ti64 is an excellent example of metal matrix composites. A suitably porous Ti64 scaffold's Young's modulus can be comparable to native bone, which reduces stress shielding risks. To promote osseointegration, the porous Ti64 scaffold can be coated with CaP coating [43], barium titanate coating [44], TiCu/Ti-Cu-N coating [45], polydopamine coating [46], etc. In addition, bone regeneration and blood vessel formation can also be promoted by adding BMP-2 and VEGF, respectively [47, 48]. Despite the fact that Ti alloys have numerous advantages, their non-biodegradable qualities severely limit their potential as perfect materials.

Metal scaffolds and metal matrix composite scaffolds are the focus elements of this doctoral thesis. Detailed discussion will be provided in the following sections.

0.7 Designing parameters for porous scaffold

The complexity of designing porous scaffolds is that the pore size, porosity, and pore shape are all intertwined. The ideal pore size and porosity are usually determined by a given pore shape rather than a general conclusion [49].

0.7.1 Pore size

Osteoblasts range in size from 10 to 50µm. However, in order to repair mineralized bone after implantation, they prefer larger pores (100-200µm) [50]. In the literature, scaffolds appropriate for BTE have pore sizes ranging from 100 to 900µm [51]. A scaffold should have a minimum pore size of 100µm (to permit cell proliferation and migration). The ideal pore size was around 300-500µm to facilitate the formation of new bone and blood vessels, according to several tests carried out on the scaffolds with varying pore sizes in vitro [52-54]. In general, large pores facilitate cell infiltration and inward growth of capillaries, but at the same time, they reduce mechanical strength and cell adherence [55]. The enormous surface area of the tiny pore structure encourages cell attachment and tissue ingrowth, but it also leads to pore occlusion [56, 57].

0.7.2 Porosity

A precise balance between the scaffold's porosity and strength is necessary to promote material transfer while maintaining a strong supporting framework [58]. A higher porosity scaffold has a larger overall surface area, allowing for increased cell proliferation and tissue growth [59, 60]. In addition, the porosity of the porous scaffold can be adjusted to manage its elastic modulus.

The porosity of more than 60% has been proven in studies to enhance bone growth [61]. Furthermore, studies have shown that porosity of 80-90% promotes cell motility and diffusion. The larger the porosity, the better the scaffold's permeability (facilitating the transport of nutrients and oxygen) [64]. However, while high porosity is favorable to tissue ingrowth, it compromises the scaffold's mechanical qualities [53].

0.7.3 Pore structure

Body-centered cubic, rhombic, and rhombic dodecahedral structures are some of the most prevalent pore units for scaffolds in BTEs. Other pore structures have seen more minor investigations.

Body-centered cubic structures **(Figure 0.4a)** are a straightforward design that is simple to produce. Scaffolds with body-centered cubic structures have extremely predictable dimensions due to their

high structure precision [62]. The mechanical characteristics of the scaffold corresponding to the porosity may be reliably modeled and inferred due to the predictability of the structure. As a result, body-centered-cubic scaffolds often meet the mechanical qualities predicted [63].

One of the most common pore shapes in BTEs is the diamond-shaped structure **(Figure 0.4b)**. Ti64 scaffolds with diamond pore structures have an elastic modulus similar to that of natural bone [61]. The diamond pore sturcture is an excellent alternative for building porous scaffolds [64, 65]. Furthermore, multiple studies have demonstrated that the diamond structure can stimulate bone ingrowth in degradable and non-degradable scaffolds [61, 66, 67]. It is noteworthy that the mechanical properties of scaffolds with diamond-shaped components are nearly identical in different directions. In BTE, the diamond-shaped scaffold can be used in situations where the scaffold must withstand multidirectional stress [62].

The rhombic dodecahedron **(Figure 0.4c)** is a centrosymmetric construction with mechanical properties that are identical in all three dimensions. Furthermore, the highly symmetric structure gives the rhombic dodecahedron structure lattice stability under multidirectional compressive stresses, even in the presence of considerable scaffold porosity, making it exceedingly safe for clinical use [68]. Furthermore, the rhombic dodecahedron-structured scaffolds show outstanding biological characteristics. This pore structure provides the cells with the nutrition and oxygen they require, as well as an ideal osteogenic microenvironment for osteoblast integration into the scaffold [69].
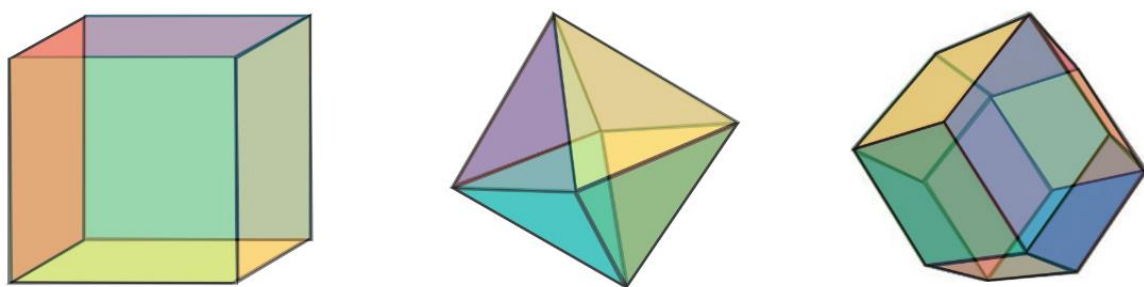

Figure 0.4. The body-centered cubic structure (left), diamond structure (middle) and rhombic dodecahedron structure (right) in BTE scaffolds.

0.7.3.1 Parametric design of the scaffolds

Scaffolds with simple structures are no longer sufficient for experimental or clinical needs, thanks to advances in AM technology. AM technology may be used to create scaffolds with a variety of

complicated structures. Algorithms are a sophisticated technique for creating porous structures. The Voronoi-Tessellation approach is the most used way of creating porous structures using the algorithm [63]. Bone scaffolds with the best porosity design should have complex and anisotropic porous structures, just like genuine bone [70]. Random-structure BTE scaffolds are better at allowing nutrients to penetrate than fixed-structure scaffolds, and they are better at allowing bone formation than fixed-structure scaffolds [71].

The Voronoi structure is morphologically comparable to the microstructure of natural bone. The Voronoi structure generates a network structure based on random discrete points [72, 73]. Currently, the critical research investigations have concentrated on the reverse reconstruction of irregular spots from CT images in order to generate a Voronoi model, which is the most straightforward technique for constructing a bone-like scaffold [74]. The Voronoi design is one of the most skeleton-like designs known in biomimicry [71]. The behavior of 3D-printed Voronoi scaffolds in vitro and in vivo has to be studied further.

0.8 Manufacturing of porous scaffold

CAD/CAM techniques can be used to design and fabricate scaffolds with customizable designs. AM is a layer-by-layer manufacturing technology that allows 3D parts to be manufactured using CAD/CAM. It can produce unique and complicated structures in a short amount of time. Today, there are several metal 3D-printing systems on the market. SLM [75] and EBM [76] techniques are the most commonly used methods in 3D-printing of biomedical metal implants [77], both of which have been successfully implemented to produce osteogenic scaffolds.

The primary advantage of AM techniques is the capacity to create porous networks with repeatable and specified cells. In this way, the inserted implant and the host bone can be perfectly matched [55, 78]. Pore size and shape are predefined, and pore morphology is placed in a regular pattern [79]. Additionally, because porosity has an effect on the elastic modulus and compressive strength of the implant, the mechanical characteristics of the implant can be adjusted so that they closely resemble those of natural bone. As a result, the stress shielding effect after scaffold implantation can be prevented by adequately managing the implant's porosity [80, 81].

0.9 Fields to improve porous scaffold

The optimum surface qualities (microstructure and chemical composition) for metal scaffolds are essential for the scaffold's adhesion to the adjacent bone tissue and extracellular matrix, and can influence the scaffold's lasting effectiveness [82]. Surface modification of metal scaffolds can be

used to boost bioactivity and biocompatibility, as well as improve biological performance [83, 84].

Surface modification of metal scaffolds can currently be accomplished in two ways. The first is to roughen the surface (sandblasting, etching, or sandblasting/etching), and the second is to coat the scaffold with a bioactive coating [85-87]. The former tries to boost cell adhesion and proliferation by modifying the scaffold surfaces' structure and roughness, while the latter enhances biocompatibility. Porous metal scaffolds are typically modified with surface coatings [88]. Different coating materials, including CaP, hydroxyapatite, zirconia, titanium carbide/titanium nitride, and carbon, have been used to improve surface qualities [89-94].

One of the bioceramics, named CaP, can be applied to scaffold surfaces to increase their osteoconductive properties [95]. The CaP coating is chemically comparable to natural bone, and it promotes proliferation and differentiation of the osteoblasts. Ti implants with CaP coating can induce bone formation, and inflammation can be reduced if antibiotics are added to the coating [96, 97].

Plasma spraying, sol-gel process, and biomimetic coating processes are all options for producing CaP coatings [98-100]. The porous metal scaffolds were successfully and uniformly coated in a biomimetic procedure by submerging the metal implants in simulated body fluids at physiological pH (7.4) and temperature (37°C) [101]. Furthermore, bioactive chemicals can be carried by the biomimetic CaP material without altering its biological activity.

BMP-2 is one of the most often used bioactive agents in BTE. It is a topically applied osteoinductive protein that promotes bone growth around scaffolds [102]. BMP-2 is a growth factor that can promote the formation of osteoblasts from mesenchymal stem cells and osteoprogenitor cells [103]. BMP-2 has been shown in studies to encourage the creation of new bone surrounding Ti scaffolds [80, 104, 105]. Furthermore, BMP-2 can also be used in conjunction with CaP or CaP-based materials to act as an osteoinductive agent and effectively stimulate bone growth [106-108].

0.10   Aims and hypotheses

The use of autologous bone grafts to correct maxillofacial bone defects currently has a number of drawbacks. Using AM technology to fabricate porous scaffolds as implants could offer a new method for repairing maxillofacial bone defects. Metal materials would be an ideal choice for constructing porous scaffolds. In this doctoral thesis, the aim is to develop 3D-printed metal scaffolds to repair maxillofacial bone defects and enhance their osteoinductive properties using surface modification techniques. In addition, we will also test the osteogenic ability of these metal scaffolds in animal models. Our findings will be a resource for researchers and will help to progress

BTE research. This doctoral thesis is divided into four parts, each with its own aim.

Part Ⅰ: Morbidities in autologous bone grafting

While autologous bone transplantation is the gold standard for BTE, it has a number of drawbacks, including the risk of complications. The literature lacks a comprehensive review of both donor- and recipient-site complications associated with VFF and VIF, the most commonly used two autologous flaps in bone reconstruction. Research into the intra- and postoperative complications related to these flaps could help surgeons estimate the imminent risks. Within this context, a review of the complication rate based on the accumulated evidence might enable surgeons to predict in advance the likelihood of patients developing postoperative morbidities.

The objective is:

To report the post-surgical donor- and recipient-site morbidities following mandibular reconstruction with VFF and VIF.

Part II: 3D-printed BTE scaffolds in animal studies

AM technology has advanced significantly and been successfully employed in the medical industry in the last few decades. Although the benefits of AM-fabricated Ti64 scaffolds have been well documented, the material is physiologically inert and lacks osteoinductive characteristics. The animal experiment is the most efficient way to assess the osteogenic potential of functionally modified Ti64 scaffolds. Therefore, it is necessary to review the state of the existing Ti64 scaffold's manufacturing and preclinical testing to better understand the osteogenic potential of the scaffolds.

The objective is:

To report the current evidence related to the application of Ti64 scaffolds to repair long bone defects in animal models and to investigate potential influencing factors that may affect their osteogenic capacity.

Part III: Surface modification of Ti alloy scaffolds

Surface modification of metal scaffolds improves the physical and chemical properties of the scaffolds and enhances osseointegration. Micro/nanoscale surface roughness has been shown to aid in bone and scaffold adhesion. CaP is the most common mineral in bone minerals, and its

degradation products provide rich Ca and P for osteoblasts to promote bone regeneration. BMP-2 is a growth factor that may drive the differentiation of mesenchymal stem cells and osteoprogenitor cells into osteoblasts, making it one of the most effective growth factors for inducing osteogenesis. At physiological temperature (37 °C) and pH (7.4), BMP-2 integrated biomimetic CaP materials were produced, and BMP-2 retained biological activity during co-precipitation with inorganic components.

The objectives are:

To design and fabricate 3D-printed Ti scaffolds using 3D-printing technology and coat the scaffolds with a BMP-2 integrated biomimetic CaP coating. Examine the osteogenic capacity of the surface-modified scaffolds in an animal model.

1. Test the osteogenic property of the scaffold in the ectopic site in the beagle dog models.

2. Test the osteogenic property of the scaffold in the mandibular bicortical bone defect in the beagle dog models.

Hypothesis: the porous Ti scaffolds coated with BMP-2 integrated biomimetic CaP coating exhibit excellent osteogenic ability in both ectopic sites and bone defects.

Part IV: Explore the biodegradable WE43 scaffold

To enable complete regeneration of bone defects, an ideal biomaterial should have mechanical qualities that imitate bone, a fully linked porous structure, and appropriate biodegradation behaviors, which is not possible with Ti and Ti alloys. Mg alloy implants promote the creation of new bone. As a result, Mg alloys play an essential role in developing orthopedic implants.

The objectives are:

To design and fabricate porous Mg alloy scaffold made of 3D-printing technique and to test that scaffold in vivo for its biocompatibility and degradation rate, and its osteogenic ability.

Hypothesis: porous 3D-printed WE43 scaffolds have good biocompatibility, have a reasonable degradation rate, and are able to induce osteogenesis in vivo.

0.11 References

1. Qu H, Fu H, Han Z, Sun Y. Biomaterials for bone tissue engineering scaffolds: a review. RSC advances. 2019;9:26252-62.

2. Hart NH, Newton RU, Tan J, Rantalainen T, Chivers P, Siafarikas A, et al. Biological basis of bone strength: anatomy, physiology and measurement. Journal of musculoskeletal & neuronal interactions. 2020;20:347.

3. Bharadwaz A, Jayasuriya AC. Recent trends in the application of widely used natural and synthetic polymer nanocomposites in bone tissue regeneration. Materials Science and Engineering: C. 2020;110:110698.

4. Liebschner M, Wettergreen M. Optimization of bone scaffold engineering for load bearing applications. Topics in tissue engineering. 2003.

5. Sikavitsas VI, Temenoff JS, Mikos AG. Biomaterials and bone mechanotransduction. Biomaterials. 2001;22:2581-93.

6. Salgado AJ, Coutinho OP, Reis RL. Bone tissue engineering: state of the art and future trends. Macromolecular bioscience. 2004;4:743-65.

7. Zhang XY, Fang G, Zhou J. Additively Manufactured Scaffolds for Bone Tissue Engineering and the Prediction of their Mechanical Behavior: A Review. Materials. 2017;10:50.

8. Niinomi M, Liu Y, Nakai M, Liu H, Li H. Biomedical titanium alloys with Young's moduli close to that of cortical bone. Regenerative biomaterials. 2016;3:173-85.

9. Wubneh A, Tsekoura EK, Ayranci C, Uludağ H. Current state of fabrication technologies and materials for bone tissue engineering. Acta Biomaterialia. 2018;80:1-30.

10. Jodati H, Yılmaz B, Evis Z. A review of bioceramic porous scaffolds for hard tissue applications: Effects of structural features. Ceramics International. 2020;46:15725-39.

11. Ghassemi T, Shahroodi A, Ebrahimzadeh MH, Mousavian A, Movaffagh J, Moradi A. Current concepts in scaffolding for bone tissue engineering. Archives of bone and joint surgery. 2018;6:90.

12. Ho-Shui-Ling A, Bolander J, Rustom LE, Johnson AW, Luyten FP, Picart C. Bone regeneration strategies: Engineered scaffolds, bioactive molecules and stem cells current stage and future perspectives. Biomaterials. 2018;180:143-62.

13. Jonitz A, Lochner K, Lindner T, Hansmann D, Marrot A, Bader R. Oxygen consumption, acidification and migration capacity of human primary osteoblasts within a three-dimensional tantalum scaffold. Journal of Materials Science: Materials in Medicine. 2011;22:2089-95.

14. Chen K, Lin X, Zhang Q, Ni J, Li J, Xiao J, et al. Decellularized periosteum as a potential biologic scaffold for bone tissue engineering. Acta biomaterialia. 2015;19:46-55.

15. Petite H, Viateau V, Bensaid W, Meunier A, de Pollak C, Bourguignon M, et al. Tissue-engineered bone regeneration. Nature biotechnology. 2000;18:959-63.

16. Lobb DC, DeGeorge Jr BR, Chhabra AB. Bone graft substitutes: current concepts and future expectations. The Journal of hand surgery. 2019;44:497-505.

17. Bauer TW, Muschler GF. Bone graft materials: an overview of the basic science. Clinical Orthopaedics and Related Research. 2000;371:10-27.

18. Wang W, Yeung KW. Bone grafts and biomaterials substitutes for bone defect repair: A review. Bioactive materials. 2017;2:224-47.

19. Chocholata P, Kulda V, Babuska V. Fabrication of scaffolds for bone-tissue regeneration. Materials. 2019;12:568.

20. Fillingham Y, Jacobs J. Bone grafts and their substitutes. The bone & joint journal. 2016;98:6-9.

21. Albrektsson T, Johansson C. Osteoinduction, osteoconduction and osseointegration. European spine journal. 2001;10:S96-S101.

22. Roberts TT, Rosenbaum AJ. Bone grafts, bone substitutes and orthobiologics: the bridge between basic science and clinical advancements in fracture healing. Organogenesis. 2012;8:114-24.

23. Khan SN, Cammisa Jr FP, Sandhu HS, Diwan AD, Girardi FP, Lane JM. The biology of bone grafting. JAAOS-Journal of the American Academy of Orthopaedic Surgeons. 2005;13:77-86.

24. Yu X, Tang X, Gohil SV, Laurencin CT. Biomaterials for bone regenerative engineering. Advanced healthcare materials. 2015;4:1268-85.

25. Haleem A, Javaid M, Khan RH, Suman R. 3D-printing applications in bone tissue engineering. Journal of clinical orthopaedics and trauma. 2020;11:S118-S24.

26. He S-y, Zhang Y, Zhou Y, Bao N, Cai Y, Zhou P, et al. Modeling osteoinduction in titanium bone scaffold with a representative channel structure. Materials Science and Engineering: C. 2020;117:111347.

27. Hara D, Nakashima Y, Sato T, Hirata M, Kanazawa M, Kohno Y, et al. Bone bonding strength of diamond-structured porous titanium-alloy implants manufactured using the electron beam-melting technique. Materials science & engineering C. 2016;59:1047-52.

28. Hutmacher DW. Scaffolds in tissue engineering bone and cartilage. Biomaterials. 2000;21:2529-43.

29. Porter JR, Ruckh TT, Popat KC. Bone tissue engineering: a review in bone biomimetics and drug delivery strategies. Biotechnology progress. 2009;25:1539-60.

30. Dorozhkin SV. Bioceramics of calcium orthophosphates. Biomaterials. 2010;31:1465-85.

31. Chen Y, Frith JE, Dehghan-Manshadi A, Attar H, Kent D, Soro NDM, et al. Mechanical properties and biocompatibility of porous titanium scaffolds for bone tissue engineering. Journal of the Mechanical Behavior of Biomedical Materials. 2017;75:169-74.

32. Zimmer.https://www.zimmerbiomet.com/en/products-and-solutions/specialties/spine/trelloss-tc-porous-ti-interbody-system.html. 2019.

33. Zimmer.https://www.zimmerbiomet.com/en/products-and-solutions/specialties/hip/osseoti-porous-metal-technology.html. 2016.

34. Nuvasive I. Https://Www.Nuvasive.Com/Surgical-Solutions/Advanced-Materials-Science/Modulus-Titanium-Technology/. 2019.

35. Spineart. https://www.spineart.com/products/juliet-ti-tl/. 2020.

36. Rodriguez-Contreras A, Punset M, Calero JA, Gil FJ, Ruperez E, Manero JM. Powder metallurgy with space holder for porous titanium implants: A review. Journal of Materials Science & Technology. 2021;76:129-49.

37. Vagaská B, Bačáková L, Filovaá E, Balík K. Osteogenic cells on bio-inspired materials for bone tissue engineering. Physiological Research. 2010;59:309-22.

38. Filippi M, Born G, Chaaban M, Scherberich A. Natural polymeric scaffolds in bone regeneration. Frontiers in Bioengineering and Biotechnology. 2020;8:474.

39. Donnaloja F, Jacchetti E, Soncini M, Raimondi MT. Natural and synthetic polymers for bone scaffolds optimization. Polymers. 2020;12:905.

40. Ma H, Feng C, Chang J, Wu C. 3D-printed bioceramic scaffolds: From bone tissue engineering to tumor therapy. Acta biomaterialia. 2018;79:37-59.

41. Bohner M. Calcium orthophosphates in medicine: from ceramics to calcium phosphate cements. Injury. 2000;31:37-47.

42. Johnson AJW, Herschler BA. A review of the mechanical behavior of CaP and CaP/polymer composites for applications in bone replacement and repair. Acta biomaterialia. 2011;7:16-30.

43. Huang H, Lan PH, Zhang YQ, Li XK, Zhang X, Yuan CF, et al. Surface characterization and in vivo performance of plasma-sprayed hydroxyapatite-coated porous Ti6Al4V implants generated by electron beam melting. Surface & Coatings Technology. 2015;283:80-8.

44. Fan B, Guo Z, Li X, Li S, Gao P, Xiao X, et al. Electroactive barium titanate coated titanium scaffold improves osteogenesis and osseointegration with low-intensity pulsed ultrasound for large segmental bone defects. Bioactive Materials. 2020;5:1087-101.

45. Guo Y, Ren L, Xie K, Wang L, Yu B, Jiang W, et al. Functionalized TiCu/Ti-Cu-N-Coated 3D-Printed Porous Ti6Al4V Scaffold Promotes Bone Regeneration through BMSC Recruitment.

Advanced Materials Interfaces. 2020;7:1901632.

46. Li L, Li Y, Yang L, Yu F, Zhang K, Jin J, et al. Polydopamine coating promotes early osteogenesis in 3D-printing porous Ti6Al4V scaffolds. Annals of Translational Medicine. 2019;7:240.

47. van der Stok J, Koolen MK, de Maat MP, Yavari SA, Alblas J, Patka P, et al. Full regeneration of segmental bone defects using porous titanium implants loaded with BMP-2 containing fibrin gels. European Cells & Materials. 2015;29:141-53.

48. Lv J, Xiu P, Tan J, Jia Z, Cai H, Liu Z. Enhanced angiogenesis and osteogenesis in critical bone defects by the controlled release of BMP-2 and VEGF: implantation of electron beam melting-fabricated porous Ti6Al4V scaffolds incorporating growth factor-doped fibrin glue. Biomedical Materials. 2015;10:035013.

49. Chen Z, Yan X, Yin S, Liu L, Liu X, Zhao G, et al. Influence of the pore size and porosity of selective laser melted Ti6Al4V ELI porous scaffold on cell proliferation, osteogenesis and bone ingrowth. Materials science & engineering C. 2020;106:110289.

50. Iviglia G, Kargozar S, Baino F. Biomaterials, current strategies, and novel nano-technological approaches for periodontal regeneration. Journal of functional biomaterials. 2019;10:3.

51. Surmeneva MA, Surmenev RA, Chudinova EA, Koptioug A, Tkachev MS, Gorodzha SN, et al. Fabrication of multiple-layered gradient cellular metal scaffold via electron beam melting for segmental bone reconstruction. Materials & Design. 2017;133:195-204.

52. Karageorgiou V, Kaplan D. Porosity of 3D biomaterial scaffolds and osteogenesis. Biomaterials. 2005;26:5474-91.

53. Alice C, Aiza H, David JC, Barbara DB, Zvi S. Additively manufactured 3D porous Ti-6Al-4V constructs mimic trabecular bone structure and regulate osteoblast proliferation, differentiation and local factor production in a porosity and surface roughness dependent manner. Biofabrication. 2014;6:045007.

54. Lv J, Jia Z, Li J, Wang Y, Yang J, Xiu P, et al. Electron beam melting fabrication of porous Ti6Al4V scaffolds: cytocompatibility and osteogenesis. Advanced Engineering Materials. 2015;17:1391-8.

55. Tamimi F, Torres J, Al-Abedalla K, Lopez-Cabarcos E, Alkhraisat MH, Bassett DC, et al. Osseointegration of dental implants in 3D-printed synthetic onlay grafts customized according to bone metabolic activity in recipient site. Biomaterials. 2014;35:5436-45.

56. Du Y, Guo JL, Wang J, Mikos AG, Zhang S. Hierarchically designed bone scaffolds: From internal cues to external stimuli. Biomaterials. 2019:119334.

57. Onal E, Frith JE, Jurg M, Wu X, Molotnikov A. Mechanical properties and in vitro behavior of additively manufactured and functionally graded Ti6Al4V porous scaffolds. Metals. 2018;8:200.

58. Ryan G, Pandit A, Apatsidis DP. Fabrication methods of porous metals for use in orthopaedic applications. Biomaterials. 2006;27:2651-70.

59. Balla VK, Bodhak S, Bose S, Bandyopadhyay A. Porous tantalum structures for bone implants: fabrication, mechanical and in vitro biological properties. Acta biomaterialia. 2010;6:3349-59.

60. Jeon H, Lee H, Kim G. A surface-modified poly (ε-caprolactone) scaffold comprising variable nanosized surface-roughness using a plasma treatment. Tissue Engineering Part C: Methods. 2014;20:951-63.

61. Li G, Wang L, Pan W, Yang F, Jiang W, Wu X, et al. In vitro and in vivo study of additive manufactured porous Ti6Al4V scaffolds for repairing bone defects. Scientific reports. 2016;6:34072.

62. Chen H, Han Q, Wang C, Liu Y, Chen B, Wang J. Porous Scaffold Design for Additive Manufacturing in Orthopedics: A Review. Frontiers in Bioengineering and Biotechnology. 2020;8:609.

63. Yang L. Experimental-assisted design development for an octahedral cellular structure using additive manufacturing. Rapid Prototyping Journal. 2015;21:168-76.

64. Reznikov N, Boughton OR, Ghouse S, Weston AE, Collinson L, Blunn GW, et al. Individual response variations in scaffold-guided bone regeneration are determined by independent strain- and injury-induced mechanisms. Biomaterials. 2019;194:183-94.

65. Li Y, Ding Y, Munir K, Lin J, Brandt M, Atrens A, et al. Novel β-Ti35Zr28Nb alloy scaffolds manufactured using selective laser melting for bone implant applications. Acta biomaterialia. 2019;87:273-84.

66. Li Y, Jahr H, Lietaert K, Pavanram P, Yilmaz A, Fockaert LI, et al. Additively manufactured biodegradable porous iron. Acta biomaterialia. 2018;77:380-93.

67. Li Y, Zhou J, Pavanram P, Leeflang M, Fockaert L, Pouran B, et al. Additively manufactured biodegradable porous magnesium. Acta biomaterialia. 2018;67:378-92.

68. Yu T, Gao H, Liu T, Huang YD, Wang C. Effects of immediately static loading on osteointegration and osteogenesis around 3D-printed porous implant: A histological and biomechanical study. Materials Science & Engineering C. 2020;108:110406.

69. Nune K, Misra R, Li S, Hao Y, Yang R. C ellular response of osteoblasts to low modulus Ti-24Nb-4Zr-8Sn alloy mesh structure. Journal of Biomedical Materials Research Part A. 2017;105:859-70.

70. Wang GJ, Shen LD, Zhao JF, Liang HX, Xie DQ, Tian ZJ, et al. Design and Compressive

Behavior of Controllable Irregular Porous Scaffolds: Based on Voronoi-Tessellation and for Additive Manufacturing. ACS Biomaterials Science & Engineering. 2018;4:719-27.

71. Du Y, Liang H, Xie D, Mao N, Zhao J, Tian Z, et al. Design and statistical analysis of irregular porous scaffolds for orthopedic reconstruction based on voronoi tessellation and fabricated via selective laser melting (SLM). Materials Chemistry and Physics. 2020;239:121968.

72. Ragone V, Canciani E, Arosio M, Olimpo M, Piras LA, von Degerfeld MM, et al. In vivo osseointegration of a randomized trabecular titanium structure obtained by an additive manufacturing technique. Journal of materials science Materials in medicine. 2020;31:17.

73. Liu T, Guessasma S, Zhu J, Zhang W. Designing Cellular Structures for Additive Manufacturing Using Voronoi-Monte Carlo Approach. Polymers. 2019;11:1158.

74. Chen H, Liu Y, Wang C, Zhang A, Chen B, Han Q, et al. Design and properties of biomimetic irregular scaffolds for bone tissue engineering. Computers in Biology and Medicine. 2021;130:104241.

75. Chen C, Hao Y, Bai X, Ni JJ, Chung SM, Liu F, et al. 3D printed porous Ti6Al4V cage: Effects of additive angle on surface properties and biocompatibility; bone ingrowth in Beagle tibia model. Materials & Design. 2019;175:107824.

76. Crovace AM, Lacitignola L, Forleo DM, Staffieri F, Francioso E, Di Meo A, et al. 3D biomimetic porous titanium (Ti6Al4V ELI) scaffolds for large bone critical defect reconstruction: An experimental study in sheep. Animals. 2020;10:1389.

77. Herzog D, Seyda V, Wycisk E, Emmelmann C. Additive manufacturing of metals. Acta Materialia. 2016;117:371-92.

78. Warnke PH, Douglas T, Wollny P, Sherry E, Steiner M, Galonska S, et al. Rapid prototyping: porous titanium alloy scaffolds produced by selective laser melting for bone tissue engineering. Tissue engineering part c: Methods. 2008;15:115-24.

79. Ide Y, Nayar S, Logan H, Gallagher B, Wolfaardt J. The effect of the angle of acuteness of additive manufactured models and the direction of printing on the dimensional fidelity: clinical implications. Odontology. 2017;105:108-15.

80. Nune K, Kumar A, Murr L, Misra R. Interplay between self-assembled structure of bone morphogenetic protein-2 (BMP-2) and osteoblast functions in three-dimensional titanium alloy scaffolds: Stimulation of osteogenic activity. Journal of biomedical materials research Part A. 2016;104:517-32.

81. Shah FA, Snis A, Matic A, Thomsen P, Palmquist A. 3D printed Ti6Al4V implant surface promotes bone maturation and retains a higher density of less aged osteocytes at the bone-implant

interface. Acta biomaterialia. 2016;30:357-67.

82. Gittens RA, McLachlan T, Olivares-Navarrete R, Cai Y, Berner S, Tannenbaum R, et al. The effects of combined micron-/submicron-scale surface roughness and nanoscale features on cell proliferation and differentiation. Biomaterials. 2011;32:3395-403.

83. Yavari SA, van der Stok J, Chai YC, Wauthle R, Birgani ZT, Habibovic P, et al. Bone regeneration performance of surface-treated porous titanium. Biomaterials. 2014;35:6172-81.

84. Goriainov V, Cook R, Latham JM, Dunlop DG, Oreffo RO. Bone and metal: an orthopaedic perspective on osseointegration of metals. Acta biomaterialia. 2014;10:4043-57.

85. Singh R, Dahotre NB. Corrosion degradation and prevention by surface modification of biometallic materials. Journal of Materials Science: Materials in Medicine. 2007;18:725-51.

86. Geetha M, Singh AK, Asokamani R, Gogia AK. Ti based biomaterials, the ultimate choice for orthopaedic implants-a review. Progress in materials science. 2009;54:397-425.

87. Chen Q, Thouas GA. Metallic implant biomaterials. Materials Science and Engineering: R: Reports. 2015;87:1-57.

88. Wang X, Xu S, Zhou S, Xu W, Leary M, Choong P, et al. Topological design and additive manufacturing of porous metals for bone scaffolds and orthopaedic implants: a review. Biomaterials. 2016;83:127-41.

89. Liu X, Chu PK, Ding C. Surface modification of titanium, titanium alloys, and related materials for biomedical applications. Materials Science and Engineering: R: Reports. 2004;47:49-121.

90. Ching HA, Choudhury D, Nine MJ, Osman NAA. Effects of surface coating on reducing friction and wear of orthopaedic implants. Science and technology of advanced materials. 2014;15:014402.

91. Roy RK, Lee KR. Biomedical applications of diamond-like carbon coatings: A review. Journal of Biomedical Materials Research Part B. 2007;83:72-84.

92. Cheang P, Khor K. Addressing processing problems associated with plasma spraying of hydroxyapatite coatings. Biomaterials. 1996;17:537-44.

93. Langhoff J, Voelter K, Scharnweber D, Schnabelrauch M, Schlottig F, Hefti T, et al. Comparison of chemically and pharmaceutically modified titanium and zirconia implant surfaces in dentistry: a study in sheep. International journal of oral and maxillofacial surgery. 2008;37:1125-32.

94. Koch F, Weng D, Krämer S, Biesterfeld S, Jahn-Eimermacher A, Wagner W. Osseointegration of one-piece zirconia implants compared with a titanium implant of identical design: a histomorphometric study in the dog. Clinical oral implants research. 2010;21:350-6.

95. LeGeros RZ. Properties of osteoconductive biomaterials: calcium phosphates. Clinical Orthopaedics and Related Research. 2002;395:81-98.

96. Habibovic P, Van der Valk C, Van Blitterswijk C, De Groot K, Meijer G. Influence of octacalcium phosphate coating on osteoinductive properties of biomaterials. Journal of Materials Science: Materials in Medicine. 2004;15:373-80.

97. Cox SC, Jamshidi P, Eisenstein NM, Webber MA, Hassanin H, Attallah MM, et al. Adding functionality with additive manufacturing: Fabrication of titanium-based antibiotic eluting implants. Materials Science and Engineering: C. 2016;64:407-15.

98. Nguyen H, Deporter D, Pilliar R, Valiquette N, Yakubovich R. The effect of sol-gel-formed calcium phosphate coatings on bone ingrowth and osteoconductivity of porous-surfaced Ti alloy implants. Biomaterials. 2004;25:865-76.

99. Denry I, Kuhn LT. Design and characterization of calcium phosphate ceramic scaffolds for bone tissue engineering. Dental Materials. 2016;32:43-53.

100. Zyman Z, Weng J, Liu X, Zhang X, Ma Z. Amorphous phase and morphological structure of hydroxyapatite plasma coatings. Biomaterials. 1993;14:225-8.

101. Barrere F, Layrolle P, Van Blitterswijk C, De Groot K. Biomimetic coatings on titanium: a crystal growth study of octacalcium phosphate. Journal of Materials Science: Materials in Medicine. 2001;12:529-34.

102. Boyne P, Jones SD. Demonstration of the osseoinductive effect of bone morphogenetic protein within endosseous dental implants. Implant dentistry. 2004;13:180-4.

103. Cheng H, Jiang W, Phillips FM, Haydon RC, Peng Y, Zhou L, et al. Osteogenic activity of the fourteen types of human bone morphogenetic proteins (BMPs). The Journal of bone and joint surgery. 2003;85:1544-52.

104. Jahr H, Zadpoor A, De Maat M, Koolen M, Van der Stok J, Amin Yavari S, et al. Full regeneration of segmental bone defects using porous titanium implants loaded with BMP-2 containing fibrin gels. European Cells & Materials. 2015;29:141-54.

105. Lv J, Xiu P, Tan J, Jia Z, Cai H, Liu Z. Enhanced angiogenesis and osteogenesis in critical bone defects by the controlled release of BMP-2 and VEGF: implantation of electron beam melting-fabricated porous Ti6Al4V scaffolds incorporating growth factor-doped fibrin glue. Biomedical Materials. 2015;10:035013.

106. Liu Y, De Groot K, Hunziker EB. BMP-2 liberated from biomimetic implant coatings induces and sustains direct ossification in an ectopic rat model. Bone. 2005;36:745-57.

107. Yu X, Wei M. Preparation and evaluation of parathyroid hormone incorporated CaP coating via a biomimetic method. Journal of Biomedical Materials Research Part B: Applied Biomaterials. 2011;97:345-54.

108.   Hunziker EB, Enggist L, Küffer A, Buser D, Liu Y. Osseointegration: the slow delivery of BMP-2 enhances osteoinductivity. Bone. 2012;51:98-106.

Part I

Morbidity in autologous bone grafting

Article 1

Donor- and recipient-site morbidity of vascularized fibular and iliac flaps for mandibular reconstruction: A systematic review and meta-analysis

Yifei Gu[1], Hongyang Ma[1], Sohaib Shujaat[1], Kaan Orhan[1,2], Wim Coucke[3], Mehdi Salar Amoli[1], Michel Bila[1], Constantinus Politis[1], Reinhilde Jacobs[1, 4]

[1]OMFS IMPATH research group, Department of Imaging & Pathology, Faculty of Medicine, KU Leuven and Department of Oral and Maxillofacial Surgery, University Hospitals Leuven, Leuven (3000), Belgium.

[2]Ankara University Faculty of Dentistry, Department of Dentomaxillofacial Radiology, Ankara (00680), Turkey.

[3]Freelance Statistician, Heverlee (3001), Belgium.

[4]Department of Dental Medicine, Karolinska Institutet, Stockholm, Sweden.

1.1   Abstract

The aim of this article is to evaluate the early and late morbidities of the donor- and recipient-site in patients undergoing mandibular reconstruction using either vascularized VFF or VIF. Electronic databases, including PubMed, Web of Science, Cochrane Central and Embase, were explored for literature published until October 2020. A total of twenty-four articles reporting complications following mandibular reconstruction surgery with follow-up periods ranging from six to 63 months were selected based on the exclusion criteria. For each research, the JBI Critical Assessment Tool and the ROBINS-I Tool were used to analyze the methodological quality and the risk of bias. A single-arm meta-analysis was performed to have a synthesized analysis of the donor- and recipient-site early and late morbidities. Results showed that the early morbidities in VFF group ranged from 3% to 12%, and the late morbidities in VFF group ranged from 5% to 67%. In VIF group, the early morbidities ranged from 3% to 16%, and the donor-site late morbidities ranged from 6% to 43%. Complications with the top three morbidities in the VFF group were: chronic sensory disturbances at the donor-site (67%), malocclusion (22%) and chronic lower limb weakness (20%); and in the VIF group were: chronic sensory disturbances at the donor-site (43%), chronic pain at the donor-site (26%), chronic gait disturbance (20%). Further controlled clinical trials are needed to assess the long-term outcome of VFF or VIF grafting.

Keywords: systematic review; mandibular reconstruction; morbidity; postoperative complications; Head and neck neoplasm

1.2   Introduction

Mandibular bone defect is often attributed to trauma, surgical removal of benign/malignant tumors and congenital abnormalities. The loss of jawbone continuity leads to aesthetic, functional and psychosocial effects which undermine the patients' quality of life. At present, vascularized autologous bone grafting is considered as a gold standard for mandibular reconstruction following tumor resection. The two most utilized autologous grafts for mandibular reconstruction include vascularized fibula flap (VFF) and vascularized iliac flap (VIF). Both flaps have certain benefits and limitations. For instance, VFF provides sufficient bone with adequate pedicle length, however it has less height compared to the native mandibular area and bone straightening require osteotomies for achieving mandibular curvature which can compromise the perfusion of the flap [1]. On the other hand, VIF is naturally curved to the hemi-mandibular region with abundant bone height and length offering adequate osseointegration and higher survival rate of implants [2]. However, VIF is difficult to harvest with a higher donor-site morbidity compared to VFF.

Several intra-operative, immediate and delayed donor- and recipient-site complications have been reported following mandibular reconstruction with either VFF or VIF. These complications might vary depending on the reconstructive technique or the patient cohort resulting in reduced quality of life. Most of the previous systematic reviews have either focused on short and long-term aesthetic/ functional outcomes, quality of life or only donor-site morbidities. We believe a gap exists in literature related to the comprehensive review of both donor- and recipient-site complications associated with VFF and VIF. Research into the intra- and post-operative complications related to these flaps could help surgeons estimate the imminent risks, prevent occurrence of complications if possible and further facilitate their management. Within this context, a review of complication rate based on the accumulated evidence might enable surgeons to predict in advance the likelihood of patients developing post-operative morbidities. Therefore, the current systematic review and meta-analysis was conducted to report the post-surgical donor- and recipient-site morbidities following mandibular reconstruction with VFF and VIF.

1.3   Materials and Methods

The protocol was registered at PROSPERO (CRD42018117322). PRISMA guidelines were used to guarantee the clarity and comprehensiveness of this systematic review. Two researchers (GYF, MHY) individually conducted a search of electronic databases in PubMed, Embase, Cochrane, and Web of Science for relevant studies published before October 2020. A search strategy containing a broad range of strings was performed using the following keywords: ("fibula" OR "Ilium") AND

("Mandibular reconstruction"). The detailed search strings can be found in Appendix 1. Reference lists and citation indices of the studies chosen in the selection phase were manually checked for additional related publications. Identified items were imported into Endnote online software (Thompson Reuters, Philadelphia, PA, USA) to remove duplicates.

The full texts of the relevant articles were obtained against the following inclusion criteria: 1) studies reporting on mandibular reconstruction in humans with VFF or VIF; 2) studies with follow-up time of at least six months; 3) studies with more than ten patients; 4) articles in English. Non-English articles, cadaver or animal studies, reviews, case reports and letters to the editors were excluded. To reduce the confounding impact related to variant underlying pathophysiology and remaining bone stock quality, patients requiring grafting following trauma were also excluded. Two researchers (GYF, MHY) examined the article titles, abstracts and full-text documents based on the eligibility criteria, and the decision for inclusion was made based on consensus. Joanna Briggs Institute Critical Appraisal of Systematic Reviews tool [3] was used to determine the methodological quality of articles and to decide on the inclusion of the article. Each study was required to meet five or more items from the checklist to be included. The risk of bias was assessed by the ROBINS-I risk of bias tool. A judgment was expressed in terms of 'no information,' 'low risk,' 'moderate risk,' 'serious risk' or 'critical risk' for different domains of bias. Two observers (GYF and MHY) independently completed the quality and risk of bias assessment. Any disagreements during the screening process were resolved by a third researcher (RJ).

The key characteristics of the included articles were extracted independently by two authors (GYF and MHY) following the "PICOS principle" [4].

Population: sample size (during surgery and during follow-up), mean age and age range, smoking habit, comorbidity.

Intervention/exposure: flap type (VIF or VFF), flap number, mean flap size, mean defect size, primary/secondary reconstruction, follow-up time, radiation, restoration processes.

Comparison: not applicable.

Outcome: morbidity, which was defined as "the incidence of a certain group of complications following autologous bone grafting surgeries."

Studies: all controlled clinical trials, observational clinical studies (either prospective or retrospective), and case series with ten or more patients were included.

A single-arm meta-analysis and the heterogeneity test were conducted with meta-library from R, version 3.5.1 to combine across studies the number of the donor- and recipient-site complications and to calculate the proportion of each complication with a 95% confidence interval. The

heterogeneity was calculated using I^2 statistics, and we considered a heterogeneity of more than 50% as an indicator of substantial heterogeneity. A p-value of <0.05 was considered as statistically significant.

1.4   Results

1.4.1 Study selection

Figure 1.1 describes the process of study selection based on PRISMA guidelines. The search through PubMed, Embase, Cochrane, and Web of Science databases provided a total of 7114 studies and following removal of the duplicates 2652 studies were yielded. 1923 papers were excluded after the screening of the titles and abstracts. The full text of the remaining 729 articles was examined, and 705 studies were further excluded. Eventually, 24 studies were included in the quantitative synthesis and 23 in the qualitative synthesis. In total, 13 case series, ten non-randomized retrospective cohort studies, and one prospective study were included. The characteristics of the selected studies are outlined in **Table 1.1**.
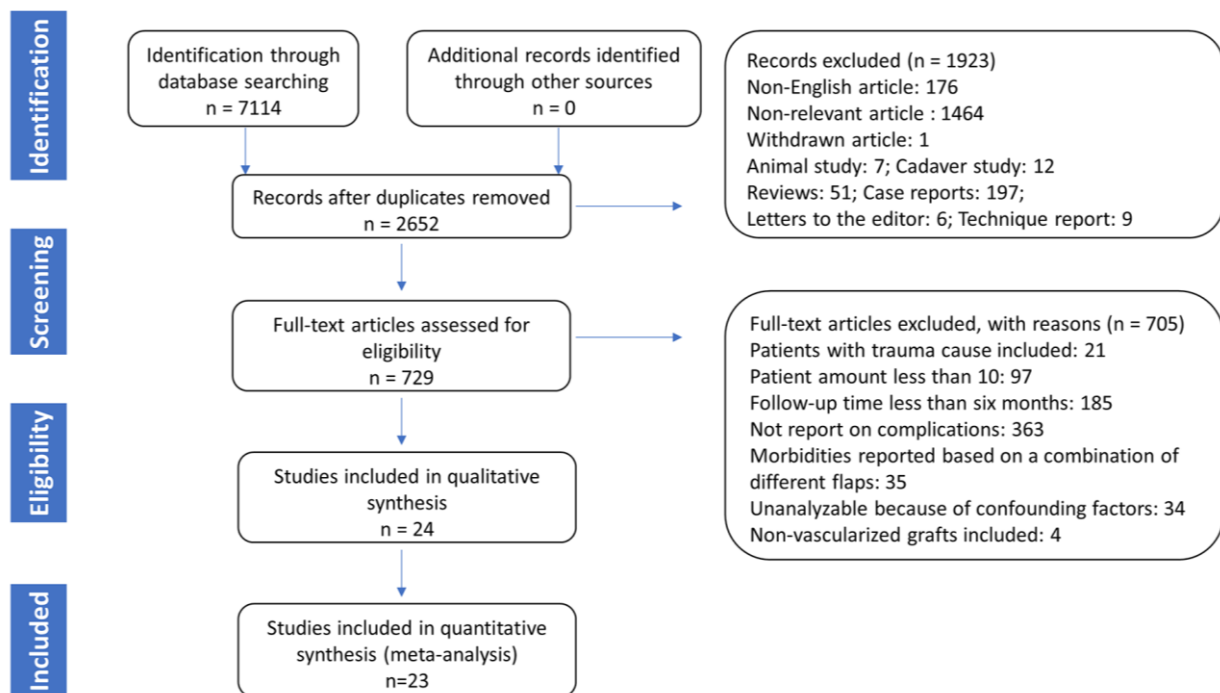

Figure 1.1. the process of study selection in the systematic review.

1.4.2 Risk of bias

All selected studies were evaluated to have an acceptable methodological quality, and the risk of bias of the comparative studies was assessed using the ROBINS-I tool (**Table 1.2**). Nine out of eleven comparative studies were determined to have a moderate risk of bias, one had a serious risk, and one was assessed to have a low risk of bias. One study [20] (Rogers, et al., 2003) showed a serious risk of bias and was excluded from the meta-analysis.

1.4.3 Participant characteristics

The selected articles included a total of 872 patients (599 males and 273 females), who underwent mandibular reconstruction with either VFF (n=737) or VIF (n=140). The mean age of all patients was 51.4 years old (range: 5-96 years). The indications for reconstruction included malignant tumor resection (75%, n= 654), benign tumor resection (15%, n=126), osteoradionecrosis, osteonecrosis or osteomyelitis (5%, n=45), mandibular atrophy and vasculopathy (1%, n=9), and unknown reasons (4%, n=38). In VFF group the follow-up time ranged from six to 63 months, and in VIF group ranged from six to 29 months.

1.4.4 Surgical characteristics

The mandibular defect in seven studies was classified based on HCL system suggested by Jewer et al., one articles utilized Urken classification, whereas 16 studies failed to classify the defect. Seven articles [5-7, 9, 15, 17, 26] measured the mean length of the defect to be reconstructed. The mean defect length in VFF group ranged from 5.2 to 11.2cm, while that of the VIF group was 6 to 8.5 cm. Eight studies [8, 12, 13, 16, 18, 19, 25, 27] measured the mean length of the graft utilized for the reconstruction ,where the mean length of VFF ranged from 7.1 to 18.3cm and VIF ranged from 6.3 to 7.6cm. In VFF group, seven studies [6, 12, 21, 24-27] described donor- and recipient-site wound closure. 54.8% (74/135) of the donor-site wound and 45.7% (32/70) of the recipient-site wound were closed with skin grafts. Fourteen articles [1, 8, 10, 14-18, 21, 23-27] described the type of the reconstructive surgery. In VFF group 89.9% patients (461/513) underwent primary surgery, and in VIF group 71.9% patients (41/57) underwent primary surgery. The final restoration process was mentioned in ten articles [1, 6, 7, 11, 15-17, 22-24]. Oral rehabilitation was carried out with wither dental implant or conventional partial/complete denture.

1.4.5 Complications

All the complications were evaluated either subjectively or objectively by the patient or surgeon. In the subjective evaluation, patients were interviewed and evaluated with a point evaluation system or through self-administered questionnaires. Based on happening frequency, complications graded as "never" or "rarely" happened and evaluations graded by severity and graded as "not at all" or "acceptable" were excluded. The complications from each study were extracted and categorized into four groups separately for patient who underwent VFF and VIF reconstruction: early/late donor-site complications and early/late recipient-site complications. Early complications were defined as complications that occurred during the immediate postoperative period and required intervention. Late complications included those reported by patients or examined by surgeons during the follow-up. It should be noted that only complications that have been mentioned in two or more studies were involved in the following review and meta-analysis. A single-arm meta-analysis was performed, and forest plots (Appendix 2) were generated for assessing the rate of each complication in VFF and VIF group.

The synthesized morbidities in VFF and VIF groups are shown in **Table 1.3**. The early donor-site morbidities in VFF group ranged between 3% to12%, and in VIF group 3% to 8%. The late donor-site morbidities in the VFF group ranged between 5% to 67%, and in the VIF group 6% to 43%. The early recipient-site morbidities in the VFF group were between 4% to 10%, and in the VIF group 16% (only delayed wound healing was reported). The late recipient-site morbidities in the VFF group were between 8% to 22%, whereas no late recipient-site morbidities were observed in the included studies in the VIF group. Donor-site chronic sensory disturbance had the highest morbidity in both VFF and VIF groups. The top three morbidities in the VFF group were donor-site chronic sensory disturbance (67%), malocclusion (22%) and chronic lower limb weakness (20%); in VIF group were donor-site chronic sensory disturbance (43%), donor-site chronic pain (26%) and gait disturbance (20%). Substantial heterogeneity was detected with four complications and were all from the VFF group: limited walking or stair climbing ability (I^2=75%, p=0.05), limited toe mobility (I^2=52%, p=0.08), recipient-site cosmesis problem (I^2=73%, p<0.01), reconstruction plate exposure or fracture (I^2=57%, p=0.03). Rest of the data was found to be homogenous.

Table 1.1. Articles included in final review.

Author, Year (Reference)	Study design	Sample size during surgery(N)	Sample size during follow-up(N)	Mean age and range (Year)	Smoking habit (N)	Comorbidity(N)	Flap (N)	Mean defect size (cm)	Mean flap size (cm)	Pri/Sec reconstruction (N)	Radiation (N)	Restoration method (N)	Follow-up (month)
Al-Bustani et al., 2016 [5]	Retro	25	25	47.3 (18-74)	7	M(25)	VFF(25)	7.4	N/A	N/A	6	N/A	27
Chiapasco et al., 2006 [1]	Cs	46	46	48.7 (13-69)	N/A	M(34),B(5), O(7)	VFF(46)	N/A	N/A	Pri(33) Sec(13)	N/A	Implant (11)	55
Crosby et al., 2008 [6]	Cs	11	11	10 (5-14)	N/A	M(5),B(6)	VFF(11)	9.0	N/A	N/A	Pre (2) Post (1)	Implant(1)	40.8
Dean et al., 2012 [7]	Retro	51	51	66.5 (31-96)	N/A	M(49),B(2)	VFF(51)	5.2	N/A	N/A	Pre (15) Post (24)	Denture(4)	20.2
Gazyakan et al., 2016 [8]	Retro	121	121	51.4 (20-85)	82	M(121)	VFF(121)	N/A	8.9	Pri(121)	121	N/A	29
Ghassemi et al., 2013 [9]	Retro	54	52	49 (12-81)	N/A	M(37),B(7), O(9), A(1)	VIF(54)	>6	N/A	N/A	N/A	N/A	12
Hoezle et al., 2007 [10]	Cs	54	54	54 (17-78)	30	M(38),O(8), A(4), V(4)	VFF(54)	N/A	N/A	Pri(29) Sec(25)	Pre (4) Post (7) Both (3)	N/A	63
Katsuragi et al., 2010 [11]	Cs	12	12	56.3 (14-80)	N/A	M(11),B(1)	VFF(12)	N/A	N/A	N/A	Post (2)	Implant(1) Denture(7)	16
Kuo et al., 2010 [12]	Cs	20	20	48.7 (30-74)	N/A	M(20)	VFF(20)	N/A	7.3	N/A	N/A	N/A	12
Ling et al., 2013 [13]	Retro	19	19	53.1	N/A	N/A	VFF(19)	N/A	8.6	N/A	N/A	N/A	6
		15	15	37.6	N/A	N/A	VIF(15)	N/A	7.6	N/A	N/A	N/A	6
Lyons et al., 2005 [14]	Cs	18	18	49.9 (12-72)	N/A	M(13),B(2), O(2),U(1)	VIF(18)	N/A	N/A	Pri(18)	N/A	N/A	6
Ooi et al., 2014 [15]	Cs	30	26	27.3 (12-59)	N/A	B(30)	VFF(32)	8.2	N/A	Pri(32)	N/A	Implant(3) Denture(15)	59
Parbo et al., 2013 [16]	Cs	36	36	54 (9-77)	N/A	M(28),B(3), O(2),U(3)	VFF(36)	N/A	7.1	Pri(36)	Pre (10)	Implant(16)	22
Politi et al., 2012 [17]	Retro	12	12	N/A	N/A	M(19),B(5)	VFF(12)	9.5	N/A	Pri(12)	N/A	Implant(12)	12
Politi et al., 2012 [17]	Retro	12	12	N/A	N/A	M(19),B(5)	VIF(12)	8.5	N/A	Pri(12)	N/A	Implant(11)	12
Rashid et al., 2012 [18]	Cs	18	18	12 (8-16)	N/A	B(18)	VFF(18)	N/A	12	Pri(18)	N/A	N/A	48

Rendenbach et al., 2018 [19]	Retro	14	14	54	N/A	M(8),B(5),O(1)	VIF(14)	N/A	6.3	N/A	2	N/A	29
Rogers et al., 2003 [20]	Retro	16	16	61 (45-74)	N/A	M(16)	VFF(16)	N/A	N/A	N/A	12	N/A	27
Schardt et al., 2017 [21]	Retro	19	19	N/A	N/A	M(28),B(9),O(9)	VFF(19)	N/A	N/A	Pri(14) Sec(5)	N/A	N/A	14
Schardt et al., 2017 [21]	Retro	27	27	N/A	N/A	M(28),B(9),O(9)	VIF(27)	N/A	N/A	Pri(11) Sec(16)	N/A	N/A	14
Sieg et al., 1999 [22]	Cs	53	53	51 (15-81)	N/A	M(48),B(5)	VFF(53)	N/A	N/A	N/A	Pre (15) Post (23)	Implant(8)	21.5
Van Gemert et al., 2018 [23]	Cs	76	76	61.3 (26-81)	50	M(76)	VFF(79)	N/A	N/A	Pri(79)	Post (67)	Implant(7/76)	27
Wolff et al., 1996 [24]	Cs	24	24	64 (37-77)	N/A	M(23),O(1)	VFF(24)	N/A	N/A	Pri(22) Sec(2)	N/A	Implant(8/24)	29
Xu et al., 2017 [25]	Pros	30	30	45.7 (20-66)	N/A	M(10),B(20)	VFF(30)	N/A	18.3	Pri(30)	N/A	N/A	>12
Zavalishina et al., 2014 [26]	Cs	17	11	52.3 (15-77)	4	M(13),B(2),O(2)	VFF(17)	11.2	N/A	Pri(17)	5	N/A	>12
Zimmermann et al., 2001 [27]	Retro	42	38	48(15.5-70.1)	N/A	M(32),B(6),O(4)	VFF(42)	N/A	9.7	Pri(35) Sec(7)	N/A	N/A	35

Indications: N/A= not applicable; Retro= retrospective cohort study; Pros= prospective study; Cs= case series; M= malignant tumor; B= Benign tumor; O= osteoradionecrosis, osteonecrosis or osteomyelitis; A= atrophy; V= vasculopathy; U= Unidentifiable; Pri= primary reconstruction; Sec=secondary reconstruction; Pre=pre-surgical; Post= post-surgical.

Table 1.2. Risk of bias analysis based on the ROBINS-I tool

Author, Year	Domains(D)							Overall
	D1	D2	D3	D4	D5	D6	D7	
Al-Bustani et al., 2016 [5]	2	3	1	1	1	2	1	Moderate
Dean et al., 2012 [7]	1	2	2	1	1	2	1	Moderate
Gazyakan et al., 2016 [8]	2	3	1	1	1	2	1	Moderate
Ghassemi et al., 2013 [9]	2	2	1	1	1	2	1	Moderate
Ling et al., 2013 [13]	2	3	1	1	1	1	1	Moderate
Politi et al., 2012 [17]	2	2	1	1	1	2	1	Moderate
Rendenbach et al., 2018 [19]	2	2	1	1	1	2	1	Moderate
Rogers et al., 2003 [20]	2	3	3	1	1	2	1	Serious
Schardt et al., 2017 [21]	2	1	1	1	2	1	1	Moderate
Xu et al., 2017 [25]	1	1	1	1	1	1	1	Low
Zimmermann et al., 2001 [27]	2	2	1	1	1	1	1	Moderate

Indications: Domain 1: confounding; Domain 2: selection of participants; Domain 3: classification of intervention; Domain 4: deviation from interventions; Domain 5: missing outcome data; Domain 6: measurement of outcomes; Domain 7: selection of reported result; Overall. Risk of bias assessment: 0—No information; 1—Low; 2—Moderate; 3—Serious; 4—Critical.

Table 1.3. Synthesized morbidities in VFF and VIF group

VFF group	Complications	Number of studies	Synthesized morbidity (95% CI)	Heterogenity (p-value)
Early donor-site	Wound infection	4	6% (3%, 11%)	0% (p=0.27)
	Wound dehiscence	2	12% (6%, 22%)	2% (p=0.17)
	Skin graft loss	4	9% (5%, 16%)	0% (p=0.47)
	Compartment syndrome	2	3% (1%, 10%)	0% (p=0.81)
Late donor-site	Pain	7	18% (13%, 24%)	49% (p=0.06)
	Sensory disturbance	5	67% (59%, 75%)	0% (p=0.33)
	Lower limb weakness	3	20% (13%, 29%)	0% (p=0.47)
	Gait disturbance	3	14% (8%, 24%)	0% (p=0.63)
	Limited walking or stair climbing ability	5	17% (12%, 23%)	75% (p=0.05)
	Limited toe mobility	9	16% (11%, 22%)	52% (p=0.08)
	Cosmesis problem	6	5% (2%,9%)	0% (p=0.64)
Early recipient-site	Wound infection	11	8% (6%, 12%)	42% (p=0.09)
	Wound dehiscence	7	8% (6%, 12%)	0% (p=0.84)
	Hematoma	5	6% (3%, 11%)	0% (p=0.38)
	Compromised circulation	7	10% (7%, 13%)	12% (p=0.52)
	Fistula	4	6% (3%, 10%)	45% (p=0.10)
	Partial flap necrosis	9	8% (6%, 11%)	21% (p=0.34)
	Flap loss	17	4% (3%, 6%)	0% (p=0.94)
Late recipient-site	Pain	2	17% (10%, 28%)	0% (p=0.09)
	Cosmesis problem	2	14% (2%, 52%)	73% (p<0.01)
	Contour deformity	2	18% (12%, 26%)	0% (p=0.42)
	Malocclusion	2	22% (9%, 43%)	0% (p=0.54)
	Plate exposure or fracture	6	8% (4%, 15%)	57% (p=0.03)
VIF group	**Complications (N)**	**Number of studies**	**Morbidity**	**Heterogenity**
Early donor-site	Wound infection	3	4% (2%, 10%)	0% (p=0.53)
	Wound dehiscence	2	8% (4%, 17%)	0% (p=0.62)
	Hernia	6	3% (1%, 7%)	11% (p=1.00)
Late donor-site	Pain	3	26% (18%, 36%)	43% (p=0.09)
	Sensory disturbance	4	43% (32%, 55%)	25% (p=0.19)
	Gait disturbance	3	20% (12%, 32%)	0% (p=0.52)
	Limited walking or stair climbing ability	2	6% (3%, 14%)	0% (p=0.23)
Early recipient-site	Delayed wound healing	2	16% (7%, 32%)	31% (p=0.11)

1.5   Discussion

This systematic review aimed to provide comprehensive evidence related to the donor- and recipient-site complications in patients who underwent mandibular reconstruction with VFF and VIF. Donor-site wound dehiscence and infection were higher in the VFF group, which was mostly related to the skin graft loss. The loss of skin graft increases the risk of delayed wound healing and wound dehiscence, which may result in wound contamination and infection [28, 29]. Several techniques, including negative pressure wound therapy over skin grafts and the harvest of a fat-fascia-only flap, have been proposed to reduce the wound healing problems following skin grafting [30, 31]. Nevertheless, controversy exists related to the wound dehiscence rate between primary closure and skin graft, where some studies show a lower complication rate with primary closure [28, 32] while others recommend skin graft [33, 34]. Skin graft should only be applied in cases where primary closure is not possible with modest tension as high tension might lead to tissue ischemia or compartment syndrome [35]. Although the incidence of compartment syndrome was relatively low compared to other morbidities, it cannot be ignored. Surgeons should pay attention to whether the patient has shown unexplained pain or decreased nerve sensitivity to prevent the occurrence of compartment syndrome [36]. Similarly, herniation was observed in only 3% of the cases with VIF, nevertheless, a careful closure of adjacent muscle tissue can further reduce the incidence of this complication [37].

Neurosensory disturbance showed the highest morbidity in both VFF and VIF group. This could have resulted due to peroneal nerve damage during the dissection and harvesting of VFF proximally at the fibular neck level where the nerve is most prone to injury. In the VIF group, the sensory disturbance could be mainly related to the damage of the lateral femoral cutaneous nerve or the superior cluneal nerve [38]. Our findings were consistent with a previous study which also suggested a higher morbidity of sensory disturbance in VFF group compared with VIF group, since the superficial peroneal nerve was more prone to damage because of the surgical exposure [20]. Furthermore, the high disturbance rate related to both flaps could be attributed to the surgical technique, volume of graft harvested or method of evaluation. Chronic donor-site pain was also a commonly seen complication in both VIF and VFF group, and it is one of the reasons driving a sustained search for an alternative to autograft [39]. The reason for chronic donor-site pain remained unclear, it is suggested that the chronic donor-site pain may be caused by the adhesion of detached muscles to the adhesive tissue, or it might occur secondarily to sensory nerve injury [40]. Psychosomatic disorder also attributes to this problem and therefore may not be entirely controlled [41]. Technical modifications as well as the use of post-operative regional anesthesia have been suggested to overcome this problem [42].

Gait disturbance and limited walking or stair climbing ability were interrelated and were seen in both VFF and VIF groups, with higher morbidities found in VIF group. It was suggested that VIF harvest usually leads to worse mobility after surgery due to the excessive stripping of the hip abductors during exposure as well as the loss of anterior superior iliac spine [13, 19, 43]. In VFF group, the patients' gait would not be adversely affected unless the muscle groups such as soleus

muscle and gastrocnemius muscle fail to function [44]. A previous study showed a higher incidence of late donor-site complications with VIF than VFF [45], which was consistent with our findings. The highest recipient-site early morbidity in VFF group was compromised circulation, which included arterial / venous thrombosis and dysfunction due to damage to the blood vessels. The high prethrombotic activity in the irradiated blood vessel is an important cause of thrombosis. In the VFF group, three articles reported on the radiotherapy rate of patients (193/213) [8, 23, 26], which could adversely affect the circulation. Two articles in the VIF group that reported delayed wound healing at the recipient-site did not give a specific reason. Delayed wound healing might have happened due to inflammation, dehiscence, hematoma, and other single or mixed factors. Postoperative malocclusion is rarely reported in the literature and is easily neglected, but it had a morbidity of 22% in the VFF group. The most likely reason could be inadequate contouring or improper positioning of the temporomandibular joint following osteotomy could result in malocclusion [46]. We believe that virtual 3D planning of the osteotomy, utilization of 3D-printed surgical guides and adopting aggressive postoperative physiotherapies can further help minimize both donor- and recipient-site complication rate.

The study had certain limitations. Firstly, the recipient-site late complications could only be collected in the VFF group due to the lack of reported data. Secondly, most of the studies were retrospective in nature. Thirdly, medium-high heterogeneity was observed for some complications (limited walking or stair climbing ability, limited toe mobility, recipient-site cosmesis problem and reconstruction plate exposure or fracture) which would have influenced the statistical pooling and misled interpretation.

1.6   Conclusion

Amongst all the complication, delayed neurosensory disturbance at the donor-site was the most frequently reported in both VFF and VIF groups. Furthermore, this review provided accumulated evidence for surgeons to estimate the likelihood of the occurrence of post-surgical complications which can further guide to improve the informed consent and decision-making process.

1.7   References

1.   Chiapasco M, Biglioli F, Autelitano L, Romeo E, Brusati R. Clinical outcome of dental implants placed in fibula-free flaps used for the reconstruction of maxillo-mandibular defects following ablation for tumors or osteoradionecrosis. Clinical oral implants research. 2006;17:220-8.

2.   Flint PW, Haughey BH, Niparko JK, Richardson MA, Lund VJ, Robbins KT, et al. Cummings Otolaryngology-Head and Neck Surgery E-Book: Head and Neck Surgery, 3-Volume Set. Elsevier Health Sciences; 2010.

3.   Aromataris E, Fernandez R, Godfrey CM, Holly C, Khalil H, Tungpunkom P. Summarizing systematic reviews: methodological development, conduct and reporting of an umbrella review approach. International journal of evidence-based healthcare. 2015;13:132-40.

4.   Davies KS. Formulating the evidence based practice question: a review of the frameworks. Evidence Based Library and Information Practice. 2011;6:75-80.

5.   Al-Bustani S, Austin GK, Ambrose EC, Miller J, Hackman TG, Halvorson EG. Miniplates Versus Reconstruction Bars for Oncologic Free Fibula Flap Mandible Reconstruction. Annals of plastic surgery. 2016;77:314-7.

6.   Crosby MA, Martin JW, Robb GL, Chang DW. Pediatric mandibular reconstruction using a vascularized fibula flap. Head & neck. 2008;30:311-9.

7.   Dean NR, Wax MK, Virgin FW, Magnuson JS, Carroll WR, Rosenthal EL. Free flap reconstruction of lateral mandibular defects: Indications and outcomes. Otolaryngology - Head and Neck Surgery (United States). 2012;146:547-52.

8.   Gazyakan E, Wu CW, Huang JJ, Engel H, Valerio IL, Cheng MH. Minimizing osteoradionecrosis after mandibular reconstruction and radiation in advanced head and neck cancer patients. Journal of surgical oncology. 2016;114:399-404.

9.   Ghassemi A, Ghassemi M, Modabber A, Knobe M, Fritz U, Riediger D, et al. Functional long-term results after the harvest of vascularised iliac bone grafts bicortically with the anterior superior iliac spine included. The British journal of oral & maxillofacial surgery. 2013;51:47-50.

10. Hoezle F, Kesting MR, Hoezle G, Watola A, Loeffelbein DJ, Ervens J, et al. Clinical outcome and patient satisfaction after mandibular reconstruction with free fibula flaps. International Journal of Oral and Maxillofacial Surgery. 2007;36:802-6.

11. Katsuragi Y, Kayano S, Akazawa S, Nagamatsu S, Koizumi T, Matsui T, et al. Mandible reconstruction using the calcium-sulphate three-dimensional model and rubber stick: A new method, 'mould technique', for more accurate, efficient and simplified fabrication. Journal of Plastic, Reconstructive and Aesthetic Surgery. 2011;64:614-22.

12. Kuo YR, Shih HS, Chen CC, Boca R, Hsu YC, Su CY, et al. Free fibula osteocutaneous flap with soleus muscle as a chimeric flap for reconstructing mandibular segmental defect after oral cancer ablation. Annals of plastic surgery. 2010;64:738-42.

13. Ling XF, Peng X, Samman N. Donor-Site Morbidity of Free Fibula and DCIA Flaps. Journal of Oral and Maxillofacial Surgery. 2013;71:1604-12.

14. Lyons AJ, James R, Collyer J. Free vascularised iliac crest graft: An audit of 26 consecutive

cases. British Journal of Oral and Maxillofacial Surgery. 2005;43:210-4.

15. Ooi A, Feng JJ, Tan HK, Ong YS. Primary treatment of mandibular ameloblastoma with segmental resection and free fibula reconstruction: Achieving satisfactory outcomes with low implant-prosthetic rehabilitation uptake. Journal of Plastic Reconstructive and Aesthetic Surgery. 2014;67:498-505.

16. Parbo N, Murra NT, Andersen K, Buhl J, Kiil B, Nørholt SE. Outcome of partial mandibular reconstruction with fibula grafts and implant-supported prostheses. International Journal of Oral and Maxillofacial Surgery. 2013;42:1403-8.

17. Politi M, Toro C. Iliac flap versus fibula flap in mandibular reconstruction. Journal of craniofacial surgery. 2012;23:774-779.

18. Rashid M, Tamimy MS, Ehtesham Ul H, Sarwar SU, Rizvi ST. Benign paediatric mandibular tumours: experience in reconstruction using vascularised fibula. Journal of plastic, reconstructive & aesthetic surgery. 2012;65:325-31.

19. Rendenbach C, Goehler F, Hansen L, Kohlmeier C, Amling M, Hanken H, et al. Evaluation of long-term functional donor-site morbidity after deep circumflex iliac crest artery bone flap harvest. Microsurgery. 2018;39:304-9.

20. Rogers SN, Lakshmiah SR, Narayan B, Lowe D, Brownson P, Brown JS, et al. A comparison of the long-term morbidity following deep circumflex iliac and fibula free flaps for reconstruction following head and neck cancer. Plastic and reconstructive surgery. 2003;112:1517-25.

21. Schardt C, Schmid A, Bodem J, Krisam J, Hoffmann J, Mertens C. Donor site morbidity and quality of life after microvascular head and neck reconstruction with free fibula and deep-circumflex iliac artery flaps. Journal of cranio-maxillo-facial surgery. 2017;45:304-11.

22. Sieg P, Hasse A, Zimmermann CE. Versatility of vascularized fibula and soft tissue graft in the reconstruction of the mandibulofacial region. International journal of oral and maxillofacial surgery. 1999;28:356-61.

23. van Gemert JTM, Abbink JH, van Es RJJ, Rosenberg A, Koole R, Van Cann EM. Early and late complications in the reconstructed mandible with free fibula flaps. Journal of surgical oncology. 2018;117:773-80.

24. Wolff KD, Ervens J, Herzog K, Hoffmeister B. Experience with the osteocutaneous fibula flap: an analysis of 24 consecutive reconstructions of composite mandibular defects. Journal of cranio-maxillo-facial surgery. 1996;24:330-8.

25. Xu ZF, Bai S, Zhang ZQ, Duan WY, Wang ZQ, Sun CF. A critical assessment of the fibula flap donor site. Head & neck. 2017;39:279-87.

26. Zavalishina L, Karra N, Zaid WS, El-Hakim M. Quality of life assessment in patients after mandibular resection and free fibula flap reconstruction. Journal of oral and maxillofacial surgery. 2014;72:1616-26.

27. Zimmermann CE, Börner BI, Hasse A, Sieg P. Donor site morbidity after microvascular fibula transfer. Clinical oral investigations. 2001;5:214-9.

28. Ling XF, Peng X. What is the price to pay for a free fibula flap? A systematic review of donor-

site morbidity following free fibula flap surgery. Plastic and reconstructive surgery. 2012;129:657-74.

29. Akinbami BO, Akadiri OA. Reconstruction of the mandible following benign tumor ablations: An audit of 20 cases. Journal of Oral and Maxillofacial Surgery Medicine and Pathology. 2015;27:650-5.

30. Bach CA, Guilleré L, Yildiz S, Wagner I, Darmon S, Chabolle F. Comparison of negative pressure wound therapy and conventional dressing methods for fibula free flap donor site management in patients with head and neck cancer. Head & neck. 2016;38:696-9.

31. Mohindra A, Parmar S, Praveen P, Martin T. The fat-fascia paddle only with a composite fibula flap: marked reduction in donor site morbidity. International journal of oral and maxillofacial surgery. 2016;45:964-8.

32. Shpitzer T, Neligan P, Boyd B, Gullane P, Gur E, Freeman J. Leg morbidity and function following fibular free flap harvest. Annals of Plastic Surgery. 1997;38:460-4.

33. Shindo M, Fong BP, Funk GF, Karnell LH. The fibula osteocutaneous flap in head and neck reconstruction: a critical evaluation of donor site morbidity. Archives of Otolaryngology-Head & Neck Surgery. 2000;126:1467-72.

34. Vittayakittipong P. Donor-site morbidity after fibula free flap transfer: a comparison of subjective evaluation using a visual analogue scale and point evaluation system. International Journal of Oral and Maxillofacial Surgery. 2013;42:956-61.

35. Matsen F, Winquist RA, Krugmire R. Diagnosis and management of compartmental syndromes. The Journal of Bone and Joint Surgery. 1980;62:286-91.

36. Klein S, Hage JJ, Woerdeman LA. Donor-site necrosis following fibula free-flap transplantation: A report of three cases. Microsurgery. 2005;25:538-42.

37. Cowley S, Anderson L. Hernias through donor sites for iliac-bone grafts. Journal of Bone and Joint Surgery. 1983;65:1023-5.

38. Loeffler BJ, Kellam JF, Sims SH, Bosse MJ. Prospective observational study of donor-site morbidity following anterior iliac crest bone-grafting in orthopaedic trauma reconstruction patients. Journal of Bone and Joint Surgery. 2012;94:1649-54.

39. Schwartz CE, Martha JF, Kowalski P, Wang DA, Bode R, Li L, et al. Prospective evaluation of chronic pain associated with posterior autologous iliac crest bone graft harvest and its effect on postoperative outcome. Health and quality of life outcomes. 2009;7:1-8.

40. Joshi A, Kostakis G. An investigation of post-operative morbidity following iliac crest graft harvesting. British dental journal. 2004;196:167-71.

41. Kalk WW, Raghoebar GM, Jansma J, Boering G. Morbidity from iliac crest bone harvesting. Journal of Oral and Maxillofacial Surgery. 1996;54:1424-9.

42. Adenike OA, Olukunle AT, Olusegun IA, Ifeolu AV, Tunde AJ. Perioperative findings and complications of non-vascularised iliac crest graft harvest: The experience of a Nigerian tertiary hospital. Nigerian Medical Journal. 2014;55:224-9.

43. Ebraheim NA, Elgafy H, Xu R. Bone-graft harvesting from iliac and fibular donor sites: techniques and complications. Journal of the American Academy of Orthopaedic Surgeons.

2001;9:210-8.

44. Lin JY, Djohan R, Dobryansky M, Chou SW, Hou WH, Chen MH, et al. Assessment of donor-site morbidity using balance and gait tests after bilateral fibula osteoseptocutaneous free flap transfer. Annals of plastic surgery. 2009;62:246-51.

45. Winters HA, van Loenen DK. A comparison between fibula and iliac crest in mandibular reconstruction. European Journal of Plastic Surgery. 2007;29:205-8.

46. Chang YM, Chana JS, Wei FC, Tsai CY, Chen SH. Osteotomy to treat malocclusion following reconstruction of the mandible with the free fibula flap. Plastic and reconstructive surgery. 2003;112:31-6.

Part II

3D-printed BTE scaffolds in animal studies

3D-printed porous Ti64 scaffolds for long bone repair in animal models: a systematic review

Yifei Gu[1], Yi Sun[1], Sohaib Shujaat[1], Annabel Braem[2], Constantinus Politis[1], Reinhilde Jacobs[1,3]

[1] OMFS IMPATH research group, Department of Imaging & Pathology, Faculty of Medicine, KU Leuven and Department of Oral and Maxillofacial Surgery, University Hospitals Leuven, Leuven (3000), Belgium.

[2] Biomaterials and Tissue Engineering research group, Department of Materials Engineering, KU Leuven, Leuven (3000), Belgium.

[3] Department of Dental Medicine, Karolinska Institutet, Stockholm, Sweden.

2.1   Abstract

Ti and its alloys have been widely employed for bone tissue repair and implant manufacturing. The rapid development of 3D-printing technology has allowed fabrication of porous Ti scaffolds with controllable microstructures, which is considered to be an effective method for promoting rapid bone formation and decreasing bone absorption. The purpose of this systematic review was to evaluate the osteogenic potential of 3D-printed porous Ti64 scaffold for repairing long bone defects in animal models and to investigate the influential factors that might affect its osteogenic capacity. Electronic literature search was conducted in the following databases: PubMed, Web of Science, and Embase up to September 2021. The SYRCLE's tool and the modified CAMARADES list were used to assess the risk of bias and methodological quality, respectively. Due to heterogeneity of the selected studies in relation to protocol and outcomes evaluated, a meta-analysis could not be performed. The initial search revealed 5858 studies. Only 46 animal studies were found to be eligible based on the inclusion criteria. Rabbit was the most commonly utilized animal model. A pore size of around 500-600μm and porosity of 60-70% were found to be the most ideal parameters for designing the Ti64 scaffold, where both dodecahedron and diamond pores optimally promoted osteogenesis. Histological analysis of the scaffold in a rabbit model revealed that the maximum BA/TA reached 59.3±8.1% at week 8-10. Based on micro-CT assessment, the maximum BV/TV was found to be 34.0±6.0% at week 12. Ti64 scaffold might act as a promising medium for providing sufficient mechanical support and a stable environment for new bone formation in long bone defects.

Keywords: Ti alloy,Ti64, 3D-printing, animal study, BTE

2.2   Introduction

Since the early 1970s, Ti and its alloys have been widely incorporated in the biomedical field for manufacturing implants and repairing bone defects. These alloys offer a lower Young's modulus compared to other materials, such as stainless steel, cobalt-chromium alloys and tantalum. Nevertheless, an elastic modulus mismatch still exists between Ti and bone tissue which could lead to bone atrophy, fracture, osteoporosis and early implant failure due to the stress shielding effect. To overcome this limitation, porous Ti scaffolds have been designed for reducing the modulus and mimicking the strength of natural bone. Thereby, allowing prevention of the stress shielding [1, 2] and promotion of scaffold fixation into the surrounding tissues [3, 4]. The interconnected pores of the scaffold also offer a shorter healing time with an improved vascularization and exchange of nutrients. At present, porous Ti scaffolds have been employed in the manufacturing of 3D-printed implants such as, artificial lumbar fusion cages and acetabular joints [5-8]. These implants offer high compressive strength, bone-like elastic modulus, and promote long-term bone ingrowth. Furthermore, they have an optimal wear resistance for resisting scratches, cracks, and peeling [9]. These characteristics make porous Ti-based implants an excellent candidate for repairing bone defects.

Currently, porous Ti64 scaffold is one of the most commonly used material for manufacturing load-bearing implants and repairing bone defects owing to its superior mechanical properties and osseointegration compared to commercially pure Ti and other alloys [10]. Many conventional material processing methods have been employed for fabricating porous Ti64 scaffolds, which include sintering [11], solid-state foaming [12] and polymeric sponge replication [13]. In comparison, recent introduction of AM technology and processes, such as, SLM and EBM, have allowed the fabrication of customizable Ti64 scaffolds which offer predictable and predetermined unit cells. Both the aforementioned technologies belong to the powder bed fusion category, where the heat generated from an energy source (SLM: fiber laser, EBM: electronic beam) is used to selectively melt and fuse powder layer-by-layer based on the CAD model. When one layer of powder has been selectively melted, the build platform is lowered to a predetermined distance and the next layer is deposited. The process is repeated with each successive layer until the desired part is entirely constructed [14].

These 3D-printed porous scaffolds have the potential to replace other BGS (allograft, autograft) for treating long bone defects, which are prone to certain risks such as restricted blood supply, disease transmission and high morbidity rate. The key to reducing these risks is to utilize a porous Ti64 scaffold with interconnected pores having sufficient pore size (>100μm), which has the ability

to promote cell proliferation and migration, as well as allow generation of new bone and capillaries [15]. Additionally, these scaffolds have a high coefficient of friction against cancellous bone (μ=1.09), which ensures a stable environment for new bone formation [16]. At an early stage following implantation, porous scaffolds also provide mechanical support to the damaged hard tissue [17].

Although the advantages of Ti64 scaffold have been well documented, it is biologically inert and lacks osteoinductivity. Consequently, it allows new bone formation only from the edges where it is in contact with the pre-existing bone, which leads to a delayed complete fill-up of the defect. Ideally, the new bone should start forming at the center of the scaffold. Many studies have attempted to improve the osteogenic effect and fixation of Ti64 scaffold to the surrounding bone for increasing its long-term success rate, which include surface modification techniques (etching, nano-structuring, coating) and addition of growth factors [18]. However, clinical trials involving the implantation of a functional Ti64 porous scaffold are still rare, owing to the technique sensitivity and high costs.

Animal models are the most effective method for confirming the osteogenic potential of these modified functional Ti64 scaffolds by investigating the macroscopic and microscopic changes of the bone environment during osseointegration [19]. While testing the modified Ti64's osteogenic performance, it is common to use pristine Ti64 scaffold as a control group [4, 20-22], which allows exclusion of any inherent impact from other scaffold modifying materials. However, no data exists confirming the osteogenic properties of a pristine Ti64 scaffold, which in turn could impact the testing process with biased outcomes. It is also crucial to design the experiments more efficiently. For instance, if an experiment time period is set for too long, then both the control and experimental group might show equally distributed bone formation due to overgrowth, making it difficult to analyze the osteogenic differences between both groups without any discernible contrast. Furthermore, there is still room for improvement in AM technology for reducing excessive residual stress and surface roughness of the scaffold. Therefore, it is necessary to review the state of existing Ti64 scaffold's manufacturing and preclinical testing to better understand its osteogenic potential and yield more effective strategies for improving its clinical applicability.

The following systematic review aimed to report the current evidence related to the application of Ti64 scaffold for repairing long bone defects in animal models and to investigate the potential influential factors that might affect its osteogenic ability. The scope of this systematic review is shown in **Figure 2.1**.
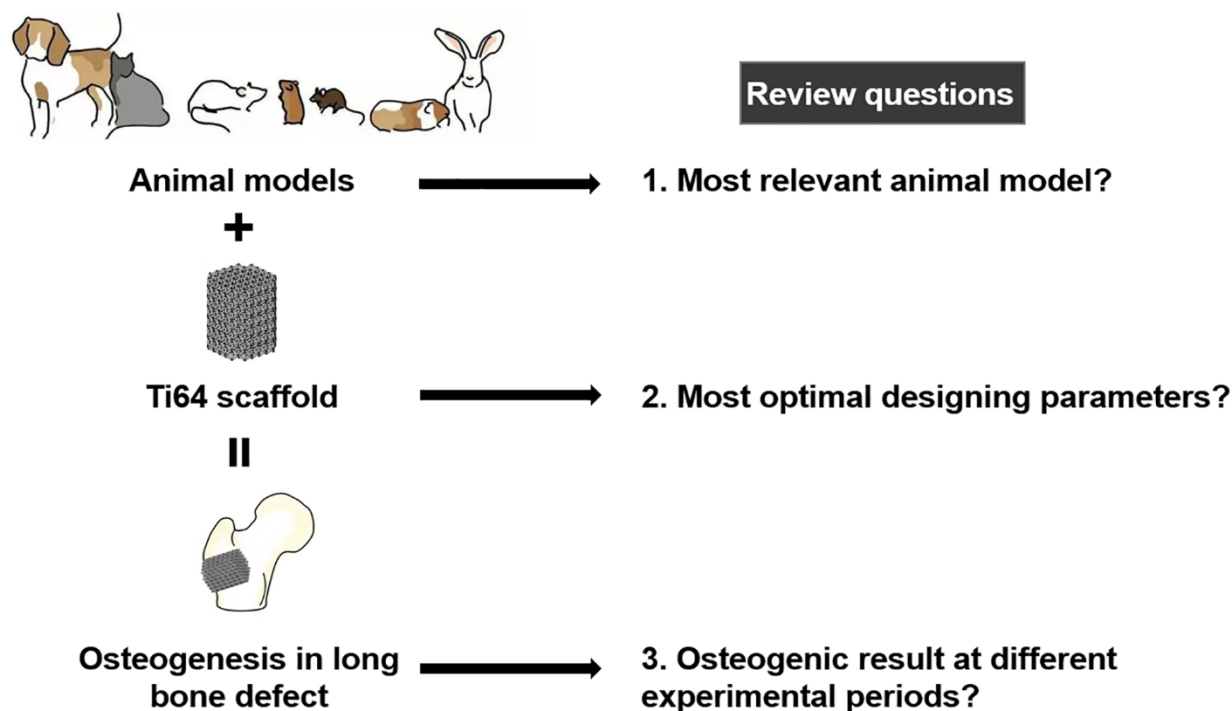
Figure 2.1. The scope of the systematic review.

2.3 Materials and Methods

The study protocol was registered in the PROSPERO database under the number CRD42020194100. The systematic review followed the PRISMA guidelines. Two researchers (GYF, SY) searched the electronic databases of PubMed, Embase, and Web of Science for relevant studies published till September 2021. Search keywords were ("Bone/bone regeneration/bone reconstruction") and ("Ti alloy") and ("3D-printing"). The detailed search strings are presented in Appendix 1. Grey literature and references within the selected studies were also screened. Identified studies were imported into Endnote online software (Thomson Reuters, Philadelphia, PA, USA) for removing duplicates.

Table 2.1 describes the inclusion and exclusion criteria. All animal studies which reported on the application of Ti64 scaffold for long bone defect repair were included. "Long bone" was defined as a bone consisting of a tubular shaft (diaphysis) and two extremities (epiphyses) and "Ti64 scaffold" referred to a 3D-printed structure with a network of fully interconnected pores [23].

Two researchers (GYF, SY) independently screened the relevant articles based on the titles and abstracts, and then read the full text of the included studies. Any disagreement was resolved through consensus. If an agreement could not be reached, a third researcher (RJ) was consulted. Risk of bias was assessed according to the SYRCLE's tool [24], and the CAMARADES list

(www.camarades.info) was used for determining the methodological quality of the included articles. The extracted data included scaffold characteristics (scaffold size and shape, fabrication method, pore size, porosity), study characteristics (animal model, implantation time, bone defect) and the reported osteogenic outcomes (BA, BV).

The PICO (Population, Intervention, Comparison, and Outcome) criteria were follows [25]:

Population: animals with long bone defect.

Intervention/exposure: application of Ti64 scaffold for repairing long bone defect.

Comparison: not applicable.

Outcome: quantitative assessment of the new bone tissue formation.

Table 2.1. Inclusion and exclusion criteria used in this study

Inclusion criteria	Exclusion criteria
All In vivo studies which reported on the application of Ti64 scaffold for long bone defect repair.	1. Non-English papers 2. Descriptive studies, in vitro studies, and clinical trials. 3. Studies used materials other than Ti64. 4. Partially porous Ti64 implant or Ti64 implant with only a textured surface layer. 5. Animal models with comorbidities (hypertension, diabetes, etc.) 6. Not a long bone defect (defect in cranial bone, jaw bone, etc.)

2.4   Results

Figure 2.2 illustrates the screening flow diagram based on the PRISMA guidelines. The PRISMA checklist can be found in Appendix 2. The search strategy retrieved 5858 articles. Following removal of duplicates, title and abstract screening and full-text reading, 46 studies were eligible to be included in the review ranging from year 2013 till 2021, with the majority articles being published in 2020 (**Figure 2.3**).
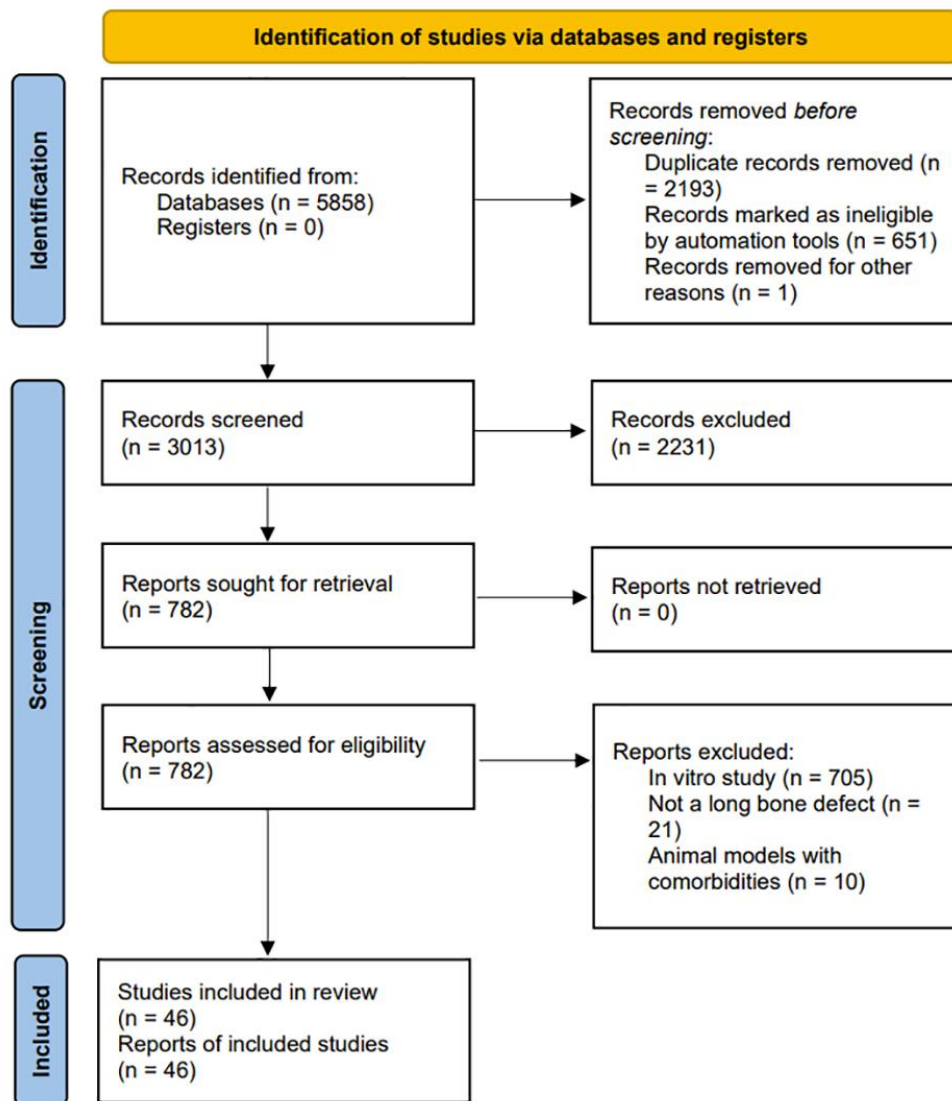
Figure 2.2. Screening flow diagram based on the PRISMA guidelines.
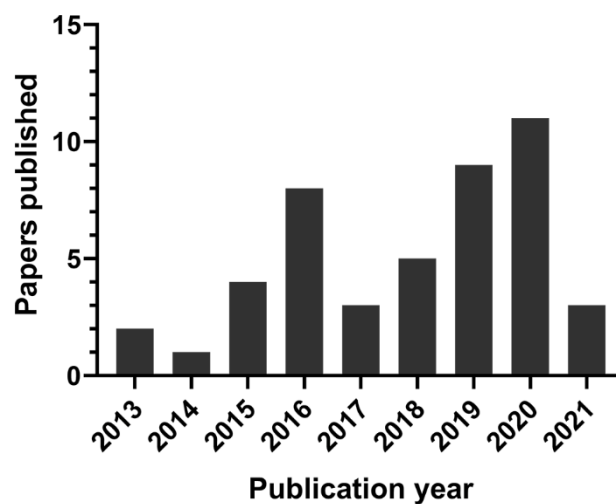
Figure 2.3. Relationship between the year of publication and number of included articles.

2.4.1 Quality of the included studies

2.4.1.1 Risk of bias

Figure 2.4 shows the findings of the SYRCLE's risk of bias analysis. The allocation sequence of animals was adequately generated in 41 studies (89%), and the baseline characteristics of experimental animals were similar in all studies. No study mentioned whether the allocation was adequately concealed. Only one study stated that the animals were housed randomly. There was no explicit description of blind intervention or outcome evaluation. Most studies (45 articles, 98%) did not randomly select animals for outcome assessment due to the high cost of animals. In addition to the items mentioned above, many other items in the questionnaire were rated as "unclear", implying that reporting of these animal studies (mainly experimental designs) should be improved.
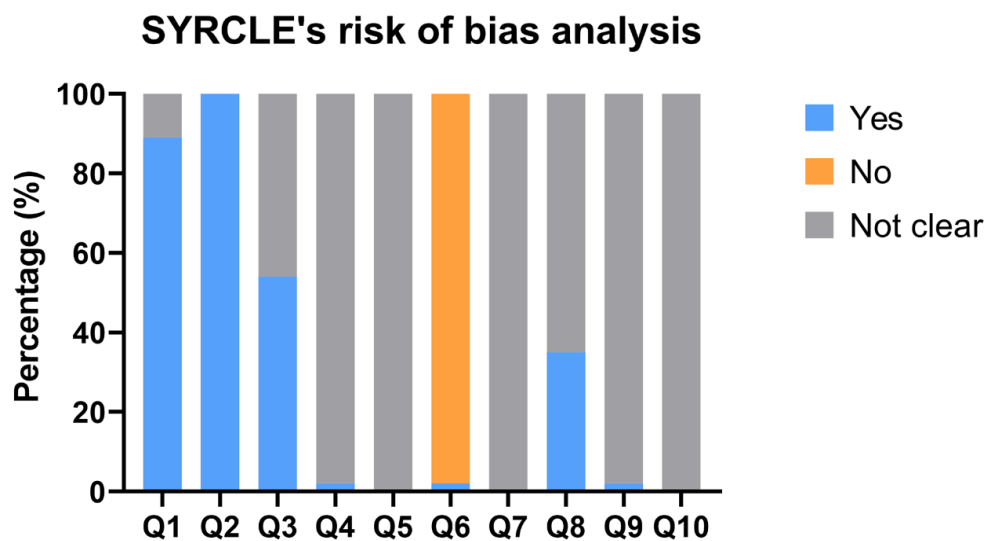
Figure 2.4. The results of SYRCLE's risk of bias analysis.

2.4.1.2 Methodological quality

Figure 2.5 illustrates the CAMARADES checklist-assisted methodological quality assessment. The outcomes of evaluating items such as animal allocation, allocation concealment, and blind operation assessment were similar to those of the "risk of bias" assessment. Animals in all the studies were healthy and a neuroprotective anesthetic was administered in some studies (12 articles, 26%). Only one article mentioned the sample size calculation method. Most studies (34

articles, 74%) clarified the adherence to relevant operating guidelines during animal experiments. Furthermore, the rest of the items were rated as "unclear" which matched the description as in "risk of bias" assessment.
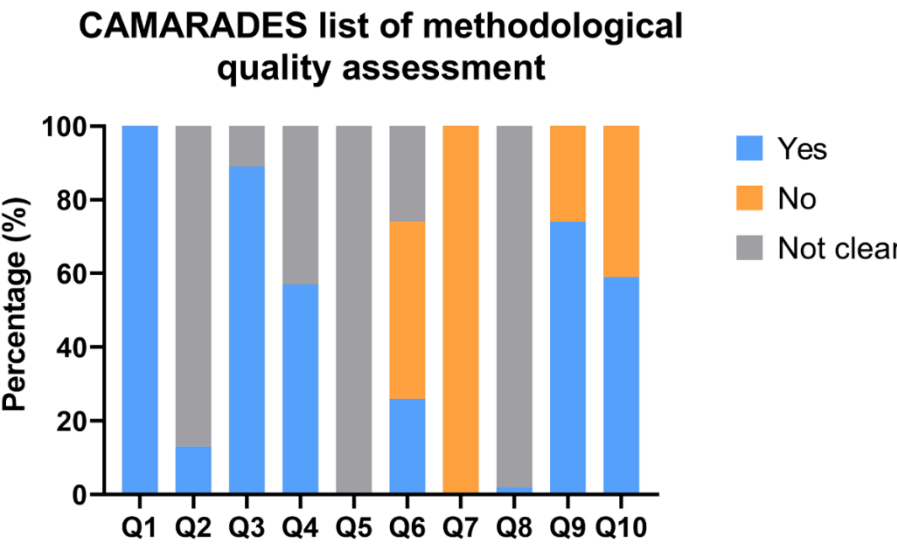

Figure 2.5. The results of CAMARADES list of methodological quality assessment.

2.4.2 Characteristics of the included studies

2.4.2.1 Scaffold design and animal study setup

Table 2.2 summarizes the design of the included articles and **Figure 2.6** represents an example illustrating a schematic workflow of a typical animal experiment. If the author's last name was the same in different articles, a number was used after the last name to distinguish the authors.
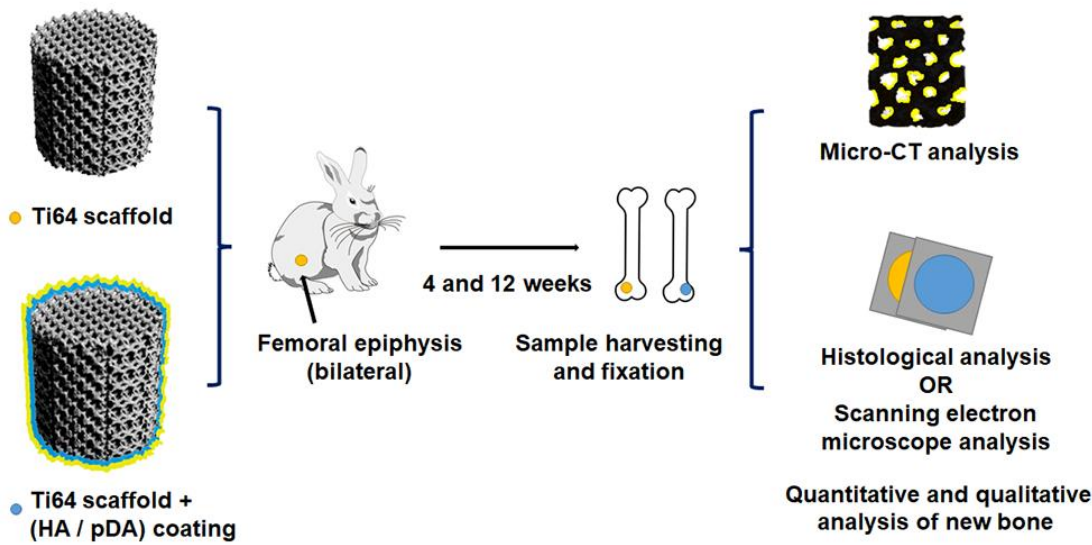
Figure 2.6. Schematic workflow of a typical animal experiment (Li4 et al. [41]).

A total of 29 studies (63%) mentioned the type of Ti64 powder for 3D-printing, with particle sizes ranging from 15 to 100μm. In 16 studies, Grade 23 Ti64 powder was incorporated. The 3D-printing technique was mentioned in 44 studies (96%), which included SLM, (26 studies, 59%), EBM (16 studies, 36%), and SLS (2 studies, 5%). Post-processing of the Ti64 scaffold with ultrasonic cleaning, sandblasting, or acid treatment for removing the excess powder was mentioned in 30 studies (65%).

A cylindrical Ti64 scaffold was the design of choice in most studies (40 studies, 87%) with the size variation depending on the animal model and reconstruction method. The strut size varied between 60 to 3600μm, mostly ranging between 200-400μm (20 studies, 77%). The reported pore size (in 41 studies) was 100-1500μm, with the size of 500-700μm in majority of the studies (23 studies, 56%), followed by 300-499μm (16 studies, 39%). The porosity of the Ti64 scaffold ranged from 25% to 90% in 40 studies, however 60-70% was applied in most of the studies (22 studies, 55%). Various pore shapes could be observed depending on the unit cell for designing the lattice structure, where some studies reported on more than one pore shape. Rhombic dodecahedron (8 studies, 27%) and diamond (8 studies, 27%) were the most applied unit cell shapes. Others included octahedron, tetrahedron, cube, spiral tetrahedron, hexagon and TPMS-based cells. Most studies (42 studies, 91%) adopted a regularly arranged lattice structure, while others adopted a randomly generated or arranged irregular pore structure [16, 22-24]. In this review, the randomly distributed pore structures were divided into the following categories: 1. Pore structure designed based on the Voronoi tessellation method [22]; 2. Pore structure designed using TPMS models [25]; 3. Randomly generated pore structure with varying pore sizes and shapes [16]; 4. Pore structure with regular-shaped and regular-sized but randomly arranged pores [23, 24].

The mechanical strength of the Ti64 scaffold was reported in 15 studies, ranging from 14 to 606MPa, where 10 studies (66%) described its strength between 30-200MPa. The elastic modulus varied from 0.32 to 7.56GPa, with the majority falling between 0 to 3GPa (12 studies, 63%).

Rabbit was the most commonly utilized animal model (25 articles, 54%). Other animal models included rat, sheep, dog, goat and pig. Femur was the preferred implantation site in the majority of studies (36 studies, 78%, femoral diaphysis: n=15, femoral epiphyses: n=21), while other sites included tibia and radius. Non-segmental bone defects accounted for most cases (35 studies, 76%). The experiment duration ranged from 4 weeks to 12 months, and the follow-up time period for most articles was less than 12 weeks (36 studies, 78%). Additionally, half of the studies assessed outcomes at two or more time points (26 papers, 57%).

Table 2.2. List of Ti64 scaffolds and animal study designs.

Author, date	Fabrication method	Scaffold shape and size (∅*h, in mm)	Strut size (μm)	Pore size (μm)	Porosity (%)	Unit cell	Modifications to improve biocompatibility	Animal model	Bone defect	Implantation time (weeks)
Arabnejad et al., 2016 [30]	SLM	C(5*10)	200-400	438-772	56-70	Tetrahedron Octahedron	/	Dog	Femur	4 and 8
Bandyopadhyay et al., 2019 [4]	SLM	C(3*5)	/	60-700	25	/	Anodization treatment	Rat	F-epi	12
Chen1 et al., 2019 [31]	SLM	C(6*6)	300	600	70	Sphere	/	Dog	Tibia	4 and 12
Chen2 et al., 2020 [32]	SLM	C(3*4)	/	500-700	60-70	Octahedron	/	Rat	F-epi	4 and 12
Crovace et al., 2020 [33]	EBM	C(12*400)	/	3600	90	Gyroid	/	Sheep	Tibia(s)	48
Fan et al., 2020 [34]	EBM	C(5*13)	382-383	659-663	70-71	/	Barium titanate coating	Rabbit	Radius (s)	6 and 12
Gilev et al., 2019 [35]	SLM	Cubic	/	/	/	/	/	Rabbit	Tibia	1,2,6,12 and 48
Guo1 et al., 2020 [36]	SLM	C(5*10)	/	340-360	70-75	/	Ti-Cu/Ti-Cu nitride multilayer coating	Rabbit	F-epi	4, 8 and 12
Guo2 et al., 2018 [22]	SLM	C(5*10)	/	316	74	Cubic	/	Rabbit	F-epi	4, 8 and 12
Han et al., 2016 [37]	EBM	C(5*5)	400	600-800	55-67	Cubic	Anodization treatment and strontium incorporation	Rabbit	F-epi	4 and 12
Hara et al., 2016 [16]	EBM	C(5*12)	/	501-933	65-70	Diamond	/	Rabbit	Femur	4 and 12
Huang et al., 2017 [20]	EBM	C(10*20)	238	514	69	Diamond	Hydroxyapatite coating	Goat	F-epi	8 and 16
Kelly et al., 2021 [38]	SLM	C(4.5*8)	/	739-1076	70	TPMS-based cell	/	Rat	Femur (s)	12
Koolen et al., 2020 [39]	SLS	C(5*6)	211	244	79	Rhombic dodecahedron	AlAcH treatment	Rat	Femur (s)	11
Li1 et al., 2019 [40]	SLM	C(5*6)	/	400	45	Cubic	Polydopamine coating	Rabbit	F-epi	5

Study	Tech	C(d*h)		Pore size	Porosity	Unit cell	Coating/Additive	Animal	Location	Weeks
Li2 et al., 2019 [29]	SLM	C(8*10)	/	100-700	50	TPMS-based cell	/	Pig	Tibia	5
Li3 et al., 2016 [3]	EBM	C(10*30)	200	315	34	Diamond	/	Goat	Metatarsus(s)	12, 24 and 48
Li4 et al., 2015 [41]	EBM	C(5*10)	/	710	68	/	Polydopamine-assisted hydroxyapatite coating	Rabbit	F-epi	4 and 12
Liu1 et al., 2016 [42]	EBM	C(5*16)	400	640	76	/	Addition of simvastatin and hydrogel	Rabbit	Tibia	4 and 8
Liu2 et al., 2020 [43]	SLM	C(10*10)	/	600	65	/	/	Rabbit	F-epi	4, 6, 8, 10 and 12
Luan et al., 2019 [44]	EBM	C(5*4)	/	334-402	55-78	/	/	Rabbit	Femur	12
Lv et al., 2015 [45]	EBM	C(5*6)	/	640	/	Hexagonal	Addition of bone BMP-2, VEGF and fibringel	Rabbit	F-epi	4
Lyu et al., 2020 [46]	/	C(2*5)	320	650	70	/	/	Rabbit	F-epi	12
Ma1 et al., 2018 [47]	SLM	C(5*6)	/	400	76	/	Addition of mineralized collagen	Rabbit	Radius(s)	4 and 12
Ma2 et al., 2021 [48]	SLM	C(15*20)	/	400	76	/	Addition of gelatin methacrylate	Rabbit	Radius(s)	4 and 12
Mumith et al., 2020 [49]	SLS	C(8*14.5)	300-750	700-1500	70-75	/	Hydroxyapatite coating, silicon-substituted or strontium-substituted hydroxyapatite coating	Sheep	F-epi	6
Palmquist1 et al., 2017 [50]	EBM	C(5.2*5)	350	550	70	Diamond	/	Sheep	Femur and tibia	24
Palmquist2 et al., 2013 [51]	EBM	C(5.2*7)	500-1000	500-700	65-70	/	/	Sheep	F-epi	26
Ragone et al., 2020 [26]	SLM	C(6.2*11)	200	450-1200	75-90	Irregular-shaped	/	Sheep	Femur and tibia	6, 10 and 14
Ran et al., 2018 [52]	SLM	C(4*13)	300-400	401-801	/	Circle	/	Rabbit	F-epi	4 and 12

Study	Method	Shape				Pore structure	Surface treatment	Animal	Location	Weeks
Shah1 et al., 2016 [53]	EBM	C(5.2*7)	583	/	63	/	/	Sheep	F-epi	24
Shah2 et al., 2016 [54]	EBM	C(5.2*5)	341	470-545	70	Diamond	/	Sheep	F-epi	26
Song et al., 2019 [55]	SLM	C(3*6)	200-400	/	65-86	Diamond	Hydroxyapatite coating	Rabbit	Femur	12 and 24
Tanzer et al., 2019 [19]	SLM	C(5.2*10)	/	450	50-65	Irregular-shaped	Hydroxyapatite coating	Dog	Femur	/
Tsai et al., 2019 [56]	SLM	C(6.5*10)	/	350	/	Cubic	Mg-calcium silicate and chitosan coating	Rabbit	Femur	6
van der Stok1 et al., 2015 [57]	SLM	Femur-shape	165	577	85	Rhombic dodecahedron	AlAcH surface treatment and addition of BMP-2 and fibrin gel	Rat	Femur (s)	12
van der Stok2 et al., 2015 [58]	SLM	Femur-shape	120	500	88	Rhombic dodecahedron	AlAcH surface treatment and osteostatin coating	Rat	Femur (s)	12
van der Stok3 et al., 2013 [17]	SLM	Femur-shape	120-230	490	68-88	Rhombic dodecahedron	AlAcH treatment	Rat	Femur (s)	4,8 and 12
Wang1 et al., 2018 [27]	SLM	C(4.8*8)	410-449	427-458	61-66	Diamond Tetrahedron	/	Rabbit	Femur	4 and 8
Wang2 et al., 2018 [59]	/	C(8*10)	/	200	/	/	Strontium ion incorporated zeolite coating	Rabbit	F-epi	4
Xiu1 et al., 2017 [60]	EBM	C(6*5)	400	640	73	Rhombic dodecahedron	Hybrid micro-arc oxidation and hydrothermal treatment	Rabbit	F-epi	8
Xiu2 et al., 2017 [61]	EBM	C(6*5)	400	640	73	Rhombic dodecahedron	Hybrid micro-arc oxidation	Rabbit	F-epi	8
Yavari et al., 2014 [62]	SLM	Femur-shape	160-180	577-596	85-89	Rhombic dodecahedron	Acid-alkali treatment, AlAcH treatment and anodizing-heat treatment	Rat	Femur (s)	4, 8 and 12
Yu et al., 2020 [28]	SLM	Cone-shape	200	650	90	Rhombic dodecahedron	/	Rabbit	Femur	4 and 8

| Zhang et al., 2021 [63] | SLM | C(5*10) | 300 | / | 68 | Diamond | Bioactive glass and mesoporous bioactive glass coating | Rabbit | F-epi | 6 and 9 |
| Zhong et al., 2020 [64] | SLM | C(6*10) | / | / | / | / | / | Rabbit | F-epi | 6 and 12 |

* C: cylinder; HA: hydroxyapatite; AlAcH: alkali-acid-heat; F-epi: femoral epiphysis; s: segmental bone defect; wk: weeks; m: months.

* Data are all average values, and parameters were reserved for integers.

* If multiple Ti64 scaffold design parameters have been applied in a single article, the parameters are expressed in ranges

2.4.2.2 Bone tissue outcomes

Quantitative evaluation of the new bone tissue formation was performed by either histomorphometric analysis, SEM or 3D micro-CT assessment. The most reported outcomes included BA/TA (new BA over scaffold pore area) as a 2D parameter and BV/TV (new BV over scaffold pore volume) as a 3D parameter. An overview of these outcomes is summarized in **Table 2.3** and **Table 2.4**. As the addition of coating material, surface treatment, or other additives might significantly alter the osteogenic performance of Ti64 scaffold, these conditions were not considered. Furthermore, segmental bone defects have been excluded from the BA/TA and BV/TV analyses as well, as in this case new bone can only grow inward from both scaffold ends. This results in a relatively low bone ingrowth, which cannot reliably be compared to the case in which most of the scaffold surface is covered by bone. Due to the heterogeneity in protocols and reported outcomes amongst the included studies, no meta-analysis could be performed.

2.4.2.2.1 BA/TA analysis (**Table 2.3**)

The majority of BA/TA data were obtained from rabbit models (12/19 articles, 63%). In five of these studies, Ti64 scaffold was implanted in the femoral diaphysis and seven in the femoral epiphysis. The BA/TA in rabbit models ranged from 1.5±0.1% to 46.3±13.7% at week 4-6, 8.2±2.3% to 59.3±8.1% at week 8-10, 2.4±0.4% to 51.6±6.4% at week 12-14, and 35.6±5.3% at week 24-26 (only reported by Song et al. [51]). The maximum BA/TA at weeks 4 and 8 were only reported by Yu et al. [24]. In addition, Hara et al. [12] observed that the depth of new bone ingrowth at week 12 exceeded 1.5mm in a rabbit model.

Four studies provided BA/TA data in sheep models, and only Palmquist2 et al. [47] found that BA/TA reached 44.7±4.4% in femoral epiphysis at week 26. The remaining three studies calculated the BA/TA in different scaffold regions (central part vs. peripheral part; cortical bone vs. cancellous bone). The new bone formation was significantly higher in the cortical and peripheral region of the Ti64 scaffold compared to cancellous bone and central area [22, 46, 50].

Three studies assessed BA/TA in the femoral or tibial diaphysis of beagle dog models. It was within the range of 11.9±2.2% to 41.5±8.2% at week 4-6, 41.3±4.3% to 56.9±4.0% at week 8-10 (only reported by Arabnejad et al. [27]), and 64.4±2.8% at week 12-14 (only reported by Tanzer et al.,2019 [16]).

2.4.2.2.2   BV/TV analysis (**Table 2.4**)

As BA/TA is limited to 2D sections, BV/TV from micro-CT analysis provides a more comprehensive quantification of bone ingrowth. Rabbit model was applied in the majority of studies (11/14 studies, 79%). Eight studies implanted Ti64 scaffold in femoral epiphysis and three in femoral diaphysis. The BV/TV in rabbit model ranged from 4.3±1.0% to 27.3±8.4% at week 4-6, 16.6±2.18% to 29.8±2.2% at week 8-10, and 8.6±2.7% to 34.0±6.0% at week 12. Similar to the BA/TA data, the maximum BV/TV at week 4-6 and week 8-10 are also reported by Yu et al. [24].

The BV/TV results in the pig, goat, and rat models are also reported [17, 26, 29]. The maximum BV/TV in pig models reached 12.8±3.9 at week 4-6, 23.4±1.6% in rat models at week 12, and 6.3±2.2% in goat models at week 16.

Table 2.3. Summary of reported BA/TA for pristine Ti64 scaffolds in the reviewed studies.

Author, date	Animal and bone defect	Group	BA/TA (%)			
			4-6 weeks	8-10 weeks	12-14 weeks	24-26 weeks
Arabnejad *et al.*,2016 [30]	Beagle dog, femur	Tetrahedron cell	28.6±11.6	41.3±4.3	/	/
		Octet truss cell	35.5±1.9	56.9±4.		
Chen1 *et al.*,2019 [31]	Beagle dog, tibia	/	11.9±2.2	/	15.9±4.9	/
Guo1 *et al.*,2020 [36]	Rabbit, f-epi	/	11.6±1.9	12.2±2.0	24.1±3.0	/
Guo2 *et al.*,2018 [22]	Rabbit, f-epi	/	13.2±2.7	35.6±2.7	55.9±2.0	/
Han *et al.*,2016 [37]	Rabbit, f-epi	Pore size 600µm	2.3±0.4	/	3.5±0.5	/
		Pore size 800µm	1.5±0.1	/	2.4±0.4	/
Hara *et al.*,2016 [16]	Rabbit, femur	Pore size 500µm	34.9±6.8	/	50.1±8.3	/
		Pore size 640µm	37.0±5.0	/	50.9±6.7	/
		Pore size 800µm	27.2±7.2	/	51.6±6.4	/
		Pore size 1000µm	34.7±8.4	/	35.1±2.7	/
Li4 *et al.*,2015 [41]	Rabbit, f-epi	/	5.8±2.2	/	12.2±2.2	/
Lv *et al.*,2015 [45]	Rabbit, f-epi	/	7.8±2.8	/	/	/
Palmquist1 *et al.*,2017 [50]	Sheep, femur and tibia	Scaffold in femur	/	/	/	Central:26.5±9.2 Peripheral:57.2±10.9
		Scaffold in tibia	/	/	/	Central: 45.6±19.5 Peripheral: 8.0±10.4
Palmquist2 et al., 2017 [51]	Sheep, f-epi	/	/	/	/	44.7±4.4
Ragone *et al.*,2020 [26]	Sheep, femur and tibia	/	Cortical:75.0±13.5 Cancellous:27.0±15.0	Cortical:82.0±5.0 Cancellous:36.0±10.5	Cortical:82.0±9.0 Cancellous:51.0±14.0	/
Shah2 *et al.*,2016 [54]	Sheep, f-epi	/	/	/	/	Central: 32.9±4.8 Peripheral:60.0±4.6
Song *et al.*,2019 [55]	Rabbit, femur	/	/	/	6.8±2.9	35.6±5.3
Tanzer *et al.*,2019 [19]	Beagle dog, femur	/	41.5±8.2	/	64.4±2.8	/
Tsai *et al.*,2019 [56]	Rabbit, femur	/	2.5±0.8	/	/	/
Wang1 *et al.*,2018 [27]	Rabbit, femur	Diamond cell (r)	34.0±5.9	36.3±1.0	/	/

		Diamond cell (ir)	33.7±5.0	36.8±2.3	/	/
		Diamond cell (g)	30.2±3.3	32.3±4.9	/	/
		Tetrahedron cell	20.5±3.0	24.3±1.9	/	/
Xiu1 *et al.*,2017 [60]	Rabbit, f-epi	/	/	8.2±2.3	/	/
Xiu2 *et al.*,2017 [61]	Rabbit, f-epi	/	/	10.8±3.4	/	/
Yu *et al.*,2020 [28]	Rabbit, femur	/	46.3±13.7	59.3±8.1	/	/

* F-epi: femoral epiphysis; r: regularly distributed pores; ir: irregularly distributed pores; g: gradient distributed pores.

* The data are all represented as means ± standard deviations, and reserved for one decimal point.

Table 2.4. Summary of reported BV/TV for pristine Ti64 scaffolds in the reviewed studies.

Author, date	Animal and bone defect	Group	BV/TV (%) 4-6 weeks	8-10 weeks	12 weeks	16 weeks
Chen2 et al., 2020 [32]	Rat, f-epi	Porosity 60%, pore size 500µm	/	/	23.4±1.6	/
		Porosity 60%, pore size 600µm	/	/	21.0±2.1	/
		Porosity 60%, pore size 700µm	/	/	12.8±2.1	/
		Porosity 70%, pore size 500µm	/	/	23.2±1.8	/
		Porosity 70%, pore size 600µm	/	/	22.3±1.0	/
		Porosity 70%, pore size 700µm	/	/	18.3±1.4	/
Guo1 et al., 2020 [36]	Rabbit, f-epi	/	11.6±1.8	17.1±1.6	25.5±2.6	/
Han et al., 2016 [37]	Rabbit, f-epi	Pore size 600µm	8.4±1.3	/	16.2±3.6	/
		Pore size 800µm	4.3±1.0	/	8.6±2.7	/
Huang et al., 2017 [20]	Goat, f-epi	/	/	5.1±1.8	/	6.3±2.2
Li1 et al., 2019 [40]	Rabbit, f-epi	/	13.7	/	/	/
Li2 et al., 2019 [29]	Pig, tibia	Pore size 300-500µm	12.7±3.6	/	/	/
		Pore size 200-600µm	12.0±3.6	/	/	/
		Pore size 100-700µm	12.8±3.9	/	/	/
Li4 et al., 2015 [41]	Rabbit, f-epi	/	5.9±2.2	/	11.0±2.6	/
Liu1 et al., 2016 [42]	Rabbit, tibia	/	26.7±1.0	28.9±1.4	/	/
Luan et al., 2019 [44]	Rabbit, femur	Porosity 55%, pore size 334µm	/	/	21.4±2.2	/
		Porosity 65%, pore size 383µm	/	/	24.6±2.0	/
		Porosity 78%, pore size 400µm	/	/	26.7±0.9	/
Lyu et al., 2020 [46]	Rabbit, f-epi	/	/	/	34.0±6.0	/
Wang2 et al., 2018 [59]	Rabbit, f-epi	/	6.0±0.2	/	/	/
Yu et al., 2020 [28]	Rabbit, femur	/	27.3±8.4	29.8±2.2	/	/
Zhang et al., 2021 [63]	Rabbit, f-epi	/	13.4±1.0	16.6±2.18	/	/
Zhong et al., 2020 [64]	Rabbit, f-epi	/	13.9±1.5	/	16.0±1.3	/

* F-epi: femoral epiphysis. *The data are all represented as means ± standard deviations, and reserved for one decimal point.

2.4.2.3 Variables affecting the osteogenic capacity of Ti64 scaffold

From the selected studies and the data presented in **Table 2.3** and **Table 2.4**, some variables have been summarized below, which might impact the osteogenic ability of Ti64 scaffold：

Implantation site: Ragone et al. [22] found that the new bone formation of Ti64 scaffold in the cortical bone region was significantly greater than that of the cancellous bone and the osseointegration of Ti64 scaffold was almost complete after 2 months.

Implantation time: The maximum BA/TA values in rabbit models peaked at week 8-10. The maximum BV/TV values in rabbit models and the maximum BA/TA values in beagle dog models increased from week 4 to week 12.

Pore size and porosity: Hara et al. [12] proposed that the pore size of 500-800μm was optimal for new bone growth. Similarly, Ran et al. [48] observed that Ti64 scaffold with pore sizes of 600-800μm had greater osteogenic ability compared to Ti64 scaffold with pore sizes of 400μm. Furthermore, Chen et al. and Han et al. found that Ti64 scaffold with pore sizes of 500-600μm have more osteogenic capability compared to 700-800μm [29, 34]. In terms of porosity, Luan et al. suggested that Ti64 scaffold with 78% porosity had a higher osteogenic capacity than Ti64 scaffold with 65% and 55% porosity.

Pore shape: Within a Ti64 scaffold with high porosity(>50%), Arabnejad et al. [27] observed that new bone formation in the octagonal pore structure was more prominent compared to tetrahedral structure. Furthermore, Wang1 et al. [23] discovered that bone formation in the tetrahedral pore structure was smaller than in the diamond pore structure.

2.5   Discussion

Over the past few years, animal experimentations for confirming the osteogenic potential of Ti64 scaffolds have gradually gained attention in the biomedical field. Therefore, the following review was conducted to accumulate evidence and report on the osteogenic ability of Ti64 scaffold for repairing long bone defects and to investigate influential factors which might impact its effectiveness. Meta-analysis could not be performed due to the presence of significant heterogeneity amongst the selected studies related to the scaffold design and size, defect type, and observation time. However, the qualitative evidence synthesis suggested certain critical commonalities and limitations associated within the methodologies of the included studies for fabricating Ti64 scaffold with optimal osteogenic potential, which could act as a reference guide for future comparative studies.

When considering the animal model for the validation of scaffold, it is essential to understand the

bone healing capacity of different animal species. Bone remodeling in small rodents is much faster than larger species [65]. Additionally, rabbits and dogs have a higher bone remodeling rate compared to humans. Therefore, it might be difficult to extrapolate the osteogenic response in these animals for a possible similar response in humans [66]. However, sheep, goat, and pig offer a similar bone remodeling rate to that of humans, making them a better choice for generating osteogenic responses and translating those findings to humans [67, 68].

In terms of the bone healing process, rats are considered less suitable based on the lack of haversian system. However, their bone remodeling is similar to the haversian remodeling in large animals [69]. Thereby, the absence of the haversian system should not be the sole reason for excluding rodents from studies where bone healing assessment is required. Furthermore, the bone healing process of dog, rabbit, sheep, and pig models is remarkably similar to that of humans [70, 71].

The studies using a rat model in this review created segmental bone defects and the scaffold size was very small. We believe that rats should not be considered for assessing the performance of Ti64 scaffolds due to their size limitation and inability to insert multiple implants. Based on the International Organization for Standardization (ISO10993-6:2016(E)), the recommended implant size for biological evaluation in rabbits should be 2x6mm and 4x12mm in larger animals, such as sheep, goat, and dog. The guidelines also recommend an observation time of 1 to 4 weeks' for assessing short-term outcomes and 12 weeks or more for long-term assessment. Additionally, the long-time follow-up time points for the animal models except rats should be 13, 26, 52, 78, and 104 weeks. However, the findings of the current review revealed that the experimental design in the majority of studies did not follow the international standards and had a follow-up period of less than 12 weeks. Hence confirming a lack of evidence related to the standardized long-term outcome evaluation of Ti64 scaffold.

Rabbit was the most applied animal model and only a few studies assessed the osteogenic capacity of the scaffold with a large animal model such as sheep, goat, dog, and pig. In contrast to large models, small animals are easier to handle, less expensive and appropriate for screening implant materials before testing in larger models. Unlike small animals, the large animal models have similar bone healing capabilities to that of humans. At the same instance, it should be kept in mind that every large animal model also has its pros and cons. For instance, dogs offer an optimal model for assessing Ti64 scaffold's effectiveness, however, due to ethical concerns and increased public scrutiny their application in animal research has been declining [72]. An adult sheep has similarities in weight, metabolism and bone remodeling rates to that of humans, and could be

considered ideal for testing the scaffold and transferring the findings to a clinical setting [73]. However, researchers tend to use young animals due to financial constraints, which might underestimate the effectiveness of the scaffold as their bones have not fully matured.

In this review, most included studies adopted the femoral condyle defect model or the transcortical defect model. The femoral condyle defect model is most relevant to plastic surgery applications [74]. When there are many groups of scaffolds to be tested on the same animal model at the same time (for example, in the paper of Arabnejad et al. [30], there are four groups of scaffolds to be tested on the same animal model at the same time), the use of transcortical defects is a viable option for achieving greater consistency within the animal. Segmental bone defects were excluded from the review as they are more prone to failure due to bending or breaking of the fixation plate, screw failure, infection and muscular and neurovascular damage. Additionally, inclusion of segmental defects would have led to bias within the findings of the review, as their mechanical integrity differs from that of a single defect which could negatively impact the osteogenic efficiency and functional recovery of the bone defect.

Based on the findings of the review, Ti64 scaffold induced remarkable osteogenesis in the cortical region compared to cancellous bone. A possible explanation could be the penetration of a lower mechanical stimulus into the cancellous bone surrounding the scaffold [49]. Additionally, the cancellous bone has a randomly distributed pore structure, which cannot be replicated by the regularly distributed simple pattern. In contrast, the randomly distributed pore structures demonstrated higher permeability allowing optimal bone ingrowth [19, 28]. The newly formed bone continues to grow over time with the maximum BA/TA and BV/TV peaking at both week 4-6 and week 8-10 due to the osteogenic effect of the randomly distributed pores which outperform a simple topological distribution [19].

The osseointegration of Ti64 scaffold is primarily determined by the pore size, structure, porosity, and interconnectivity [19]. The pore size in the included studies ranged from 100 to 900μm [75]. A large pore size promotes the growth of blood vessels but reduces the mechanical properties and cell adhesion. On the contrary, a small pore size improves cell adhesion and tissue growth, however the likelihood of pore blockage increases [76]. The findings of the review suggested that the pore sizes ranging from 500-600μm were found to be most optimal for an in vivo fabrication of Ti64 scaffold. Furthermore, an ideal porosity for porous scaffolds should be around 80-90% [76]. The majority of Ti64 scaffolds included in the review had a porosity of 60-70% for ensuring optimal mechanical strength. Furthermore, their compressive strength (33-193MPa) and elastic modulus (0.02-3GPa) were equal to that of human cortical bone for avoiding the stress shielding effect [75].

A higher porosity than the aforementioned limit should be avoided to inhibit weakening of the scaffold's mechanical properties.

The pore shape of the Ti64 scaffold varied amongst studies without any consensus on which shape offered the most optimal outcomes. The most commonly applied shapes were diamond and rhombic dodecahedron. The diamond lattice is isotropic in nature with evenly distributed deformation, which helps to reduce stress concentration. Its structure is closely similar to that of cancellous bone and has a large curvature radius which induces higher tissue amplification [27]. Based on these benefits, a diamond lattice is widely incorporated in porous scaffolds [77]. On the other hand, rhombic dodecahedron lattice has a higher yield stress and is stable under multi-directional compression forces. Thereby, making it an ideal choice for manufacturing load-bearing implants [28, 78]. However, care should be taken that the dodecahedron shape is designed with only obtuse angles, as acutely angled pores are easily damaged during the melting stage of printing. Other designed pore shapes in the review involved tetrahedral, octahedral, gyroid and TPMS lattices which are beneficial for improving the scaffold's strength and rigidity, isotropy, load resistance and surface area and permeability, respectively [30, 32, 33, 38].

In this review, all Ti64 scaffolds were implanted immediately following the creation of bone defect, which is clinically applicable for procedures where sufficient preoperative time is available for treatment planning such as lumbar intervertebral fusion and acetabular joint reconstruction. An immediate insertion allows for a reduction in potential complications and cost of the procedure. However, autologous bone graft and bone lengthening with external fixation still remain the standard for treating trauma-related bone defects, where immediate 3D-printing is not possible due to a long scaffold designing and printing time.

The review only reported the osteogenic outcomes of unmodified Ti64 scaffold, which could act as a guide for comparison with other porous biomaterials in future studies. However, the impact of scaffold's surface modification for improving its biological activity and osteogenic capacity cannot be ignored. Surface modification techniques such as anodic oxidation and micro-arc oxidation increase the surface area of the bone in contact with the oxidized scaffold, leading to a quicker and firmer integration of the implant [60, 61]. Hydroxyapatite coating has also been widely used as a coating agent which demonstrated improved osseointegration and bone ingrowth compared to an uncoated Ti64 scaffold [20, 41]. Furthermore, ion substituted hydroxyapatite coatings (strontium and silicon substituted hydroxyapatite coatings) also offer an increased bone growth compared to pure hydroxyapatite [49]. Other coatings that have also shown to improve bone ingrowth, wear resistance and osteogenic capacity of the scaffold, include polydopamine coating [40], Mg-calcium

silicate composite coating [56], osteostatin coating [58], Sr-incorporated zeolite coating [59] and Ti-Cu/Ti-Cu nitride multilayer [36]. Apart from surface modifying techniques and coatings, the Ti64 scaffold has also been tailored with growth factors such as, BMP-2 and VEGF for inducing osteogenesis and angiogenesis, respectively [41, 45, 57]. In summary, all the aforementioned factors should be considered when designing a Ti64 scaffold to allow for optimal performance.

Based on the findings of the review, future in vivo studies are warranted using large animal models. Although small animals are acceptable for proving general principles, repeated experiments with larger animal models are necessary for translating the results to humans. Furthermore, as the mechanism of bone regeneration is also dependent on the size of the bone defect, it constitutes a need for creating large sized defects that can only be set in large animal models. Future research should also be conducted with a long-term follow-up period for assessing the precise osteogenic capacity of a Ti64 scaffold. It is also recommended to follow the ISO guidelines for designing experiments and standardized parameters such as BA/TA, BV/TV, and BIC should be assessed for quantifying bone ingrowth. These proposed recommendations can greatly reduce data heterogeneity and improve study comparability.

At present, Ti64 scaffold is still a black box for researchers and further exploration is required to unravel its full potential. For instance, a more advanced functional Ti64 scaffold hierarchical design could be fabricated by combining different techniques such as topology optimization, CAD, and minimal surface formulation [9]; Furthermore, surface nano-topography modification could endow Ti64 scaffolds with additional biological functions such as antibacterial properties and enhanced osteogenic differentiation [79]. Another avenue of investigation could be the improvement of the AM processes to address the issues of unmelted powder particles and pores in the scaffold trabecula, which would negatively impact the scaffold's mechanical properties.

The review had certain limitations. Firstly, no standardization existed related to the pore size, porosity, strut size and pore shape amongst different studies. As all the parameters are correlated, thereby it was difficult to determine the best combination for designing the Ti64 scaffold. Secondly, most studies used rabbit's femoral epiphysis as the implantation site and a 5mm diameter scaffold, which is too large for a rabbit model and also it does not represent the functional Ti64 scaffold used in humans. However, it should be noted that a scaffold with a smaller diameter is difficult to manufacture by the available 3D-printing techniques. Finally, the longest follow-up time-point reported by majority of the studies was 12 weeks, hence, it was difficult to predict whether and when the new bone would outgrow the Ti64 scaffold.

2.6   Conclusion

Ti64 scaffold could be regarded as a promising medium for providing mechanical support and a stable environment for new bone formation in long bone defects. The rabbit model is the most relevant animal model, and the pore size of 500-600μm with 60-70% porosity and rhombic dodecahedron or diamond unit pore shape could be considered as the most optimal designing parameters for manufacturing Ti64 scaffold. Further studies are required using large animal models and standardized protocols for extrapolating the results of animal studies to humans for potential clinical applications.

2.7   References

1.   Warnke PH, Douglas T, Wollny P, Sherry E, Steiner M, Galonska S, et al. Rapid prototyping: porous titanium alloy scaffolds produced by selective laser melting for bone tissue engineering. Tissue Engineering - Part C: Methods. 2008;15:115-24.

2.   Tamimi F, Torres J, Al-Abedalla K, Lopez-Cabarcos E, Alkhraisat MH, Bassett DC, et al. Osseointegration of dental implants in 3D-printed synthetic onlay grafts customized according to bone metabolic activity in recipient site. Biomaterials. 2014;35:5436-45.

3.   Li G, Wang L, Pan W, Yang F, Jiang W, Wu X, et al. In vitro and in vivo study of additive manufactured porous Ti6Al4V scaffolds for repairing bone defects. Scientific Reports. 2016;6:34072.

4.   Bandyopadhyay A, Mitra I, Shivaram A, Dasgupta N, Bose S. Direct comparison of additively manufactured porous titanium and tantalum implants towards in vivo osseointegration. Additive Manufacturing. 2019;28:259-66.

5.   Zimmer.https://www.zimmerbiomet.com/en/products-and-solutions/specialties/spine/trelloss-tc-porous-ti-interbody-system.html. 2019.

6.   Zimmer.https://www.zimmerbiomet.com/en/products-and-solutions/specialties/hip/osseoti-porous-metal-technology.html. 2016.

7.   Nuvasive I. https://Www.Nuvasive.Com/Surgical-Solutions/Advanced-Materials-Science/Modulus-Titanium-Technology/. 2019.

8.   Spineart. https://www.spineart.com/products/juliet-ti-tl/. 2020.

9.   Rodriguez-Contreras A, Punset M, Calero JA, Gil FJ, Ruperez E, Manero JM. Powder metallurgy with space holder for porous titanium implants: A review. Journal of Materials Science & Technology. 2021;76:129-49.

10. Elias C, Lima J, Valiev R, Meyers M. Biomedical applications of titanium and its alloys. Jom. 2008;60:46-9.

11. Zhang X, Zheng G, Wang J, Zhang Y, Zhang G, Li Z, et al. Porous Ti6Al4V scaffold directly fabricated by sintering: preparation and in vivo experiment. Journal of Nanomaterials. 2013;2013:1-7.

12. Davis N, Teisen J, Schuh C, Dunand D. Solid-state foaming of titanium by superplastic expansion of argon-filled pores. Journal of Materials Research. 2001;16:1508-19.

13. Li J, Li S, Van Blitterswijk C, De Groot K. A novel porous Ti6Al4V: characterization and cell attachment. Journal of Biomedical Materials Research. 2005;73:223-33.

14. Sing SL, An J, Yeong WY, Wiria FE. Laser and electron-beam powder-bed additive

manufacturing of metallic implants: A review on processes, materials and designs. Journal of Orthopaedic Research. 2016;34:369-85.

15. Karageorgiou V, Kaplan D. Porosity of 3D biomaterial scaffolds and osteogenesis. Biomaterials. 2005;26:5474-91.

16. Hara D, Nakashima Y, Sato T, Hirata M, Kanazawa M, Kohno Y, et al. Bone bonding strength of diamond-structured porous titanium-alloy implants manufactured using the electron beam-melting technique. Materials Science and Engineering: C. 2016;59:1047-52.

17. Van der Stok J, Van der Jagt OP, Amin Yavari S, De Haas MF, Waarsing JH, Jahr H, et al. Selective laser melting−produced porous titanium scaffolds regenerate bone in critical size cortical bone defects. Journal of Orthopaedic Research. 2013;31:792-9.

18. Fojt J. Ti-6Al-4V alloy surface modification for medical applications. Applied Surface Science. 2012;262:163-7.

19. Tanzer M, Chuang PJ, Ngo CG, Song L, TenHuisen KS. Characterization of bone ingrowth and interface mechanics of a new porous 3D printed biomaterial: an animal study. The Bone & Joint Journal. 2019;6 Suppl B:62-7.

20. Huang H, Lan PH, Zhang YQ, Li XK, Zhang X, Yuan CF, et al. Surface characterization and in vivo performance of plasma-sprayed hydroxyapatite-coated porous Ti6Al4V implants generated by electron beam melting. Surface and Coatings Technology. 2015;283:80-8.

21. Guo Y, Wu J, Xie K, Tan J, Yang Y, Zhao S, et al. Study of Bone Regeneration and Osteointegration Effect of a Novel Selective Laser-Melted Titanium-Tantalum-Niobium-Zirconium Alloy Scaffold. ACS Biomaterials Science & Engineering. 2019;5:6463-73.

22. Guo Y, Xie K, Jiang W, Wang L, Li G, Zhao S, et al. In Vitro and in Vivo Study of 3D-Printed Porous Tantalum Scaffolds for Repairing Bone Defects. ACS Biomaterials Science & Engineering. 2019;5:1123-33.

23. Wu S, Liu X, Yeung KW, Liu C, Yang X. Biomimetic porous scaffolds for bone tissue engineering. Materials Science and Engineering: A. 2014;80:1-36.

24. Hooijmans CR, Rovers MM, De Vries RB, Leenaars M, Ritskes-Hoitinga M, Langendam MW. SYRCLE's risk of bias tool for animal studies. BMC Medical Research Methodology. 2014;14:43.

25. Davies KS. Formulating the evidence-based practice question: a review of the frameworks. Evidence Based Library and Information Practice. 2011;6:75-80.

26. Ragone V, Canciani E, Arosio M, Olimpo M, Piras LA, von Degerfeld MM, et al. In vivo osseointegration of a randomized trabecular titanium structure obtained by an additive manufacturing technique. Journal of Materials Science: Materials in Medicine. 2020;31:17.

27. Wang H, Su K, Su L, Liang P, Ji P, Wang C. The effect of 3D-printed Ti6Al4V scaffolds with various macropore structures on osteointegration and osteogenesis: A biomechanical evaluation. Journal of the Mechanical Behavior of Biomedical Materials. 2018;88:488-96.

28. Yu T, Gao H, Liu T, Huang YD, Wang C. Effects of immediately static loading on osteointegration and osteogenesis around 3D-printed porous implant: A histological and biomechanical study. Materials Science and Engineering: C. 2020;108:110406.

29. Li L, Shi J, Zhang K, Yang L, Yu F, Zhu L, et al. Early osteointegration evaluation of porous Ti6Al4V scaffolds designed based on triply periodic minimal surface models. Journal of Orthopaedic Translation. 2019;19:94-105.

30. Arabnejad S, Johnston RB, Pura JA, Singh B, Tanzer M, Pasini D. High-strength porous biomaterials for bone replacement: A strategy to assess the interplay between cell morphology, mechanical properties, bone ingrowth and manufacturing constraints. Acta Biomaterialia. 2016;30:345-56.

31. Chen C, Hao Y, Bai X, Ni JJ, Chung SM, Liu F, et al. 3D printed porous Ti6Al4V cage: Effects of additive angle on surface properties and biocompatibility; bone ingrowth in Beagle tibia model. Materials & Design. 2019;175:107824.

32. Chen Z, Yan X, Yin S, Liu L, Liu X, Zhao G, et al. Influence of the pore size and porosity of selective laser melted Ti6Al4V ELI porous scaffold on cell proliferation, osteogenesis and bone ingrowth. Materials Science and Engineering: C. 2020;106:110289.

33. Crovace AM, Lacitignola L, Forleo DM, Staffieri F, Francioso E, Di Meo A, et al. 3D biomimetic porous titanium (Ti6Al4V ELI) scaffolds for large bone critical defect reconstruction: An experimental study in sheep. Animals. 2020;10:1389.

34. Fan B, Guo Z, Li X, Li S, Gao P, Xiao X, et al. Electroactive barium titanate coated titanium scaffold improves osteogenesis and osseointegration with low-intensity pulsed ultrasound for large segmental bone defects. Bioactive Materials. 2020;5:1087-101.

35. Gilev MV, Bazarny VV, Volokitina EA, Polushina LG, Maksimova AY, Kazakova YE. Laboratory Monitoring of Bone Tissue Remodeling after Augmentation of Impression Intraarticular Fracture with Different Types of Bone Graft. Bulletin of Experimental Biology and Medicine. 2019;167:681-4.

36. Guo Y, Ren L, Xie K, Wang L, Yu B, Jiang W, et al. Functionalized TiCu/Ti–Cu-N-Coated 3D-Printed Porous Ti6Al4V Scaffold Promotes Bone Regeneration through BMSC Recruitment. Advanced Materials Interfaces. 2020;7:1901632.

37. Han TX, Chang B, Ding X, Yue GN, Song W, Tang HP, et al. Improved bone formation and ingrowth for additively manufactured porous Ti6Al4V bone implants with strontium laden nanotube

array coating. RSC Advances. 2016;6:13686-97.

38. Kelly CN, Lin AS, Leguineche KE, Shekhar S, Walsh WR, Guldberg RE, et al. Functional repair of critically sized femoral defects treated with bioinspired titanium gyroid-sheet scaffolds. Journal of the Mechanical Behavior of Biomedical Materials. 2021;116:104380.

39. Koolen M, Amin Yavari S, Lietaert K, Wauthle R, Zadpoor AA, Weinans H. Bone Regeneration in Critical-Sized Bone Defects Treated with Additively Manufactured Porous Metallic Biomaterials: The Effects of Inelastic Mechanical Properties. Materials. 2020;13:1992.

40. Li L, Li Y, Yang L, Yu F, Zhang K, Jin J, et al. Polydopamine coating promotes early osteogenesis in 3D printing porous Ti6Al4V scaffolds. Annals of Translational Medicine. 2019;7:240.

41. Li Y, Yang W, Li X, Zhang X, Wang C, Meng X, et al. Improving osteointegration and osteogenesis of three-dimensional porous Ti6Al4V scaffolds by polydopamine-assisted biomimetic hydroxyapatite coating. ACS Applied Materials & Interfaces. 2015;7:5715-24.

42. Liu H, Li W, Liu C, Tan J, Wang H, Hai B, et al. Incorporating simvastatin/poloxamer 407 hydrogel into 3D-printed porous Ti6Al4V scaffolds for the promotion of angiogenesis, osseointegration and bone ingrowth. Biofabrication. 2016;8:045012.

43. Liu LZ, Duan JH, Shi Q, Chen Q, Yao QQ, Li ZY. Mechanical effect on the evolution of bone formation during bone ingrowth into a 3D-printed Ti-alloy scaffold. Materials Letters. 2020;273:127971.

44. Luan HQ, Wang LT, Ren WY, Chu ZW, Huang YF, Lu CL, et al. The effect of pore size and porosity of Ti6Al4V scaffolds on MC3T3-E1 cells and tissue in rabbits. Science China Technological Sciences. 2019;62:1160-8.

45. Lv J, Xiu P, Tan J, Jia Z, Cai H, Liu Z. Enhanced angiogenesis and osteogenesis in critical bone defects by the controlled release of BMP-2 and VEGF: implantation of electron beam melting-fabricated porous Ti6Al4V scaffolds incorporating growth factor-doped fibrin glue. Biomedical Materials. 2015;10:035013.

46. Lyu LW, Jing Y, Wang JK, Zhang CQ. Enhanced Osseointegration of Porous Titanium Scaffold Implanted with Preload: An Experiment Study in Rabbits. International Journal of Morphology. 2020;38:909-13.

47. Ma L, Wang X, Zhao N, Zhu Y, Qiu Z, Li Q, et al. Integrating 3D Printing and Biomimetic Mineralization for Personalized Enhanced Osteogenesis, Angiogenesis, and Osteointegration. ACS Applied Materials & Interfaces. 2018;10:42146-54.

48. Ma L, Wang X, Zhou Y, Ji X, Cheng S, Bian D, et al. Biomimetic Ti-6Al-4V alloy/gelatin methacrylate hybrid scaffold with enhanced osteogenic and angiogenic capabilities for large bone

defect restoration. Bioactive Materials. 2021;6:3437-48.

49. Mumith A, Cheong VS, Fromme P, Coathup MJ, Blunn GW. The effect of strontium and silicon substituted hydroxyapatite electrochemical coatings on bone ingrowth and osseointegration of selective laser sintered porous metal implants. PLoS One. 2020;15:e0227232.

50. Palmquist A, Shah FA, Emanuelsson L, Omar O, Suska F. A technique for evaluating bone ingrowth into 3D printed, porous Ti6Al4V implants accurately using X-ray micro-computed tomography and histomorphometry. Micron. 2017;94:1-8.

51. Palmquist A, Snis A, Emanuelsson L, Browne M, Thomsen P. Long-term biocompatibility and osseointegration of electron beam melted, free-form-fabricated solid and porous titanium alloy: experimental studies in sheep. Journal of Biomaterials Applications. 2013;27:1003-16.

52. Ran Q, Yang W, Hu Y, Shen X, Yu Y, Xiang Y, et al. Osteogenesis of 3D printed porous Ti6Al4V implants with different pore sizes. Journal of the Mechanical Behavior of Biomedical Materials. 2018;84:1-11.

53. Shah FA, Snis A, Matic A, Thomsen P, Palmquist A. 3D printed Ti6Al4V implant surface promotes bone maturation and retains a higher density of less aged osteocytes at the bone-implant interface. Acta Biomaterialia. 2016;30:357-67.

54. Shah FA, Omar O, Suska F, Snis A, Matic A, Emanuelsson L, et al. Long-term osseointegration of 3D printed CoCr constructs with an interconnected open-pore architecture prepared by electron beam melting. Acta Biomaterialia. 2016;36:296-309.

55. Song P, Hu C, Pei X, Sun J, Sun H, Wu L, et al. Dual modulation of crystallinity and macro-/microstructures of 3D printed porous titanium implants to enhance stability and osseointegration. Journal of Materials Chemistry B. 2019;7:2865-77.

56. Tsai CH, Hung CH, Kuo CN, Chen CY, Peng YN, Shie MY. Improved Bioactivity of 3D Printed Porous Titanium Alloy Scaffold with Chitosan/Magnesium-Calcium Silicate Composite for Orthopaedic Applications. Materials. 2019;12:203.

57. van der Stok J, Koolen MK, de Maat MP, Yavari SA, Alblas J, Patka P, et al. Full regeneration of segmental bone defects using porous titanium implants loaded with BMP-2 containing fibrin gels. European Cells & Materials. 2015;29:141-53.

58. van der Stok J, Lozano D, Chai YC, Amin Yavari S, Bastidas Coral AP, Verhaar JA, et al. Osteostatin-coated porous titanium can improve early bone regeneration of cortical bone defects in rats. Tissue Engineering - Part A. 2015;21:1495-506.

59. Wang S, Li R, Li D, Zhang ZY, Liu G, Liang H, et al. Fabrication of bioactive 3D printed porous titanium implants with Sr ion-incorporated zeolite coatings for bone ingrowth. Journal of Materials

Chemistry B. 2018;6:3254-61.

60. Xiu P, Jia ZJ, Lv J, Yin C, Cai H, Song CL, et al. Hierarchical Micropore/Nanorod Apatite Hybrids In-Situ Grown from 3-D Printed Macroporous Ti6Al4V Implants with Improved Bioactivity and Osseointegration. Journal of Materials Science & Technology. 2017;33:179-86.

61. Xiu P, Jia Z, Lv J, Yin C, Cheng Y, Zhang K, et al. Tailored Surface Treatment of 3D Printed Porous Ti6Al4V by Microarc Oxidation for Enhanced Osseointegration via Optimized Bone In-Growth Patterns and Interlocked Bone/Implant Interface. ACS Applied Materials & Interfaces. 2016;8:17964-75.

62. Amin Yavari S, van der Stok J, Chai YC, Wauthle R, Tahmasebi Birgani Z, Habibovic P, et al. Bone regeneration performance of surface-treated porous titanium. Biomaterials. 2014;35:6172-81.

63. Zhang G, Zhao P, Lin L, Qin L, Huan Z, Leeflang S, et al. Surface-treated 3D printed Ti-6Al-4V scaffolds with enhanced bone regeneration performance: an in vivo study. Annals of Translational Medicine. 2021;9:39.

64. Zhong W, Li J, Hu C, Quan Z, Jiang D, Huang G, et al. 3D-printed titanium implant-coated polydopamine for repairing femoral condyle defects in rabbits. Journal of Orthopaedic Surgery and Research. 2020;15:102.

65. von Rechenberg B. Animal models in bone repair. Drug Discovery Today: Disease Models. 2014;13:23-7.

66. Pearce A, Richards R, Milz S, Schneider E, Pearce S. Animal models for implant biomaterial research in bone: a review. European Cells & Materials. 2007;13:1-10.

67. Reichert JC, Saifzadeh S, Wullschleger ME, Epari DR, Schütz MA, Duda GN, et al. The challenge of establishing preclinical models for segmental bone defect research. Biomaterials. 2009;30:2149-63.

68. Hakimi M, Jungbluth P, Sager M, Betsch M, Herten M, Becker J, et al. Combined use of platelet-rich plasma and autologous bone grafts in the treatment of long bone defects in mini-pigs. Injury. 2010;41:717-23.

69. Histing T, Garcia P, Holstein J, Klein M, Matthys R, Nuetzi R, et al. Small animal bone healing models: standards, tips, and pitfalls results of a consensus meeting. Bone. 2011;49:591-9.

70. Willie BM, Bloebaum RD, Bireley WR, Bachus KN, Hofmann AA. Determining relevance of a weight–bearing ovine model for bone ingrowth assessment. Journal of Biomedical Materials Research Part A. 2004;69:567-76.

71. Wancket L. Animal models for evaluation of bone implants and devices: comparative bone structure and common model uses. Veterinary Pathology. 2015;52:842-50.

72. Mangione F, Salmon B, EzEldeen M, Jacobs R, Chaussain C, Vital S. Characteristics of large animal models for current cell-based oral tissue regeneration. Tissue Engineering Part B: Reviews. 2021.

73. McGovern JA, Griffin M, Hutmacher DW. Animal models for bone tissue engineering and modelling disease. Disease Models & Mechanisms. 2018;11:033084.

74. Li Y, Chen S-K, Li L, Qin L, Wang X-L, Lai Y-X. Bone defect animal models for testing efficacy of bone substitute biomaterials. Journal of Orthopaedic Translation. 2015;3:95-104.

75. Surmeneva MA, Surmenev RA, Chudinova EA, Koptioug A, Tkachev MS, Gorodzha SN, et al. Fabrication of multiple-layered gradient cellular metal scaffold via electron beam melting for segmental bone reconstruction. Materials & Design. 2017;133:195-204.

76. Du Y, Guo JL, Wang J, Mikos AG, Zhang S. Hierarchically designed bone scaffolds: From internal cues to external stimuli. Biomaterials. 2019;218:119334.

77. Zhang X-Y, Fang G, Xing L-L, Liu W, Zhou J. Effect of porosity variation strategy on the performance of functionally graded Ti-6Al-4V scaffolds for bone tissue engineering. Materials & Design. 2018;157:523-38.

78. Huang G, Pan S-T, Qiu J-X. The osteogenic effects of porous Tantalum and Titanium alloy scaffolds with different unit cell structure. Colloids and Surfaces B. 2021;210:112229.

79. Hasan J, Jain S, Chatterjee K. Nanoscale topography on black titanium imparts multi-biofunctional properties for orthopedic applications. Scientific Reports. 2017;7:1-13.

Part III

Surface modification of Ti and Ti alloy scaffolds

BMP-2 integrated biomimetic CaP coating functionalized 3D-printed Ti64 scaffold induces ectopic bone formation in a dog model

Yifei Gu[1], Lingfei Wei[2,5], Zheru Zhang[3], Jeroen Van Dessel[1], Ronald B. Driesen[4], Ivo Lambrichts[4], Reinhilde Jacobs[1], Lei Tian*[3], Yi Sun*[1], Yuelian Liu*[2], Constantinus Politis[1]

[1] OMFS IMPATH research group, Department of Imaging & Pathology, Faculty of Medicine, KU Leuven and Department of Oral and Maxillofacial Surgery, University Hospitals Leuven, Leuven (3000), Belgium.

[2] Department of Oral Implantology and Prosthetic Dentistry, Academic Centre for Dentistry Amsterdam, University of Amsterdam and Vrije Universiteit Amsterdam, Amsterdam (1019), the Netherlands

[3] State Key Laboratory of Military Stomatology & National Clinical Research Center for Oral Diseases & Shaanxi Clinical Research Center for Oral Diseases, Department of Craniofacial Trauma and Orthognathic Surgery, School of Stomatology, FMMU, Xi'an (710000), China

[4] Biomedical Research Institute, Hasselt University, Hasselt (3500), Belgium

[5] Department of oral implantology, Yantai Stomatological Hospital, Yantai (264000), China

3.1 Abstract

The use of Ti64 in bone engineering is limited, due to the biological inertia of the surface. In this study, a porous Ti6Al4V scaffold with mechanical properties similar to cancellous bone was designed and 3D-printed. Under physiological conditions, the scaffold was immersed firstly in a 5-fold-concentrated simulated body fluid, then in a supersaturated CaP solution containing BMP-2, to form a bone-like porous micro/nano structured biomimetic coating on the surface. Scaffolds were implanted in the muscle pouches created in six beagle dogs and were retrieved four weeks later for histologic and histomorphometric analysis. Results showed that BMP-2 integrated biomimetic CaP coating induced ectopic bone formation, which was absent in other two groups. Soft tissue infiltrated the scaffold's outside 1 mm layer, while the new-formed bone was evenly distributed in the longitudinal and horizontal directions within the rest of the scaffold based on BA/TA, BIC and BA measurements. In conclusion, the BMP-2 integrated biomimetic CaP coating creates a micro/nano surface structure on the Ti64 scaffold, which helps to increase biocompatibility. The integrated BMP-2 is capable of inducing ectopic bone formation in vivo. The proposed combination may have the potential for bone reconstruction, but further studies are needed to explore its clinical applicability.

Keywords: biomimetics; 3D-printing; Ti alloy; BMP-2; CaP; bone substitutes

3.2   Introduction

The porous scaffold of different materials is one of the core elements in BTE [1]. The interconnected pores in the scaffold provide channels for cell migration and the transportation of nutrition and oxygen. These pores also ensure the space for the formation of blood vessels and prevent necrosis of the new tissue due to insufficient vascularization [2].

Ti and Ti alloys are widely used to manufacture scaffolds for their high strength-to-weight ratio, good biocompatibility, corrosion resistance and durability, strong osteointegration capability, and low cost [3, 4]. However, disadvantages also exist: the elastic modulus of Ti and Ti alloy is 4 - 10 times than that of the human skeleton, and the mismatched mechanical properties between the material and the surrounding host bone are easy to cause the stress shielding effect; also, the low surface bio-recognition ability of Ti and Ti alloys has restricted their applications [5]. There is room for improvement in scaffold design, AM technique, and surface modification.

In the medical field, 3D porous scaffolds have been produced through the AM technique (or 3D-printing technique) [6]. Interconnected porous constructs with predictable and predetermined unit cells were manufactured. The structure allows osteoblasts and mesenchymal stem cells to migrate and proliferate, as well as extramedullary tissues to infiltrate [7]. Moreover, the mechanical properties of the scaffolds can be modified by AM to approach those of human bone to relieve the stress-shielding effect [8].

Surface modification of metal scaffolds improves the physical and chemical properties of the scaffold and enhances osseointegration [9]. Surface roughness at the micro/nanoscale has been shown to aid in the bonding of bone and scaffold [10]. CaP is the most abundant mineral in bone minerals, and its degradation products provide abundant Ca and P to osteoblasts and promote bone regeneration [11]. Scaffolds coated with CaP show enhanced angiogenesis and bone formation based on its biocompatibility and osteoconductivity [12-14]. BMP-2 is one of the most potent growth factors that induce mesenchymal stem cell and osteoprogenitor cell differentiation into osteoblasts [15]. The BMP-2 integrated biomimetic CaP or CaP-based composites were fabricated under physiological temperature (37 °C) and pH conditions (7.4), and the biological activity of BMP-2 can be preserved during its coprecipitation with the inorganic components [16, 17].

In previous studies, BMP-2 integrated biomimetic CaP coating with micro/nano structure was produced, and the excellent osteoinductive effects of this composited coating have been demonstrated in in vivo studies [16]. However, no research has ever attempted to combine the BMP-2 integrated biomimetic CaP coating with a 3D-printed porous Ti scaffold, which is designed

in line with the biomechanical property of human bone. The advantages of the porous Ti scaffold mentioned above make it more conducive to repairing bone defects. More importantly, the 3D-printed Ti scaffold can be customized for clinical applications and is more worthy of investigation. The present study aimed to manufacture Ti64 scaffolds via the AM technique. Biomimetic CaP coating (OCP) and BMP-2 were deposited on the scaffold surface simultaneously to promote the osteoconductive and osteoinductive properties of the scaffolds in an ectopic model in dog's back muscles. The objective is to see whether this combined fabrication is beneficial to new bone formation after four weeks of implantation.

3.3   Materials and Methods

3.3.1 Design and 3D-printing of the scaffold

Porous cylindrical models were designed in 3-Matic software (Materialise, Leuven, Belgium), and STL files were created. The designed 3D model is shown in **Figure 3.1a**. Porous cylinder Ti64 scaffolds (diameter 10 mm, length 10 mm) were fabricated using a 3D Metal printer (ProX DMP 320, 3D Systems, Inc.) with a minimum feature size of 100μm. **Table 3.1** shows the scaffold designing parameters as well as the Ti64 powder details. Ti64 powder (LaserForm Ti Gr23 (A), 3D Systems, Inc.) was melted layer by layer in an argon atmosphere at a scanning speed of 1000mm/s. According to previous numerical simulations [18, 19], under this scanning speed, the instantaneous temperature within the molten pool during the selective laser melting of Ti64 can reach approximately 3.5×10^3K, with a heating rate of around 4.6×10^7K/s and a temperature gradient of about 5.6×10^4K/cm. A rapid solidification process was recorded (cooling rate of up to 5.5×10^5K/s) after the laser beam left the Ti64 molten pool.

In total, 42 samples were printed, and 15 samples were randomly selected for the mechanical test, and the other 27 samples were randomly distributed to three groups (nine samples per group):

Group 1 (G1): Ti64 scaffold without any coating (Ti64, **Figure 3.1b**).

Group 2 (G2): Ti64 scaffold with biomimetic CaP coating (CaP-Ti64, **Figure 3.1c**).

Group 3 (G3): Ti64 scaffold with BMP-2 integrated biomimetic CaP coating (BMP-2/CaP-Ti64).

The distribution of scaffolds and the design of the experiment were shown in a flow chart (**Figure 3.2**).

Table 3.1 Designing parameters of the scaffold and information of the Ti64 powder

Designing parameters	Pore shape	Rhombic dodecahedron
	Pore size	438 - 825µm (Randomized distribution, average 638 µm)
	Porosity	88%
	Strut size	300µm
Information of Ti64 powder (manufacturer's data)	Composition (wt%)	Ti: Balance; N ≤0.03; Al: 5.5-6.5; C ≤0.08; V: 3. -4.5; H ≤0.012; O ≤0.13; F ≤0.25; Y ≤ 0.005
	Particle size	100% <1mm
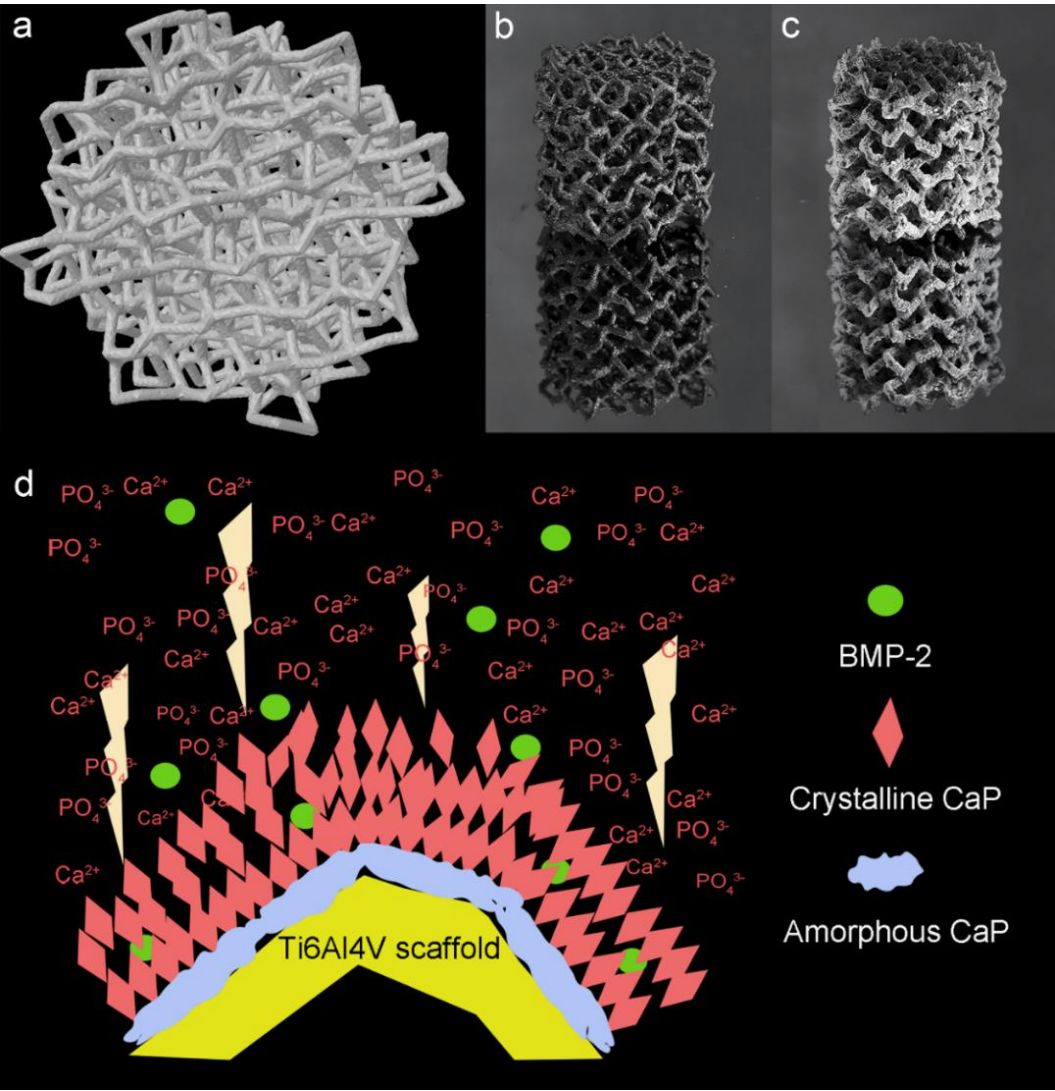
Figure 3.1. designed 3D model (a), uncoated Ti64 scaffold (b) and Ti64 scaffold with biomimetic CaP coating (c); (d) illustration of the fabrication process of biomimetic CaP coating. The lighting symbols in (d) indicate the direction of ion deposition.
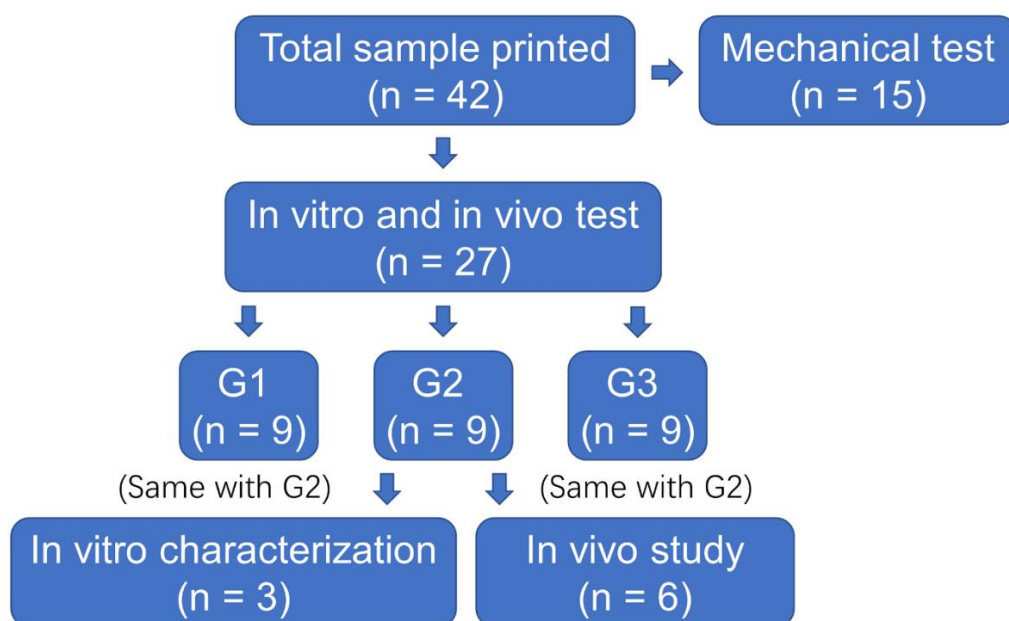
Figure 3.2. The flow chart showing the distribution of scaffolds and the design of the experiment.

3.3.2 Procedures to perform coating

Samples in G2 and G3 were coated by biomimetic CaP using a well-established protocol (**Figure 3.1d**) [20, 21]. Briefly, the substrate coating of biomimetic CaP coating was deposited by immersing the Ti64 scaffolds into 5-fold-concentrated simulated body fluid (5L, 684mM NaCl, 13.5mM KCL, 9mM $CaCl_2.2H_2O$, 2.1mM $Na_2HPO_4.2H_2O$, 59.5mM $NaHCO_3$, 5mM $MgCl_2.6H_2O$) for 24 hours under physiological condition (37°C, pH=7.4). This treatment yielded a layer of amorphous CaP onto the scaffold surface. Then the scaffolds were sterilized using a standard steam autoclave procedure. Subsequently, the outside layer of biomimetic CaP coating was deposited onto the initial amorphous CaP substratum by immersing the scaffolds into supersaturated CaP solution (75ml, 40mM HCl, 137mM NaCl, 4mM $CaCl_2.2H_2O$, 2mM $Na_2HPO_4.2H_2O$, 50mM TRIS, PH:7.4±0.05) for 48 hours under physiological condition (37°C, pH=7.4). This treatment yielded a layer of crystalline CaP onto the scaffold. In G3, recombinant human BMP-2 (rhBMP-2, Shanghai Rebone Biomaterials Co., China) was added into supersaturated CaP solution at a concentration of 5mg L^{-1} and was deposited simultaneously with the outside biomimetic CaP layer. The Ca/P ratio of the coating was determined by ICP-OES. The amount of BMP-2 integrated into the coated scaffolds was determined by the ELISA technique [22]. Scaffolds were then dried and kept at room temperature. The entire procedure was performed

under sterile conditions.

3.3.3 In vitro characterization

3.3.3.1 Mechanical test

The mechanical properties of the scaffold, including compressive strength and elastic modulus, were assessed by compression testing using a universal testing machine (Instron 4467, Instron Corp., USA) with a 5kN load cell and a crosshead speed of 1mm min^{-1} at room temperature. The ASTM E9-89a standard was followed for the compression test [23], and the tension-strain curves of the scaffold were recorded.

3.3.3.2 Micro-CT scan

Three scaffolds were randomly selected from each group (total n=9, three in each group) and scanned with a micro-CT scanner (SkyScan 1172; Bruker-microCT, Kontich, Belgium) to calculate the porosity. The scanning parameters were set as: Pixel size =10x10µm; Step size =0.25° per image; Filter =1mm thick Cu; Voltage =100kV; Current =100µA; Rotation =360°. The scanning time for each step was approximately 1.6s. The scanned images were then reconstructed with Bruker NRecon software (version 1.7.3.0) and the reconstructed axial images were analyzed by Bruker CTAn software (version 1.18.4.0). The porosity of the printed scaffolds was calculated within a selected region of interest (height: 3mm, diameter: 8mm, threshold: 128-255) in the middle of the scaffold.

3.3.3.3 SEM and EDX scan

After micro-CT scanning, the scaffolds (n =3 in each group) were scanned with SEM (Philips XL-30, FEI company, The Netherlands) to observe the surface morphology of the scaffold. Then, they were embedded with epoxy resin (Epofix resin, Struers, Copenhagen, Denmark) in cylindrical containers. The upper half (5mm) of the scaffolds were removed by polishing and the middlemost cross-sections of the scaffolds were shown. The surface morphology of these cross-sections was characterized using SEM.

For each cross-section, a field of view was chosen at random, and three struts were chosen randomly within the field of view. The thicknesses of the struts were measured twice or three times in different locations, and the average strut thickness in each scaffold group was calculated. To observe the difference in coating thickness from the inside to the outside of the scaffold, three coated surfaces on the outer side of the scaffold and three coated surfaces in the center of the scaffold were randomly selected for each cross-section in G2 and G3, and the average coating thickness was measured and compared. The chemical composition of the biomimetic CaP coatings

was characterized by an EDS attached to the SEM apparatus.

3.3.4 In vivo study

3.3.4.1 Study design

The research protocol was submitted to and approved by the Ethical Committee for Animal Experiments in The Fourth Military Medical University, China (No. 2018(K9-023)). Six adult male beagle dogs with normal health status were selected and housed separately. The animals were provided with adequate diet and water, and the indoor environment was constant: temperature 18-19°C; humidity 40-70%; routinely maintained air change 10-20 times per hour. Six scaffold samples from each group were used in the animal study.

After two weeks of adaptation and 12 hours of fasting, the animals were fixed in prone position under general anesthesia (3% pentobarbital sodium solution 1ml kg^{-1}, Intravenous injection). 8×10^6 Units of penicillin potassium were administered preoperatively. The backs of the animals were shaved and the skin was disinfected with iodophor and sealed with a hole towel. Incisions were firstly marked by methylene blue, then performed with a scalpel. The connective tissues were fully separated until the erector spinae showed. Three muscle pouches were made by separating the muscle fibers along the spine, and an about 3mm distance was kept between every muscle pouch and the spine to prevent potential nerve injuries. For each animal, one scaffold from each group was randomly selected and implanted into the three muscle pouches. After implantation, the muscle pouches, perimysium, subcutaneous tissues and skin were closed with suture in order, and the wound was cleaned with 75% ethanol and dressed tightly. The animals were given five days of anti-inflammatory drugs after surgery. At week 4 after implantation, the animals were anesthetized and fixed with the same method described above. The muscle pouches were opened again, and the scaffolds were harvested and kept in 10% formaldehyde solution, followed by storing in 4°C refrigerator. The processes of suturing, disinfecting and dressing were the same as described above, and the animals were observed and taken care of properly. The dressing was removed three days after the surgery.

3.3.4.2 Histological and histomorphometrical analysis

Retrieved scaffolds were rinsed with ultrapure water at room temperature for 24 hours and dehydrated by graded ethanol (70%-100%) for 48 hours. The samples were then vitrified with dimethylbenzene and embedded with PMMA. Five sections of 200μm in thickness were vertically cut from the scaffold (**Figure 3.3a**). The cut sections were polished into 30-50μm thick sections with sandpapers, and then stained with McNeil's Tetrachrome, basic Fuchsine and Toluidine Blue

O. The images of each slice were obtained using a light microscope (Axio-Imager M2, Carl Zeiss Microscopy, Jena, Germany) to observe new bone induction.

On each section, the most top, bottom, left and right points of the scaffold were marked using Image J software, and the center of the section was determined by crossing the top-bottom line and the left-right line. Five concentric circles, centered at the center of the scaffold and with diameters of 1 to 5mm, were drawn and called circle 1 to circle 5 respectively (**Figure 3.3b**). Based on these circles, five ROIs were set: ROI1= range of circle 1; ROI2= ring-shaped area of circle 2 minus circle 1; ROI3= ring-shaped area of circle 3 minus circle 2; ROI4= ring-shaped area of circle 4 minus circle 3; ROI5= ring-shaped area of circle 5 minus circle 4.

To observe the distribution of the new bone, the following tests were performed in horizontal and longitudinal directions:

In the horizontal direction, in each ROI, the parameters of observed new bone around the scaffold, including TA (mm2), BA (mm2) and BIC(%) were quantitatively evaluated using Image J software. The BA/TA and BIC values were compared between different ROI groups.

In the longitudinal direction, BA, BA/TA and BIC values were calculated and compared between different slice groups to evaluate the longitudinal distribution of new bone.

In the end, five regions with new bone were randomly selected in the slice 2 and slice 4 of every scaffold, respectively. The area of bone (mm^2), as well as the number of cells in the new bone (osteocytes, osteoblasts and osteoclasts) were measured and counted using Image J software, and the cell density was calculated by cell number/BA.
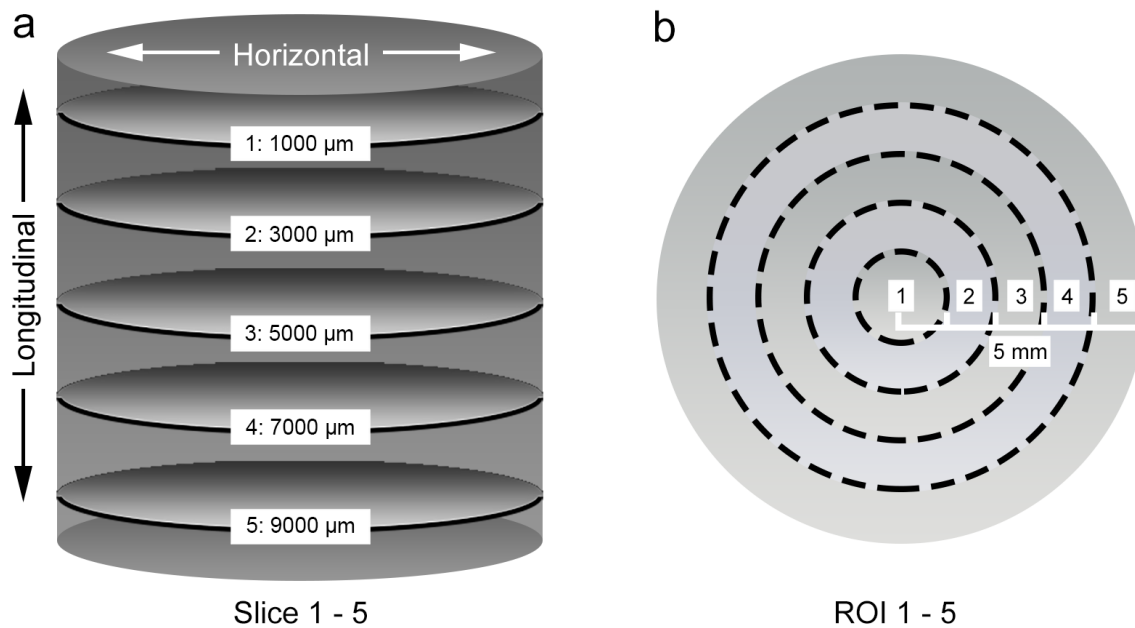
Figure 3.3. schematic diagram for slice 1-5 and ROI 1-5 in each scaffold. Slice 1-5 and ROI 1-5 were used to assess the longitudinal and horizontal distribution of new bone, respectively.

3.3.5 Statistical analysis

The data obtained from the in vitro characterization and animal study were analyzed and expressed as mean ± deviations. The statistically significant difference (p-value) was calculated using the SPSS statistics software (SPSS 26.0). Statistical method was selected based on whether the calculated data follows a normal distribution. A p-value lower than 0.05 was considered to be significant.

3.4   Results

3.4.1 In vitro characterization

The scaffolds were successfully printed and coated, and the samples remained intact without any fractures throughout the entire experimental process. The amorphous layer had a Ca/P ratio of 1.78, while the crystalline layer had a Ca/P ratio of 1.63. The loading of BMP-2 (266±41 µg per scaffold) was further confirmed by ELISA technique.

3.4.1.1 Mechanical test

With respect to the mechanical properties of Ti64 and CaP, it is unlikely that the mechanical properties of the scaffold will be changed due to the addition of biomimetic CaP coating. The mechanical test revealed that the compressive strength and elastic modulus of the tested Ti64

scaffolds were 17.4±0.7 MPa and 1.64±0.12 GPa, respectively.

3.4.1.2 Micro-CT scan

The total porosity of the scaffolds in the three groups was determined by micro-CT: G1, 84.8%; G2, 83.8%; G3, 83.8%. The presence of the biomimetic CaP coating slightly reduced the total porosity of the scaffold. Moreover, the actual porosity of the Ti64 scaffold was lower than that of the designed porosity (88%) because of the existence of unmelt pools formed during sintering.

3.4.1.3 SEM and EDS scan

Figures 3.4-3.6 show the SEM images of the surface and cross-sectional characteristics of three groups of scaffolds, respectively. SEM pictures demonstrate the rough metal surface induced by the sintering of alloy powder particles (**Figure 3.4b**) and the coated scaffold surface completely covered with micro/nanostructures (**Figure 3.4d and f**). The high magnified SEM image contrasts the rough surface of the Ti scaffold with the crystallized coating surface, which is composed of vertically stacked plate-like nano-thick crystallites (**Figure 3.5**). On cross-sections, a clear boundary can be observed between the base layer of the amorphous CaP and the outer layer of the crystalline CaP (the yellow dotted line in **Figure 3.6**). In addition, clear boundaries can also be observed between the whole CaP coating, the scaffold and the epoxy resin under the BSE mode (**Figure 3.6e and f**). According to the previous research [24], the amorphous layer is a dense and homogenous CaP film made up of spherical CaP pellets with a diameter of about 100nm that serves as seeds for the crystalline layer's secondary nucleation. Previous studies have also proved that the crystallites possess the features typical of an OCP crystal structure through the X-ray diffraction and the Fourier transform infrared spectroscopy examinations [20, 21], irrespective of the absence or presence of BMP-2 [20]. Moreover, the form of the coating was not affected by the incorporation of BMP-2.

Results of strut thickness and coating thickness measurement are shown in **Figure 3.7**. The mean strut thicknesses of scaffolds in G2 (316.8 ± 19.1µm) and G3 (322.31 ± 12.9µm) were shown to be significantly higher than that of the scaffolds in G1 (293.17 ± 27.2µm, $p < 0.05$). No significant difference was observed in the mean strut thickness between G2 and G3. The average coating thickness was significantly higher on the outer part of the scaffold than in the center of the scaffold in G2 (17.20 ± 2.03µm vs. 7.12 ± 1.24µm, $p < 0.05$), and the same result was observed in G3 (17.52 ± 2.35µm vs. 6.76 ± 0.84µm, $p < 0.05$). No significant difference was observed in the mean coating thickness between G2 and G3. EDS results confirmed that chemical elements including C, O, Na, Mg, Si, P, Cl and Ca could be observed in the biomimetic CaP coating. There was no apparent change in the elemental composition of the coatings between G2 and G3 (Appendix 1).

Mg^{2+} is used to inhibit crystal growth and promote the formation of an amorphous CaP layer, and it only exists in the amorphous layer, not the crystalline layer [16].
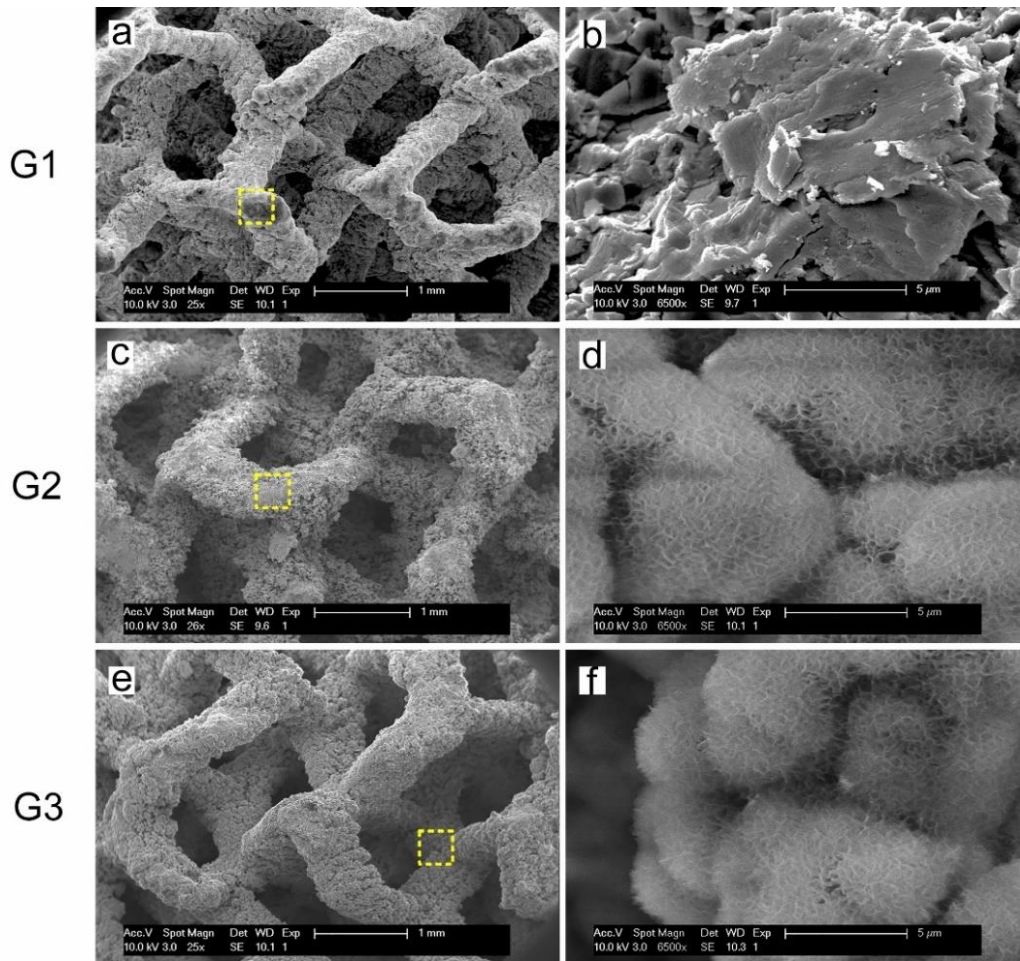
Figure 3.4. SEM images of the surface characteristics of scaffold in G1 (a and b), G2 (c and d) and G3 (e and f). The images in the right column are the magnified images of the yellow boxes in the left column.
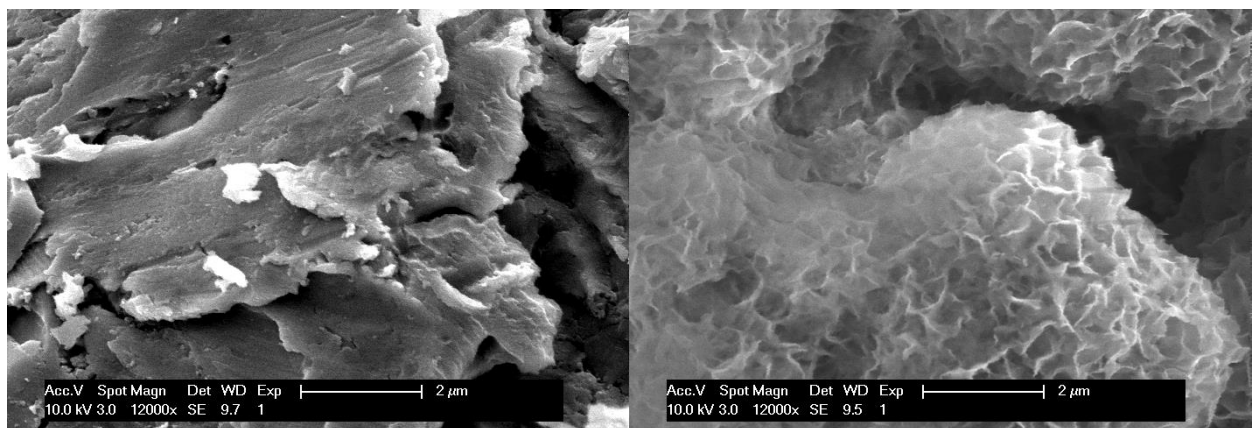

Figure 3.5. SEM images contrasting the coarse scaffold surface with the coating surface, which is made up of nano-thick plate-like crystals.
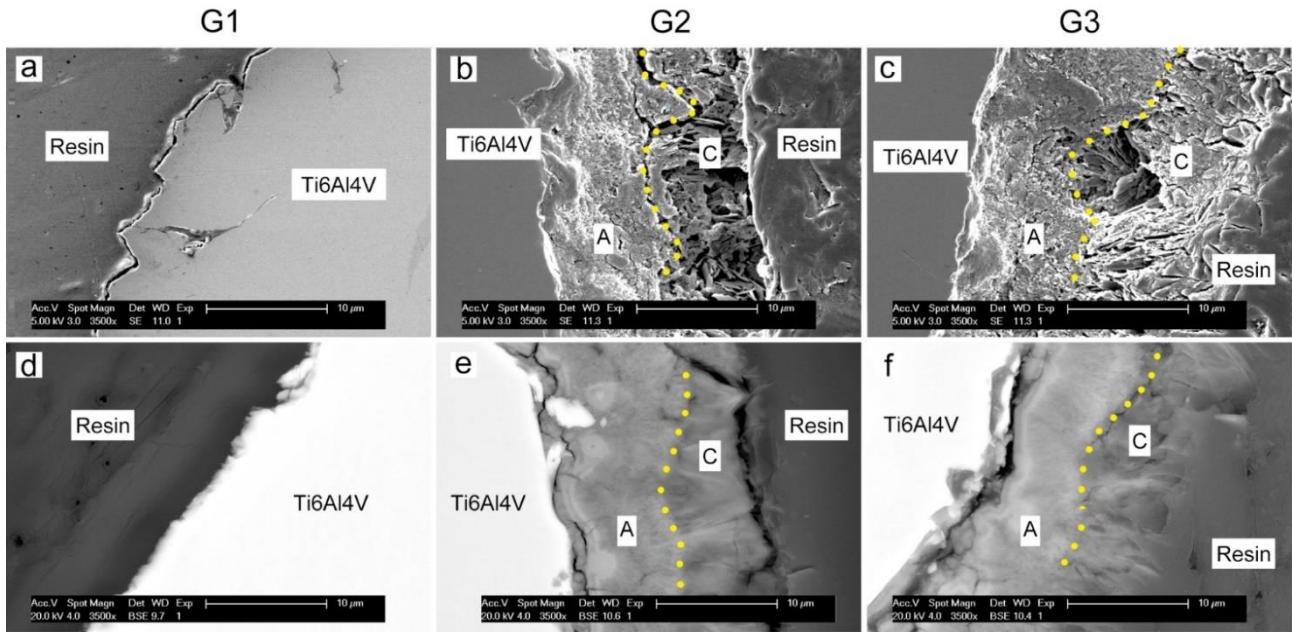
Figure 3.6. SEM images of the cross-sectional characteristics of scaffold in G1, G2 and G3. (a) to (c) are pictures viewed in the SE mode, and (d) to (f) are pictures viewed in the BSE mode. The yellow dotted line represents the boundary between the amorphous CaP coating (A) and the crystalline CaP coating (C).
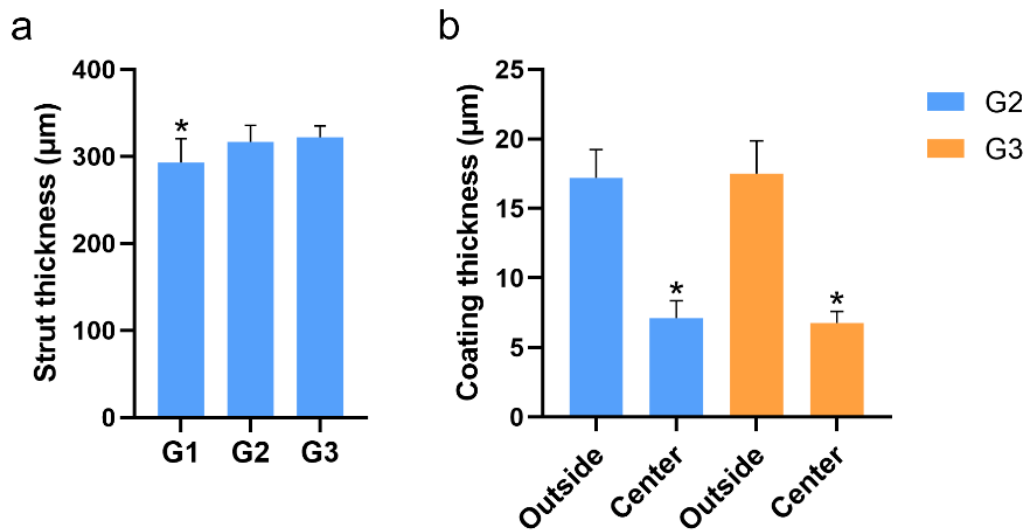
Figure 3.7. measurement results of strut thickness and coating thickness. * in (a) means the strut thickness of scaffolds in G2 and G3 was significantly different from that in G1; * in (b) means the coating thickness in the center of the scaffold was significantly different to that on the outside part of the scaffold in G2 and G3.

3.4.2 In vivo study

All animals remained alive by the end of the study. The wounds of two animals were not healed one week after the surgery and the scaffolds were rejected from the surgical site due to the inflammatory reactions. Consequently, these two animals were excluded from the subsequent study. The experimental sites in the remaining four animals healed uneventfully without significant complications. In total, there are four valid samples for our analysis in each group.

3.4.2.1 Histologic observation

Figure 3.8 showed that in G1 and G2, only loose connective tissues were observed in the scaffold. Bone induction is seen only in the BMP-2 integrated biomimetic CaP coating (G3, **Figure 3.8c**). The formed trabeculae were separated from the muscle tissue by a layer of infiltrated soft tissue (**Figure 3.8f**).

Figure 3.9 showed the details of the new bone in G3. The new bone was either attached to the scaffold surface, or grew free in the space between the scaffold struts, and the bone islands were interconnected to form a trabecular network. Around the trabeculae is the loose connective tissue full of new-forming blood vessels (**Figure 3.9a**). Direct BIC can be found (**Figure 3.9b and c**).The new-formed bone was normal in appearance, and the mineralized bone matrix, osteoblasts, osteoclasts, and osteocytes were visible (**Figure 3.9d**).
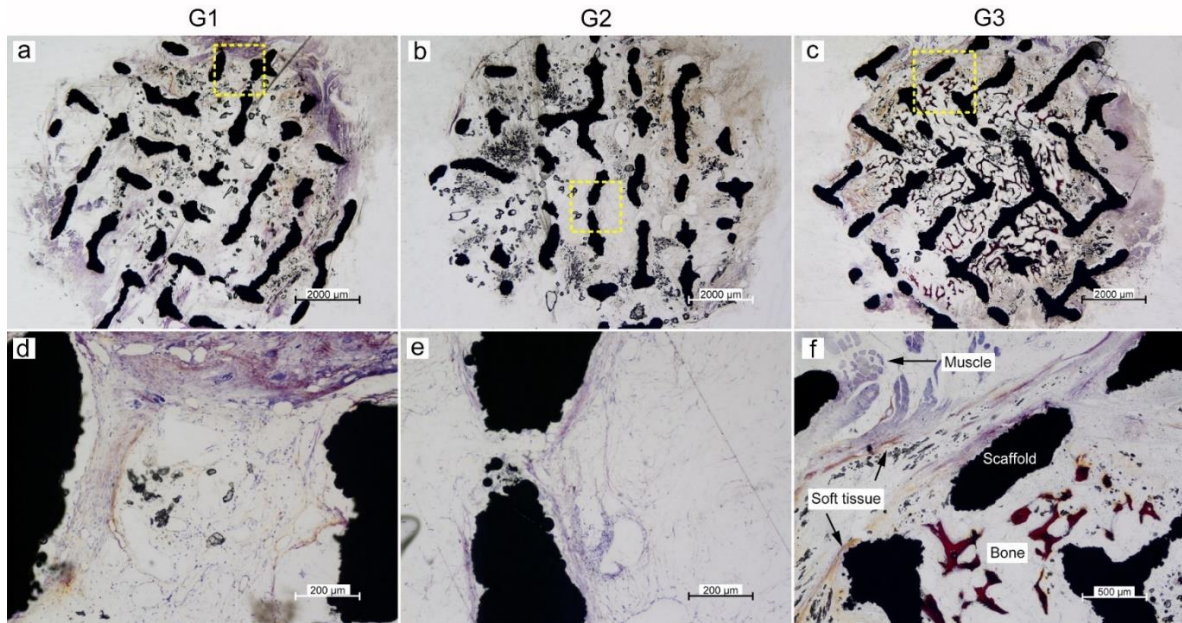
Figure 3.8. Histological images of scaffold in G1 (a and d), G2 (b and e) and G3 (c and f). The images in the bottom row are the magnified images of the yellow boxes in the top row. (f) indicates that the infiltrated soft tissue functions as a boundary between the muscle tissue and the new bone.
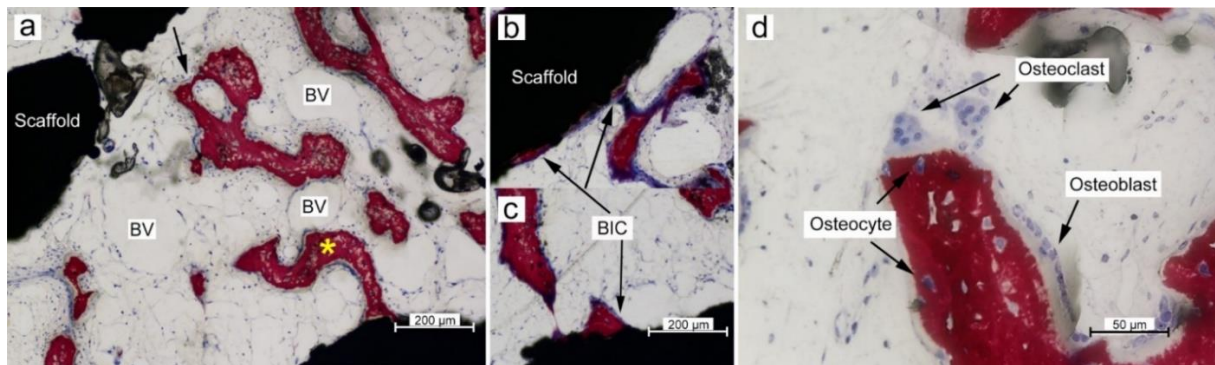
Figure 3.9. details of the new bone in the histological images of scaffold in G3. (a) shows the free bone islands and those attached to the scaffold surface (marked by *), and the interconnected trabecular network (arrows). The surrounding loose connective tissue is full of forming blood vessels (BV). (b and c) show the direct BIC between new bone and the scaffold. (d) shows the new bone with osteocytes, and the aligned osteoblasts and osteoclasts.

3.4.2.2 Histomorphometrical analysis

Histomorphometrical analysis was only performed in G3 (sample n =4, slice n =20) since no new-formed bone was observed in other two groups. The cell density in the new bone was 1274 ± 307 /mm^2. Results of BA/TA, BIC and BA measurements are shown in **Figure 3.10**.

In the horizontal direction of the scaffold, ROI5 was mostly filled with muscle fibers and soft tissues grown from the surrounding muscle tissues, so new bone formation has hardly been observed in ROI5. Normal distribution detection revealed that, except for ROI5, the BA/TA and BIC values of the other four ROI groups were consistent with normal distribution characteristics. The Kruskal-Wallis H test results showed that the distributions of BA / TA and BIC values between ROI1 to 5 groups were not all the same, and the differences were statistically significant ($p < 0.05$). The post-hoc pairwise comparison revealed that the distribution of BA/TA and BIC values in ROI5 were significantly different from that in each of the other four ROI groups ($p < 0.05$), between which there was no significant difference ($p > 0.05$). To improve the analytical precision, the ANOVA test was further applied between ROI1 to 4 groups, and no significant differences in mean BA/TA (F =2.71, p =0.05) and BIC (F =2.51, p =0.06) values were found between these four groups. The results revealed that the new bone expanded uniformly within a range of 4mm from the center of the scaffold, and the soft tissue could only penetrate around 1mm into the scaffold.

In the longitudinal direction of the scaffold, The BA/TA and BA values in slices 1 to 5 groups all followed a normal distribution, but not all of the BIC values did. ANOVA test showed no significant difference in the mean BA/TA (F =0.72, p =0.58) and BA (F =0.89, p =0.49) values between slice 1 to 5 groups. Kruskal-Wallis H test showed that no significant difference was found in the distribution of BIC values between slice 1 to 5 groups (p =0.81). These results indicate that the new bone develops uniformly along the scaffold's long axis.
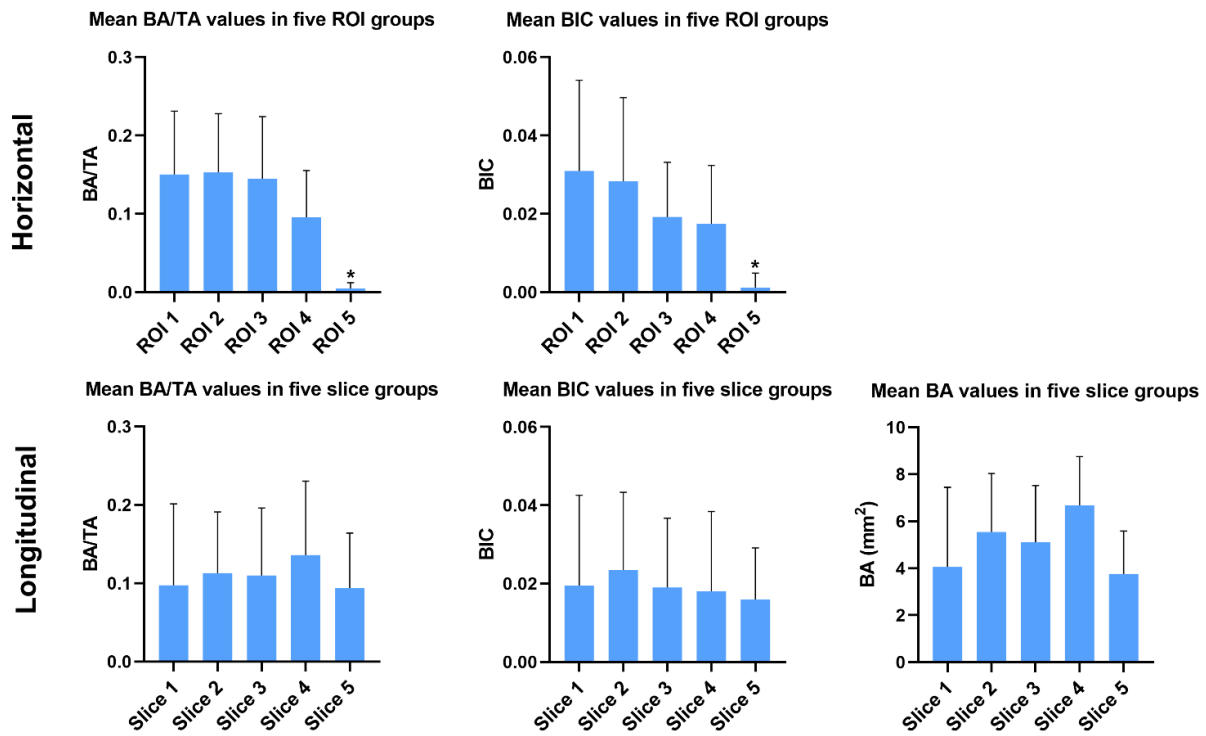
Figure 3.10. BA/TA, BIC and BA measurements in five ROI groups and five slice groups. *means the BA/TA value in ROI 5 group was significantly different from that in ROI 1 to 4 groups in BA/TA and BIC measurements.

3.5   Discussion

At present, research on AM scaffold focuses primarily on mechanical properties in vitro. factors, including design parameters, printing techniques and selection of coatings, are closely linked to the biological characteristics of the scaffold, which can be most effectively verified by in vivo studies.

Our research is the first study combining BMP-2 integrated biomimetic CaP coating with porous Ti64 scaffold, and our result has shown that this combination promotes ectopic bone formation. One of the findings in our study is that the addition of BMP-2 determines the ectopic bone formation, and the new bone tissue was observed only in G3. Only loose connective tissue was observed around the scaffold struts in G1 and G2, meaning that the biomimetic CaP coating alone was unable to stimulate bone regeneration in the muscle pouches made in beagle dogs. Another interesting finding is that in G3, although the coating thickness on the center and the outside of the scaffold was not uniform, the BA/TA,BIC and BA values were not significantly different between five slice groups in the longitudinal direction. Besides, in the horizontal direction, there were no significant differences in BA/TA and BIC values between five ROI groups. This implies that the apparent new trabeculae in the scaffold were evenly distributed both longitudinally and horizontally.

We assumed that the infiltrated soft tissue 'wrapped' the released BMP-2 and allowed it to spread in limited space within the scaffold, resulting in the new trabeculae spreading evenly throughout the scaffold.

BMP-2 belongs to the transforming growth factor-beta family and induces ectopic bone formation [25]. BMP-2 integrated biomimetic CaP composites have been prepared and coated to various materials (including Ti64) in previous in vitro and in vivo studies. The coated composite preserves the biological activity of the rat bone marrow stromal cells while also increasing their ALP activity [17]; and in another study, increases the proliferation and promote the osteogenic differentiation of MC3T3-E1 cells [26]. In addition, the long-term sustainable osteogenic differentiation capacity of the BMP-2 coating has been demonstrated at both ectopic [27-29] and orthotopic [30] sites in vivo. In addition, the long-term sustainable osteogenic differentiation capacity of the BMP-2 coating has been demonstrated at both ectopic [27-29] and orthotopic [30] sites in vivo. However, a previous study revealed that a single, rapid uptake of high dose BMP-2 stimulated resorption of newly formed bone [28]. Therefore, ensuring a long-term effect of BMP-2 on osteogenic differentiation and limiting extensive bone resorption requires a drug loading system (carrier) which permits a steady and sustained release of BMP-2.

Biomimetic CaP coating was used as a carrier of BMP-2 in this study. The micro/nano hybrid structure has been shown in studies to improve osteoblast adhesion, proliferation, and differentiation. Moreover, the micro/nano structure can provide a larger specific surface area, which can improve protein anchoring and adsorption effectiveness and ability [31]. The first precipitated amorphous CaP particles in the biomimetic coating act as nucleation sites for the subsequent crystal growth, and OCP crystals grow epitaxially on the surface of this seeding layer [32]. The morphology of the amorphous CaP particles changes when they come into contact with the supersaturated CaP solution, which was manifested as an increase in particle size and partial dissolution, which then initiates the nucleation and growth of OCP crystals perpendicular to the seeding layer [33].

It is hypothesized that the BMP-2 was liberated from the inorganic matrix based on the synergistic resorptive activities of the foreign body giant cells and the osteoclasts [20]. Moreover, this cell-mediated release process for BMP-2 is supposed to be similar to the physiological bone remodeling process by virtue of growth factors being released from the bone matrix during its degradation [16, 17]. In addition, the surmise is supported by previous studies showing that the bone induction performance of the coating-integrated BMP-2 depot was markedly higher than the utilization of a surface-absorbed BMP-2 depot [20, 34].

BMP-2 is released in a slow MC3T3-E1and sustained mode since the distribution density of BMP-2 is fixed in the supersaturated CaP solution [17, 34, 35]. The release mechanism of coating-integrated BMP-2 was determined in vivo previously by using a radiolabeled osteogenic agent (^{131}I-BMP-2) [36]. Results showed that 50% of the BMP-2 loaded was released over five weeks (5% to 10% weekly), and a stable and effective osteogenic response was obtained with a low pharmacological dose of BMP-2. Apart from being a carrier, the integration of BMP-2 also strengthens the CaP coating by surrounding the brittle CaP crystals and enhances the coating's binding to the underlying Ti alloy substrate [37]. This kind of mutual benefit grants biomimetic CaP coating a distinct advantage over other BMP-2 carriers in bone reconstruction. However, in the current study, we must admit that the low concentration ratio of BMP-2 to CaP makes it difficult to judge the strengthening effect of BMP-2. To maximize coating strength and biocompatibility, further research is required to optimize the amount of protein integrated into the coating.

We hypothesize that BMP-2 was slowly released from the progressively degraded CaP coating in a cell-mediated manner and induced an even distribution of new bone formation within the scaffold. Osteoblasts and osteoclasts around the trabeculae help to expand and reshape the trabeculae into the cancellous bone. New blood vessels around the trabeculae carry the bone progenitor cells, nutrients, and oxygen. New bone trabeculae were formed through a direct ossification mechanism instead of the enchondral mechanism, which was also identified in some previous in vivo studies [20]. Direct ossification occurs in a mechanically stable environment provided by the porous scaffold [20]. The surface of the scaffold had a thicker biomimetic CaP coating and a higher amount of integrated-in BMP-2. However, we observed that the 1 mm-thick outer rim of our scaffolds was occupied by only soft tissue. The absence of direct ossification could be explained by continuous exposure of the outer rim to a mechanically unstable environment. The latter would be induced via the frictional contact between the scaffold surface and the beagle dog's back muscles during movement.

In this study, the Ti64 scaffold was designed to meet the optimal pore size (100 to 1200μm) [38] and porosity (80% to 90%) [39] for cell proliferation and migration, as well as the smooth delivery of oxygen and nutrients. In addition, the scaffold mimicked the cancellous bone's mechanical characteristics, that is, an elastic modulus of 0.2 - 2GPa and compressive strength value of 2 - 80MPa [40]. The porous system's mechanical properties can be easily controlled by changing the porous structure, and the balance between these two aspects must be maintained. Apart from pore size and porosity, the pore unit's shape also significantly impacts the scaffold's biological and mechanical properties. However, it should be noted that, since porosity and pore size may also

change along with variations in the pore unit, it is difficult to determine which pore unit is most conducive to new bone formation. Few articles have explicitly examined the pore unit's impact on the scaffold's osteogenesis capability. With a view to optimizing pore size and porosity, we selected the rhombic dodecahedron unit, which has been extensively researched in the designing and manufacturing of porous bone scaffold [41-43], in our experiment. Several other studies have also developed 3D-printed porous Ti64 scaffolds with mechanical characteristics similar to cancellous bone, with porosity varying from 22% to 80% [44-47]. A balance has been established between high porosity and appropriate mechanical property in our designed scaffold compared to their findings.

Despite our major advancement in ectopic bone formation, our study presents some limitations. Considering the scaffold's limited permeability, the supersaturated CaP solution could not fully penetrate every part of the scaffold. As a result, the coating thickness in the middle of the scaffold was lower than that at the scaffold's surface. The limitation of permeability was partly due to the porous structure's design and, on the other hand, to the fact that a large number of Ti alloy powders were only partially remelted during the AM manufacturing process, resulting in high surface roughness of the scaffold [48]. According to our hypothesis, the infiltrated soft tissue 'wrapped' BMP-2 and allowed for good ectopic bone formation in this study. However, ensuring a uniform thickness of the coating would improve the overall osteogenic differentiation capacity of the scaffold in an open environment. Currently, the AM procedure inevitably creates defects such as irregular pore shapes or micro-pores within the AM components and thus requires further research in optimizing the AM parameter management and processing technique. A second limitation relates to the infiltration of soft connective tissue which hinders bone formation. The limited bone formation would not be conductive to the fixation of the porous scaffold if the scaffold has been applied to repair the bone defect. To prevent rapid ingrowth of soft tissue within the pores, the use of a collagen membrane should be considered to separate the scaffold's surface from the soft tissue.

Some critical challenges still remain in the phase of biomaterial development and scaffold design. First, more and more new biomaterials, such as Ti-7.5Mo alloy, have been explored with AM technology's advancement. Ti-7.5Mo alloy has been shown to have a lower elastic modulus and more potent strength/modulus combination than Ti and Ti alloy; it is also known to be a material of excellent corrosion resistance and biocompatibility [49]. Several previous studies have successfully developed Ti-7.5Mo alloy scaffolds, which comply with cancellous bone's mechanical requirements [49-51]. Using in vivo experiments to confirm this scaffold's biocompatibility is also our aim in the next step. Secondly, the perfect bone tissue scaffold material should be biodegradable, leaving

only healthy bone tissue within the human body. Thirdly, as for the scaffold design, there is still a lack of a unified standard. The optimized option of pore unit, for example, has not yet been determined. Future studies should concentrate on a general understanding of how the scaffold's geometric parameters impact the scaffold's mechanical and biological behavior. In the fourth place, the natural bone consists of four different levels of pore sizes, and the composition of the bone continually varies according to its stress state [52]. Functional grading scaffolds can mimic the shape and structure of natural bones and encourage tissue growth while maintaining mechanical strength [53]. Functionally grading scaffolding has also been widely studied in recent years, in which porosity varies within the scaffold with a particular gradient [54-56]. This structure can also be considered to repair long bone defects, which is also a key element in future research. Finally, the sterilization of BMP-2 coated implants is an important issue that has not been adequately addressed. Guillot et al. found that the osteoinductive potential of BMP-2 coated on Ti implant was retained following sterilization with the method of 25kGy gamma radiation, and the amount of BMP-2 remaining after irradiation was still sufficient to induce new bone tissue [57]. Furthermore, 25kGy gamma radiation sterilization has been used to sterilize biological materials containing BMP-2 in other studies [58-61]. This potential sterilization method may be applied to the future industrial production of the scaffold, but more research is required to verify its clinical safety and effectiveness.

3.6   Conclusion

In conclusion, we have manufactured a porous Ti64 scaffold with similar mechanical properties to the cancellous bone in a beagle dog model. Using biomimetic CaP coating as a carrier, BMP-2 was attached to the scaffold's surface to promote ectopic bone formation. BMP-2 integrated biomimetic CaP coating greatly improved new bone formation in vivo. The proposed coating of a 3D-printed porous scaffold seems to offer some future potential for bone tissue reconstruction, with more studies needed to assess its clinical feasibility.

3.7   References

1.   Haleem A, Javaid M, Khan RH, Suman R. 3D printing applications in bone tissue engineering. Journal of clinical orthopaedics and trauma. 2020;11:S118-S24.

2.   He S-y, Zhang Y, Zhou Y, Bao N, Cai Y, Zhou P, et al. Modeling osteoinduction in titanium bone scaffold with a representative channel structure. Materials Science and Engineering: C. 2020;117:111347.

3. Zhang L-C, Chen L-Y, Wang L. Surface modification of titanium and titanium alloys: technologies, developments, and future interests. Advanced Engineering Materials. 2020;22:1901258.

4.   Dong Y, Tang J, Wang D, Wang N, He Z, Li J, et al. Additive manufacturing of pure Ti with superior mechanical performance, low cost, and biocompatibility for potential replacement of Ti-6Al-4V. Materials & Design. 2020;196:109142.

5.   Kaur M, Singh K. Review on titanium and titanium based alloys as biomaterials for orthopaedic applications. Materials Science and Engineering: C. 2019;102:844-62.

6.   Qu H. Additive manufacturing for bone tissue engineering scaffolds. Materials Today Communications. 2020;24:101024.

7.   Ali MA, Rajabi M, Sali SS. Additive manufacturing potential for medical devices and technology. Current Opinion in Chemical Engineering. 2020;28:127-33.

8.   Begum SR, Kumar MS, Pruncu C, Vasumathi M, Harikrishnan P. Optimization and fabrication of customized scaffold using additive manufacturing to match the property of human bone. Journal of Materials Engineering and Performance. 2021:30:1-12.

9.   Zhu Y, Wagner WR. Design principles in biomaterials and scaffolds. Principles of Regenerative Medicine. 2019: 505-22.

10. Kim H-B, Hayashi M, Nakatani K, Kitamura N, Sasaki K, Hotta J-i, et al. In situ measurements of ion-exchange processes in single polymer particles: laser trapping microspectroscopy and confocal fluorescence microspectroscopy. Analytical chemistry. 1996;68:409-14.

11. Dee P, You HY, Teoh S-H, Le Ferrand H. Bioinspired approaches to toughen calcium phosphate-based ceramics for bone repair. Journal of the Mechanical Behavior of Biomedical Materials. 2020;112:104078.

12. Mumith A, Cheong VS, Fromme P, Coathup MJ, Blunn GW. The effect of strontium and silicon substituted hydroxyapatite electrochemical coatings on bone ingrowth and osseointegration of selective laser sintered porous metal implants. PLoS One. 2020;15:e0227232.

13. Bose S, Banerjee D, Shivaram A, Tarafder S, Bandyopadhyay A. Calcium phosphate coated

3D printed porous titanium with nanoscale surface modification for orthopedic and dental applications. Materials & design. 2018;151:102-12.

14. Biemond JE, Hannink G, Verdonschot N, Buma P. Bone ingrowth potential of electron beam and selective laser melting produced trabecular-like implant surfaces with and without a biomimetic coating. Journal of Materials Science-Materials in Medicine. 2013;24:745-53.

15. Casanova MR, Oliveira C, Fernandes EM, Reis RL, Silva TH, Martins A, et al. Spatial immobilization of endogenous growth factors to control vascularization in bone tissue engineering. Biomaterials science. 2020;8:2577-89.

16. Lin X, Chen J, Liao Y, Pathak JL, Li H, Liu Y. Biomimetic Calcium Phosphate Coating as a Drug Delivery Vehicle for Bone Tissue Engineering: A Mini-Review. Coatings. 2020;10:1118.

17. Liu Y, Hunziker EB, Layrolle P, De Bruijn JD, De Groot K. Bone morphogenetic protein 2 incorporated into biomimetic coatings retains its biological activity. Tissue engineering. 2004;10:101-8.

18. Ding L, Sun ZG, Liang ZL, Li F, Xu GL, Chang H. Investigation on Ti-6Al-4V Microstructure Evolution in Selective Laser Melting. Metals. 2019;9:1270.

19. Ninpetch P, Kowitwarangkul P, Mahathanabodee S, Chalermkarnnon P, Rattanadecho P. Computational investigation of thermal behavior and molten metal flow with moving laser heat source for selective laser melting process. Case Studies in Thermal Engineering. 2021;24:100860.

20. Liu Y, De Groot K, Hunziker EB. BMP-2 liberated from biomimetic implant coatings induces and sustains direct ossification in an ectopic rat model. Bone. 2005;36:745-57.

21. Liu Y, Layrolle P, de Bruijn J, van Blitterswijk C, de Groot K. Biomimetic coprecipitation of calcium phosphate and bovine serum albumin on titanium alloy. Journal of Biomedical Materials Research: An Official Journal of The Society for Biomaterials, The Japanese Society for Biomaterials, and The Australian Society for Biomaterials and the Korean Society for Biomaterials. 2001;57:327-35.

22. Engvall E, Perlmann P. Enzyme-linked immunosorbent assay (ELISA) quantitative assay of immunoglobulin G. Immunochemistry. 1971;8:871-4.

23. ASTM E. Standard test methods of compression testing of metallic materials at room temperature. West Conshohocken, PA: ASTM International. 2000:98-105.

24. Lin X, De Groot K, Wang D, Hu Q, Wismeijer D, Liu Y. Suppl 1-M4: A review paper on biomimetic calcium phosphate coatings. The open biomedical engineering journal. 2015;9:56.

25. Halloran D, Durbano HW, Nohe A. Bone morphogenetic protein-2 in development and bone homeostasis. Journal of Developmental Biology. 2020;8:19.

26. Zhang X, Lin X, Liu T, Deng L, Huang Y, Liu Y. Osteogenic enhancement between icariin and bone morphogenetic protein 2: A potential osteogenic compound for bone tissue engineering. Frontiers in pharmacology. 2019;10:201.

27. Wu G, Liu Y, Iizuka T, Hunziker EB. The effect of a slow mode of BMP-2 delivery on the inflammatory response provoked by bone-defect-filling polymeric scaffolds. Biomaterials. 2010;31:7485-93.

28. Wu G, Hunziker EB, Zheng Y, Wismeijer D, Liu Y. Functionalization of deproteinized bovine bone with a coating-incorporated depot of BMP-2 renders the material efficiently osteoinductive and suppresses foreign-body reactivity. Bone. 2011;49:1323-30.

29. Wu G, Liu Y, Iizuka T, Hunziker EB. Biomimetic coating of organic polymers with a protein-functionalized layer of calcium phosphate: the surface properties of the carrier influence neither the coating characteristics nor the incorporation mechanism or release kinetics of the protein. Tissue Engineering Part C: Methods. 2010;16:1255-65.

30. Liu T, Wu G, Wismeijer D, Gu Z, Liu Y. Deproteinized bovine bone functionalized with the slow delivery of BMP-2 for the repair of critical-sized bone defects in sheep. Bone. 2013;56:110-8.

31. Jiang P, Liang J, Song R, Zhang Y, Ren L, Zhang L, et al. Effect of octacalcium-phosphate-modified micro/nanostructured titania surfaces on osteoblast response. ACS applied materials & interfaces. 2015;7:14384-96.

32. Barrere F, Layrolle P, Van Blitterswijk C, De Groot K. Biomimetic calcium phosphate coatings on Ti6Al4V: a crystal growth study of octacalcium phosphate and inhibition by Mg2+ and HCO3−. Bone. 1999;25:107-11.

33. Barrere F, Layrolle P, Van Blitterswijk C, De Groot K. Biomimetic coatings on titanium: a crystal growth study of octacalcium phosphate. Journal of Materials Science: Materials in Medicine. 2001;12:529-34.

34. Hunziker EB, Enggist L, Küffer A, Buser D, Liu Y. Osseointegration: the slow delivery of BMP-2 enhances osteoinductivity. Bone. 2012;51:98-106.

35. Liu Y, Hunziker E, de Groot K, Layrolle P, editors. Introduction of ectopic bone formation by BMP-2 incorporated biomimetically into calcium phosphate coatings of titanium-alloy implants. Key Engineering Materials. 2003;240:667-70

36. Liu Y, Schouten C, Boerman O, Wu G, Jansen JA, Hunziker EB. The kinetics and mechanism of bone morphogenetic protein 2 release from calcium phosphate−based implant−coatings. Journal of Biomedical Materials Research Part A. 2018;106:2363-71.

37. Liu Y, Hunziker E, Randall N, De Groot K, Layrolle P. Proteins incorporated into biomimetically

prepared calcium phosphate coatings modulate their mechanical strength and dissolution rate. Biomaterials. 2003;24:65-70.

38. Yan Y, Chen H, Zhang H, Guo C, Yang K, Chen K, et al. Vascularized 3D printed scaffolds for promoting bone regeneration. Biomaterials. 2019;190:97-110.

39. Du Y, Guo JL, Wang J, Mikos AG, Zhang S. Hierarchically designed bone scaffolds: From internal cues to external stimuli. Biomaterials. 2019;218:119334.

40. Gibson L. The mechanical behaviour of cancellous bone. Journal of biomechanics. 1985;18:317-28.

41. Huang G, Pan S-T, Qiu J-X. The osteogenic effects of porous Tantalum and Titanium alloy scaffolds with different unit cell structure. Colloids and Surfaces B: Biointerfaces. 2021;210:112229.

42. Eltlhawy B, El-Midany T, Fouda N, Eldesouky I, editors. Finite Element Assessment of a Porous Tibial Implant Design Using Rhombic Dodecahedron Structure. Solid State Phenomena. 2021;318:71-81.

43. Abate KM, Nazir A, Yeh YP, Chen JE, Jeng JY. Design, optimization, and validation of mechanical properties of different cellular structures for biomedical application. International Journal of Advanced Manufacturing Technology. 2020;106:1253-65.

44. Wauthle R, Van Der Stok J, Yavari SA, Van Humbeeck J, Kruth JP, Zadpoor AA, et al. Additively manufactured porous tantalum implants. Acta Biomaterialia. 2015;14:217-25.

45. Zhang B, Pei X, Zhou C, Fan Y, Jiang Q, Ronca A, et al. The biomimetic design and 3D printing of customized mechanical properties porous Ti6Al4V scaffold for load-bearing bone reconstruction. Materials & Design. 2018;152:30-9.

46. Surmeneva MA, Surmenev RA, Chudinova EA, Koptioug A, Tkachev MS, Gorodzha SN, et al. Fabrication of multiple-layered gradient cellular metal scaffold via electron beam melting for segmental bone reconstruction. Materials & Design. 2017;133:195-204.

47. Li G, Wang L, Pan W, Yang F, Jiang W, Wu X, et al. In vitro and in vivo study of additive manufactured porous Ti6Al4V scaffolds for repairing bone defects. Scientific reports. 2016;6:34072.

48. Vrancken B, Thijs L, Kruth J-P, Van Humbeeck J. Heat treatment of Ti6Al4V produced by Selective Laser Melting: Microstructure and mechanical properties. Journal of Alloys and Compounds. 2012;541:177-85.

49. Hsu H-C, Hsu S-K, Tsou H-K, Wu S-C, Lai T-H, Ho W-F. Fabrication and characterization of porous Ti-7.5 Mo alloy scaffolds for biomedical applications. Journal of Materials Science: Materials in Medicine. 2013;24:645-57.

50. Hsu H-C, Wu S-C, Hsu S-K, Chang T-Y, Ho W-F. Effect of ball milling on properties of porous

Ti-7.5 Mo alloy for biomedical applications. Journal of alloys and compounds. 2014;582:793-801.

51. Hsu H-C, Wu S-C, Hsu S-K, Tsai M-S, Chang T-Y, Ho W-F. Processing and mechanical properties of porous Ti-7.5 Mo alloy. Materials & Design. 2013;47:21-6.

52. Monzón M, Liu C, Ajami S, Oliveira M, Donate R, Ribeiro V, et al. Functionally graded additive manufacturing to achieve functionality specifications of osteochondral scaffolds. Bio-Design and Manufacturing. 2018;1:69-75.

53. Onal E, Frith JE, Jurg M, Wu X, Molotnikov A. Mechanical properties and in vitro behavior of additively manufactured and functionally graded Ti6Al4V porous scaffolds. Metals. 2018;8:200.

54. Wang S, Liu LL, Li K, Zhu LC, Chen J, Hao YQ. Pore functionally graded Ti6Al4V scaffolds for bone tissue engineering application. Materials & Design. 2019;168.

55. Khrapov D, Koptyug A, Manabaev K, Leonard F, Mishurova T, Bruno G, et al. The impact of post manufacturing treatment of functionally graded Ti6Al4V scaffolds on their surface morphology and mechanical strength. Journal of Materials Research and Technology. 2020;9:1866-81.

56. Lowen JM, Leach JK. Functionally graded biomaterials for use as model systems and replacement tissues. Advanced Functional Materials. 2020;30:1909089.

57. Guillot R, Gilde F, Becquart P, Sailhan F, Lapeyrere A, Logeart-Avramoglou D, et al. The stability of BMP loaded polyelectrolyte multilayer coatings on titanium. Biomaterials. 2013;34:5737-46.

58. Ražem D, Katušin-Ražem B. The effects of irradiation on controlled drug delivery/controlled drug release systems. Radiation physics and chemistry. 2008;77:288-344.

59. Ripamonti U, Van Den Heever B, Crooks J, Tucker M, Sampath T, Rueger D, et al. Long‒term evaluation of bone formation by osteogenic protein 1 in the baboon and relative efficacy of bone‒derived bone morphogenetic proteins delivered by irradiated xenogeneic collagenous matrices. Journal of Bone and Mineral Research. 2000;15:1798-809.

60. Wientroub S, Reddi AH. Influence of irradiation on the osteoinductive potential of demineralized bone matrix. Calcified tissue international. 1988;42:255-60.

61. Pekkarinen T, Jämsä T, Määttä M, Hietala O, Jalovaara P. Reindeer BMP extract in the healing of critical-size bone defects in the radius of the rabbit. Acta orthopaedica. 2006;77:952-9.

Article 4

BMP-2 integrated biomimetic CaP coating functionalized 3D-printed Ti scaffolds promotes bone formation in a dog model with bicortical bone defects

Yifei Gu[1], Yiwen Liu[3], Jeroen Van Dessel [1], Reinhilde Jacobs[1], Lei Tian*[3], Yi Sun*[1], Yuelian Liu*[2], Constantinus Politis[1]

[1] OMFS IMPATH research group, Department of Imaging & Pathology, Faculty of Medicine, KU Leuven and Department of Oral and Maxillofacial Surgery, University Hospitals Leuven, Leuven (3000), Belgium.

[2] Department of Oral Implantology and Prosthetic Dentistry, Academic Centre for Dentistry Amsterdam, University of Amsterdam and Vrije Universiteit Amsterdam, Amsterdam (1019), the Netherlands

[3] State Key Laboratory of Military Stomatology & National Clinical Research Center for Oral Diseases & Shaanxi Clinical Research Center for Oral Diseases, Department of Craniofacial Trauma and Orthognathic Surgery, School of Stomatology, FMMU, Xi'an (710000), China

4.1 Abstract

The repair of mandibular bicortical bone defects is challenging. Advanced AM techniques can produce Ti alloy scaffolds with overall porous structures that can be used to repair bone defects. Ti scaffolds lack osteoinductivity, and surface modification is required to improve their osteogenesis results. A BMP-2 integrated CaP coating was created in this study using a biomimetic approach and coated on the surface of porous Ti scaffolds fabricated by SLM. The coated and uncoated scaffolds were characterized by micro-CT, SEM, ICP-OES, and mechanical tests. Additionally, the osteogenic capacity of coated and uncoated scaffolds was examined in a beagle dog model of mandibular bicortical bone defects. Results showed that the Ti scaffolds had compressive strength and elastic modulus comparable to the human cortical bone. Compared to uncoated scaffolds, coated scaffolds had lower porosity and increased Tb.Th, volume, and surface area. The coating has a phase of OCP and a micro/nanoscaled surface structure appropriate for cell proliferation and adhesion. According to the existing micro-CT results, the coated Ti scaffold significantly enhanced bone regeneration eight weeks after implantation in the mandibular bicortical defect in the dog models. Hence, the integrated biomimetic CaP coating of BMP-2 can improve the osteogenic potential of porous Ti scaffolds and aid in the repair of bicortical bone defects.

Keywords: biomimetics; CaP; 3D-printing; BMP-2; Ti; bone substitutes

4.2   Introduction

A variety of factors can lead to defects of the maxillofacial bone, such as trauma, tumor surgery, or congenital conditions that affect the oral and maxillofacial regions. Due to a lack of blood supply, mandibular bicortical bone defects are particularly difficult to treat. The use of autologous or allogeneic bone grafts in treating bone defects is limited due to factors such as supply constraints, donor site morbidity, disease transmission, etc. [1]. As a result, BTE has received much attention. The success of BTE lies in the design and fabrication of porous scaffolds. The 3D-printed porous scaffolds have an interconnected network structure that encourages the ingrowth of the vascular system, which delivers oxygen and nutrients to cells while also helping remove waste products. Furthermore, by modifying the design parameters, the elastic modulus of the designed scaffold can be matched to that of the natural bone tissue, preventing stress shielding effect-induced scaffold failures [2]. 3D-printing technologies enable the manufacture of 3D porous scaffolds with precisely designed and fully interconnected pores, as well as configurable and appropriate properties [3].

Ti is biocompatible and has good osteoconductivity. The Ti also has high strength, low weight, and good plasticity [4]. Therefore, Ti shows excellent promise in the fabrication of porous scaffolds. However, Ti also has obvious disadvantages: Ti has a low osteoinductivity due to its surface inertness, which induces the formation of fibrous connective tissue at the bone-metal interface and affects bone regeneration [5]. Increased osteoinductivity of Ti scaffolds can be achieved through surface modification. Rough surfaces have more anchor points that enhance cell adhesion and improve cell viability and proliferation [6].

Bone and tooth enamel are primarily composed of CaP. CaP has received much research attention in orthopedics and research in dental implants due to their biocompatibility and capacity to directly bond with the bone [7]. CaP materials can promote the adhesion and proliferation of osteoblasts, help in implant osseointegration, and enhance the deposition of Ca-containing minerals [8]. CaP coatings have been shown to improve the biological activity of porous metal scaffolds, increase the formation of new blood vessels and bone inside the scaffold, and enhance tissue integration [9-11]. Traditional CaP coating fabrication techniques, such as plasma spraying, sol-gel processes, etc., suffer from problems such as uneven coating thickness, insufficient adhesion to the substrate, and high processing temperatures, which inhibit the addition of organic components to the coating [12-15]. Wet chemical technology provides the best solution to this problem. The biomimetic coating method involves immersing the metal implants in the simulated body fluid at physiological pH and temperature. In this way, the porous metal scaffolds can be successfully coated, improving the scaffold's biocompatibility and bioactivity [16]. The biomimetic coating technique provides better

control over the coating's crystal structure, morphology, and thickness, and is relatively simple and low-cost [17].

Most importantly, the mild fabrication conditions of the biomimetic coating method allow for the deposition of biomolecules and drugs together with the inorganic CaP layer together [18-20]. One of the most frequently used growth factors in BTE is BMP-2, which promotes the migration and proliferation of stem cells and enhances osteogenic differentiation. Despite this, BMP-2 has a few disadvantages, such as a short half-life time, side effects when overdosed, etc. The in vivo osteoinductive efficiency of BMP-2 highly depends on its delivery method [21]. The burst release of the BMP-2 fails to induce a sustained osteogenic response at the implantation site [22, 23]. To achieve long-term osteogenic effects and avoid unnecessary side effects, BMP-2 should be administered using a slow-release delivery system [24]. Biomimetic CaP coating is an excellent carrier for BMP-2, and the activity of BMP-2 can be fully preserved in the coating's inorganic components.

In previous studies, we achieved the sustained release of BMP-2 by incorporating BMP-2 into a biomimetic CaP coating [25-27]. Although this coating shows excellent potential in BTE, no direct evidence has been reported for the performance of the coating in combination with the porous scaffold in bone defects. In addition, the biosafety of this coating has not been comprehensively evaluated in vivo. Therefore, it is necessary to assess this scaffold's biocompatibility and bone repair ability in vivo, especially in large animal models that are more similar to humans in terms of the bone healing process.

The aim of the present study was to fabricate topologically ordered BMP-2 integrated biomimetic CaP coated porous Ti scaffold using SLM technique. The secondary objective was to study biocompatibility and bicortical bone defect repairing result of the fabricated scaffold using a beagle dog model.

4.3   Materials and Methods

4.3.1 Design and 3D-printing of the scaffold

A cubic scaffold (4*6*10mm) was designed with 3-MATIC software (Materialise, Leuven, Belgium), and a 2mm diameter hole was created in the scaffold center. All trabecular structures without or with only one connection point were removed, and a STL file was created. The scaffolds were fabricated using a 3D-printer (3D Systems DMP Flex 350 platform, Amnovis) using commercial pure Ti powder (Ti Grade 1, particle size 15-45μm).

The scaffold design parameters are listed in **Table 4.1**. In total, fourteen scaffolds were printed, of

which two scaffolds were used for in vitro evaluation, and twelve others were used for in vivo experiments. The scaffolds were randomly divided into two groups, each with seven scaffolds. Group 1(G1): uncoated scaffolds (**Figure 4.1a**); Group 2(G2): scaffolds with BMP-2 integrated biomimetic CaP coating (**Figure 4.1b**). Furthermore, six cubic scaffolds (15*15*15mm) were also printed for mechanical tests using the same design parameters as **Table 4.1**.

Table 4.1. Design parameters of the scaffold

	Pore shape	Rhombic dodecahedron
Design parameters	Pore size	660µm
	Porosity	87%
	Strut size	400µm
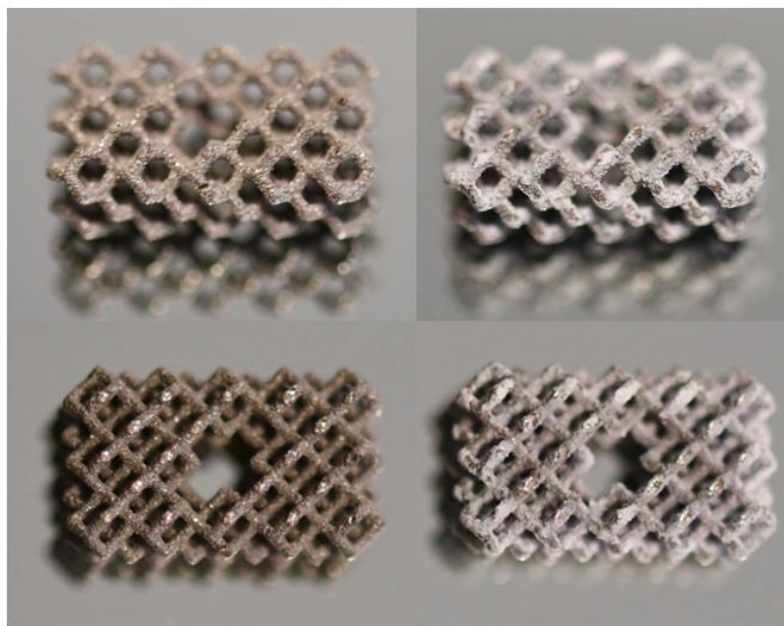
Figure 4.1. Scaffolds in G1 (left) and G2 (right), and their top views. A circular hole with a diameter of 2mm was designed in the middle of the scaffold. The hole was enlarged to form a cross after removing the trabecular structure without or with only one connection point in the STL file.

4.3.2 Preparation of the coating

The BMP-2 integrated biomimetic CaP coating was prepared as described in the previous paper [28]. In brief, scaffolds were first immersed under physiological conditions (37°C, pH =7.4) in 5x simulated body fluids for 24 hours. A uniform layer of amorphous CaP will be formed on the scaffold surface in this step. The amorphous layer is composed of small CaP particles that serve as nucleation sites for the subsequent growth of the crystalline CaP layer. The scaffolds were then autoclaved sterilized following a standard procedure. Afterwards, the scaffolds were immersed in supersaturated CaP solution under physiological conditions (37°C, pH =7.4) for 48 hours. In this

step, a crystalline CaP layer formed on top of the amorphous layer. Human recombinant BMP-2 (rhBMP-2, Shanghai Rebone Biomaterials Co., China) at a concentration of 5mg/L was added to the solution simultaneously with the precipitation of the crystalline layer. The Ca/P was detected by ICP-OES. Scaffolds were air-dried and stored at room temperature, and the entire coating preparation process was completed under sterile conditions.

4.3.3 In vitro characterization

4.3.3.1 Mechanical test

As the coating layer does not substantially alter the mechanical properties of the scaffold, the uncoated cubic scaffolds (15*15*15mm) were used for the mechanical test. Six scaffolds were compressed at room temperature at a crosshead speed of 1 mm/min with a universal tester (Instron 4467, Instron Corp., USA) and a load cell of 30kN. The compression test was conducted according to the ASTM E9-89a standard. The tension-strain curves were obtained, and elastic modulus and compressive strength of the cubic scaffolds were calculated.

4.3.3.2 Micro-CT scan

Scaffolds were scanned for porosity with a micro-CT scanner (Skyscan 1272, Bruker micro-CT, Kontich, Belgium). Two scaffolds were randomly selected from G1 and G2, respectively. The scanning parameters included: scanner voltage = 100kV; current = 100µA; rotation = 360°. Bruker NRecon software (version 1.7.3.0) was used to reconstruct scanned files, and then Bruker CTAn software (version 1.18.4.0) was used to analyze scanned images with a reconstruction threshold of 128-255.

4.3.3.3 SEM scan

Following micro-CT, the two scaffolds were scanned using SEM (Philips XL-30, FEI company, The Netherlands) to observe their surface morphology. The scaffolds were then embedded in epoxy resin (Epofix resin, Struers, Copenhagen, Denmark). A sander was used to remove the upper half of the scaffolds. The scaffold's cross-section was observed under SEM.

4.3.4 In vivo analysis

4.3.4.1 Study design

The Fourth Military Medical University Ethics Committee reviewed and approved this study (No.2018(K9-203)). Six healthy female beagle dogs were reared in separate cages and fed with a regular diet and drinking water every day. The feeding environment for experimental animals was constant [28]: temperature around 20°C; humidity 40-70%; and ventilation 10-20 times per hour.

Preoperatively, 8 * 10^6 Units of penicillin potassium were administered to the animals after a two-week acclimation and 12-hour fast. The animals were anesthetized with 3% pentobarbital sodium solution 1ml kg^{-1}, injected intravenously. The animals were immobilized in a recumbent position on their left side. Utilizing a dental handpiece and a bur, a buccolingual bone defect with a depth of 4mm and a length of 10mm was created at the lower edge of the mandible. The mandibular nerves and blood vessels were separated and severed after ligating both ends with 5-0 silk thread. After placing a scaffold in the bone defect, an orthopedic screw of 2mm length was used to fix the scaffold (**Figure 4.2**). The subcutaneous tissue and skin were then sutured sequentially, and the wound was cleaned with 75% alcohol and then tightly bandaged.
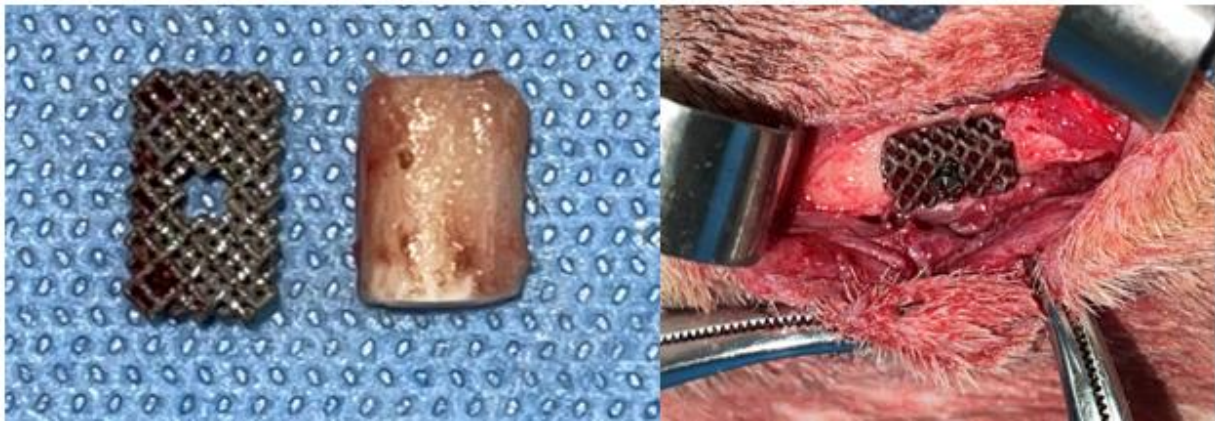
Figure 4.2. The process of creating bone defect and fixing the scaffold.

Another bone defect was created, and another scaffold was fixed in the right mandible after the beagle was switched to the right side. The two groups of scaffolds were arranged by computer-generated random numbers on either the left or right side of the mandible of the same animal. Immediately postoperative CT imaging revealed that the scaffold was successfully fixed to the mandible (Appendix 1). Anti-inflammatory drugs were given to the animals for five days following surgery. A daily examination of the animals' wound healing and general condition was conducted.

All animals were sacrificed eight weeks after surgery by overdosed anesthesia after the operation. The mandible was dissected, and the mandibular segment with the scaffold was removed, immersed in 4% paraformaldehyde, and stored at 4° C.

4.3.4.2 Micro-CT analysis

The mandibular fragments were scanned using a microtomography imaging system (AX-2000 Microfocus Industrial CT) to determine new bone formation. The micro-CT system had a maximum voltage of 120kV and a maximum current of 100μA. Additional scanning parameters include integration time of 0.6s, projection number of 1440, and resolution of 9μm. The scaffold area was

selected as the ROI. The new bone formation in the scaffolds was examined with the 3D image processing software VG Studio Max 3.0 (Volume Graphics, Heidelberg, Germany). The parameters analyzed included BV/TV, Tb.N, Tb.Th and Tb.Sp.

4.3.5 Statistical analysis

The data obtained from the in vitro characterization and animal study was analyzed and expressed as a mean ± deviation. By using SPSS statistics software (SPSS 26.0), the statistically significant difference (p-value) was calculated. Bone ingrowth into the scaffold between the two groups was compared by ANOVA analysis. A p-value of less than 0.05 was considered significant.

4.4   Results

4.4.1 In vitro characterization

The scaffolds were successfully printed, and the BMP-2 integrated biomimetic CaP coatings were prepared. We confirmed that the amorphous layer shows the hydroxyapatite phase, and the crystalline layer shows the OCP phase using Fourier-transform infrared spectroscopy and X-ray diffraction [29, 30]. Based on ICP-OES detection, the coating had a Ca/P ratio of 1.63, which shows a mixing of basal HA (Ca/P ratio 1.8) and surface OCP (Ca/P ratio 1.33).

4.4.1.1 Mechanical test

The mechanical test results showed that the scaffold had a compressive strength of 192.67±20.03Mpa (human cortical bone 33-193MPa) and elastic modulus of 23.15±4.88GPa (human cortical bone 3-30GPa). The compressive strength and elastic modulus of Ti scaffolds with design parameters used in this paper were comparable to those of human cortical bone.

4.4.1.2 Micro-CT analysis

The micro-CT results showed that the scaffold's porosity in G1 was 83.82%, the Tb.Th was 21.76 pixels, the scaffold volume was 8336356 pixels3, and the scaffold area was 2539 pixels2. In G2, the scaffold porosity was 79.20%; the Tb.Th was 26.71 pixels, which was 1.23 times that of G1. The scaffold volume was 10618830 pixel3, which was 1.27 times that of G1. the scaffold area was 1619924 pixel2, which was 638 times that of G1.

4.4.1.3 SEM scan

Figure 4.3 shows that in G1, the scaffold surface was covered with unmelted Ti droplets whose surfaces were smooth. Additionally, the scaffolds in G2 were also covered with Ti droplets, however the droplets were covered with micro/nano-scaled crystals on their surfaces. The plate-like crystals have sharp edges and are about 0.05-0.1μm thick. On the cross-section of the

scaffolds, the coating morphology was observed under both SE and BSE modes. The coating had a uniform distribution over the scaffold surface with a thickness of around 10-15μm (**Figure 4.4**).
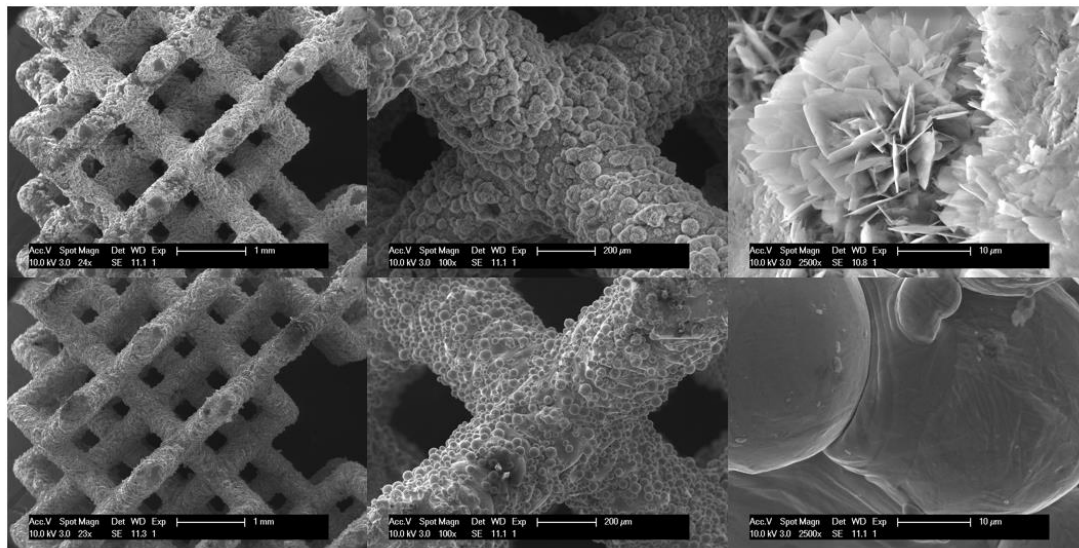

Figure 4.3. morphological observations of scaffolds in G1 (down) and G2 (up).
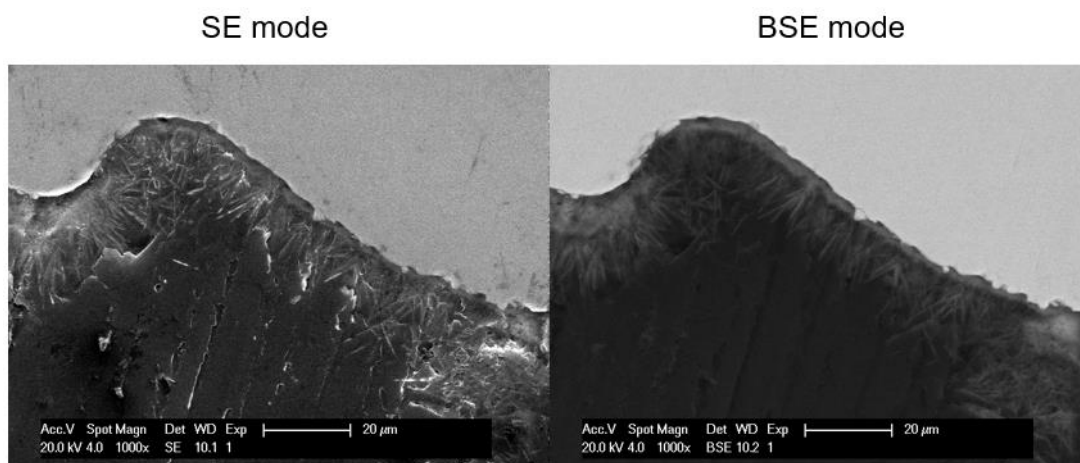

Figure 4.4. cross-sections of the scaffold and coating under SE and BSE modes in SEM analysis. The coating thickness is approximately 10-15μm.

4.4.2 In vivo study

All animals were successfully prepared with bilateral mandibular defects, and the inferior alveolar neurovascular bundles were completely isolated and successfully severed. CT examination by week 8 showed that the scaffolds were not dislodged.

4.4.2.1 Micro-CT scan

The results of the micro-CT analysis are shown in **Figure 4.5**. The amount of bone formation in G2 was significantly higher than that in G1. **Table 4.2** presents the measured osteogenesis data. G2

had a significantly higher BV/TV and Tb. N than G1 (p<0.05). In addition, g2 also had higher Tb. Th and lower Tb. Sp values (p>0.05).
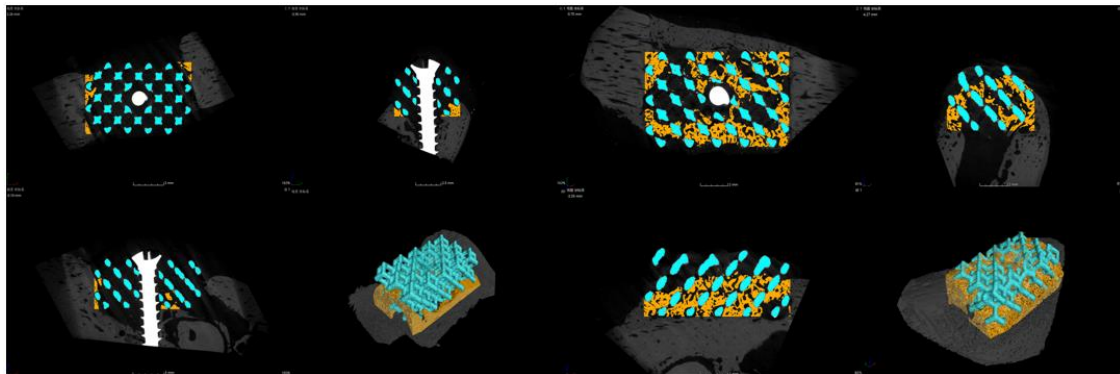
Figure 4.5. Micro-CT results of scaffolds in G1 (left) and G2 (right).

Table 4.2. Osteogenic data calculated by micro-CT analysis.

	G1	G2
BV/TV（*）	5.43% ± 1.76%	19.58% ± 6.61%
Tb,Th	0.07 ± 0.03	0.10 ± 0.04
Tb.N（*）	0.71 ± 0.46	2.00 ± 0.08
Tb.Sp	3.11 ± 4.20	0.40 ± 0.04

* means there was significant difference between G1 and G2.

4.5   Discussion

With advanced AM techniques, porous Ti alloys can be produced with controlled pore size, geometry, and porosity as appropriate materials for BTE. The main concern regarding the clinical applications of these Ti scaffolds is how to enhance their osseointegration and osteogenic properties. BMP-2 induces bone and cartilage formation in vivo and can be used in a range of therapeutic interventions. Ti scaffold combined with BMP-2 integrated biomimetic CaP coating is very attractive for achieving the long-term, stable release of BMP-2. Previous studies have successfully demonstrated the osteogenic properties of BMP-2 integrated biomimetic CaP coatings in vivo on solid implants [31, 32]. However, the key to success of BTE lies in the creation of the porous scaffold. 3D-printed porous scaffolds provide a large surface area for cells to anchor, and the newly formed bone tissue is able to fill the pores on the scaffold, thereby improving the quality of the bone defect reconstruction. We fabricated BMP-2 integrated biomimetic CaP coatings on porous Ti scaffolds in this study. In our study, the BMP-2 integrated biomimetic CaP coating resulted in better osseointegration and osteogenesis of the porous Ti scaffold within the bicortical

bone defect, repairing 20% of the defect at week 8, which is significantly better than the porous Ti scaffold without coating.

A micro/nanoscaled surface roughness can facilitate the bonding of new bone to the scaffold [33], and has been shown to enhance osteoblast adhesion, proliferation, and differentiation [34]. Furthermore, the rough surface increases the surface area of the scaffold. As demonstrated by micro-CT results, the coating increases the surface area of the scaffold by a factor of 638, which greatly improves the anchoring and adsorption of proteins [34]. In this study, the first precipitated amorphous CaP particles in the biomimetic coating serve as nucleation sites for subsequent growth of the crystalline layer. OCP crystals are epitaxially grown out of and perpendicular to this seeding layer [35]. Results of micro-CT revealed a decrease in porosity and an increase in Tb.Th. SEM revealed a noticeable change in surface morphology, indicating a successful coating fabrication.

Bicortical defects of 6 to 8mm in length in the dog's mandible did not spontaneously heal after 16 weeks [36]. The results of our control group also confirmed this: the scaffold played a much smaller role in bone repair than the coating did. In the biomimetic coating, BMP-2 determines ectopic bone formation [28]. However, the rapid ingestion of a high dose of BMP-2 stimulates the resorption of newly formed bone [26]. CaP serves as both a carrier and a sustained-release system, allowing BMP-2 to be released in a stable and sustained manner [28]. Studies have shown that coating-integrated BMP-2 is 5-70 times more osteoinductive than surface-adsorbed BMP-2 [29, 31]. Therefore, the use of CaP coating to deliver BMP-2 is both correct and effective. During coating degradation, BMP-2 is released in a manner similar to the release of growth factors from the bone matrix during bone remodeling [37]. Research has demonstrated that 50% of the BMP-2 in the coating is released within 5 weeks (5% to 10% per week) and can induce a stable and potent ectopic osteogenic response in rats and beagle dogs [28, 38].

In this study, a beagle dog model with mandibular bicortical defect was used to investigate the osteogenic properties of the scaffold and coating in vivo. Micro-CT results showed that G2 induced a significantly larger volume of regenerated bone compared with G1. Furthermore, G2 had a higher average number of trabecular bone compared to G1, indicating a higher quality of new bone in G2. These results suggest that the BMP-2 integrated biomimetic CaP coating enhances the bioactivity of porous Ti scaffolds, promoting osteogenesis results. The micro-CT results indicate that the osteogenic results between G2 and G1 are significantly different. However, an additional histological study is needed to confirm the findings of the present study. Currently, we are still in the process of producing histological sections. We predict that G2 has a more significant BA/TA

and BIC in hard tissue sections, and the quality of the new bone should be higher than that of G1, i.e., there should be more healthy bone formation markers around the new bone: osteogenesis cells, osteoclasts, and osteocytes [39]. Furthermore, we will measure the depth of bone ingrowth to quantify the osteogenic outcome and serve as a reference for the subsequent application of such coatings.

Ti scaffolds with compressive strength and elastic modulus similar to human cortical bone were also designed and printed in this study. The scaffold has a porosity of approximately 80%, which is sufficient for cell proliferation and migration [40]. By creating a balance between oxygen transport channels and mechanical properties, these scaffolds are intended to mimic actual clinical procedures.

Although Ti is a widely used BTE biomaterial, it is biodegradable. Non-degradable metal implants can cause chronic infections and interfere with patient radiological examinations [41, 42]. In future works, we will also use absorbable metals, such as Mg alloys, Zn alloys, etc. to fabricate 3D-printed scaffolds and coat them with BMP-2 integrated biomimetic CaP coating. In light of the coating's ability to promote osteogenesis, we believe this combination has great potential in BTE.

Therefore, the existing experimental results demonstrate that the BMP-2 integrated biomimetic CaP coating is promising for modifying porous Ti scaffolds to repair bicortical bone defects. These results confirm that this coating significantly improves the formation of new bone in vivo, and the coating is also safe. This coating and scaffold combination has excellent potential for BTE, but further research is necessary to assess its clinical feasibility, especially in large animal models.

4.6   Conclusion

We fabricated 3D-printed Ti scaffolds with compressive strength and elastic modulus similar to human cortical bone. Micro-CT results revealed that BMP-2 integrated biomimetic CaP coating significantly enhanced the osteogenic potential in mandibular bicortical bone defects in beagle dogs. A further histological analysis is required to confirm the results of the present study.

4.7 References

1. Gu Y, Ma H, Shujaat S, Orhan K, Coucke W, Amoli MS, et al. Donor-and recipient-site morbidity of vascularized fibular and iliac flaps for mandibular reconstruction: A systematic review and meta-analysis. Journal of Plastic, Reconstructive & Aesthetic Surgery. 2021;74:1470-9.

2. Kanwar S, Vijayavenkataraman S. Design of 3D printed scaffolds for bone tissue engineering: A review. Bioprinting. 2021;24:e00167.

3. Cheong VS, Fromme P, Coathup MJ, Mumith A, Blunn GW. Partial Bone Formation in Additive Manufactured Porous Implants Reduces Predicted Stress and Danger of Fatigue Failure. Annals of Biomedical Engineering. 2020;48:502-14.

4. Lv Y, Wang B, Liu G, Tang Y, Lu E, Xie K, et al. Metal material, properties and design methods of porous biomedical scaffolds for additive manufacturing: A review. Frontiers in Bioengineering and Biotechnology. 2021;9:194.

5. Zuo W, Yu L, Lin J, Yang Y, Fei Q. Properties improvement of titanium alloys scaffolds in bone tissue engineering: a literature review. Annals of Translational Medicine. 2021;9:1259.

6. Keller JC, Stanford CM, Wightman JP, Draughn RA, Zaharias R. Characterizations of titanium implant surfaces. Journal of biomedical materials research. 1994;28:939-46.

7. Eliaz N, Metoki N. Calcium phosphate bioceramics: a review of their history, structure, properties, coating technologies and biomedical applications. Materials. 2017;10:334.

8. Sapino S, Chindamo G, Chirio D, Manzoli M, Peira E, Riganti C, et al. Calcium Phosphate-Coated Lipid Nanoparticles as a Potential Tool in Bone Diseases Therapy. Nanomaterials. 2021;11:2983.

9. Mumith A, Cheong VS, Fromme P, Coathup MJ, Blunn GW. The effect of strontium and silicon substituted hydroxyapatite electrochemical coatings on bone ingrowth and osseointegration of selective laser sintered porous metal implants. PLoS One. 2020;15:e0227232.

10. Bose S, Banerjee D, Shivaram A, Tarafder S, Bandyopadhyay A. Calcium phosphate coated 3D printed porous titanium with nanoscale surface modification for orthopedic and dental applications. Materials & design. 2018;151:102-12.

11. Witting L, Waselau A-C, Feichtner F, Wurm L, Julmi S, Klose C, et al. Influence of coatings on degradation and osseointegration of open porous Mg scaffolds in vivo. Materialia. 2020;14:100949.

12. Müller V, Pagnier T, Tadier S, Gremillard L, Jobbagy M, Djurado E. Design of advanced one-step hydroxyapatite coatings for biomedical applications using the electrostatic spray deposition. Applied Surface Science. 2021;541:148462.

13. Su Y, Lu C, Hu X, Guo Y, Xun X, Zhang Z, et al. Improving the degradation resistance and

surface biomineralization ability of calcium phosphate coatings on a biodegradable magnesium alloy via a sol-gel spin coating method. Journal of The Electrochemical Society. 2018;165:C155.

14. Kreller T, Sahm F, Bader R, Boccaccini AR, Jonitz-Heincke A, Detsch R. Biomimetic calcium phosphate coatings for bioactivation of titanium implant surfaces: Methodological approach and in vitro evaluation of biocompatibility. Materials. 2021;14:3516.

15. Koju N, Sikder P, Ren Y, Zhou H, Bhaduri SB. Biomimetic coating technology for orthopedic implants. Current opinion in chemical engineering. 2017;15:49-55.

16. Barrere F, Layrolle P, Van Blitterswijk C, De Groot K. Biomimetic coatings on titanium: a crystal growth study of octacalcium phosphate. Journal of Materials Science: Materials in Medicine. 2001;12:529-34.

17. Bigi A, Boanini E. Functionalized biomimetic calcium phosphates for bone tissue repair. Journal of applied biomaterials & functional materials. 2017;15:e313-e25.

18. Bracci B, Torricelli P, Panzavolta S, Boanini E, Giardino R, Bigi A. Effect of Mg^{2+}, Sr^{2+}, and Mn^{2+} on the chemico-physical and in vitro biological properties of calcium phosphate biomimetic coatings. Journal of Inorganic Biochemistry. 2009;103:1666-74.

19. Yu X, Wang L, Jiang X, Rowe D, Wei M. Biomimetic CaP coating incorporated with parathyroid hormone improves the osseointegration of titanium implant. Journal of Materials Science: Materials in Medicine. 2012;23:2177-86.

20. Ciobanu G, Ciobanu O. Investigation on the effect of collagen and vitamins on biomimetic hydroxyapatite coating formation on titanium surfaces. Materials Science and Engineering: C. 2013;33:1683-8.

21. Liu Y, Enggist L, Kuffer AF, Buser D, Hunziker EB. The influence of BMP-2 and its mode of delivery on the osteoconductivity of implant surfaces during the early phase of osseointegration. Biomaterials. 2007;28:2677-86.

22. Haidar ZS, Hamdy RC, Tabrizian M. Delivery of recombinant bone morphogenetic proteins for bone regeneration and repair. Part A: Current challenges in BMP delivery. Biotechnology letters. 2009;31:1817-24.

23. Haidar ZS, Hamdy RC, Tabrizian M. Delivery of recombinant bone morphogenetic proteins for bone regeneration and repair. Part B: Delivery systems for BMPs in orthopaedic and craniofacial tissue engineering. Biotechnology letters. 2009;31:1825-35.

24. Liu Y, Hunziker EB, Layrolle P, De Bruijn JD, De Groot K. Bone morphogenetic protein 2 incorporated into biomimetic coatings retains its biological activity. Tissue engineering. 2004;10:101-8.

25. Wu G, Liu Y, Iizuka T, Hunziker EB. The effect of a slow mode of BMP-2 delivery on the inflammatory response provoked by bone-defect-filling polymeric scaffolds. Biomaterials. 2010;31:7485-93.

26. Wu G, Hunziker EB, Zheng Y, Wismeijer D, Liu Y. Functionalization of deproteinized bovine bone with a coating-incorporated depot of BMP-2 renders the material efficiently osteoinductive and suppresses foreign-body reactivity. Bone. 2011;49:1323-30.

27. Liu T, Wu G, Wismeijer D, Gu Z, Liu Y. Deproteinized bovine bone functionalized with the slow delivery of BMP-2 for the repair of critical-sized bone defects in sheep. Bone. 2013;56:110-8.

28. Gu Y, Wei L, Zhang Z, Van Dessel J, Driesen RB, Lambrichts I, et al. BMP-2 incorporated biomimetic CaP coating functionalized 3D printed Ti6Al4V scaffold induces ectopic bone formation in a dog model. Materials & Design. 2022:215:110443.

29. Liu Y, De Groot K, Hunziker EB. BMP-2 liberated from biomimetic implant coatings induces and sustains direct ossification in an ectopic rat model. Bone. 2005;36:745-57.

30. Liu Y, Layrolle P, de Bruijn J, van Blitterswijk C, de Groot K. Biomimetic coprecipitation of calcium phosphate and bovine serum albumin on titanium alloy. Journal of Biomedical Materials Research. 2001;57:327-35.

31. Hunziker EB, Enggist L, Küffer A, Buser D, Liu Y. Osseointegration: the slow delivery of BMP-2 enhances osteoinductivity. Bone. 2012;51:98-106.

32. Teng F, Wei L, Yu D, Deng L, Zheng Y, Lin H, et al. Vertical bone augmentation with simultaneous implantation using deproteinized bovine bone block functionalized with a slow delivery of BMP‒2. Clinical Oral Implants Research. 2020;31:215-28.

33. Kim H-B, Hayashi M, Nakatani K, Kitamura N, Sasaki K, Hotta J-i, et al. In situ measurements of ion-exchange processes in single polymer particles: laser trapping microspectroscopy and confocal fluorescence microspectroscopy. Analytical chemistry. 1996;68:409-14.

34. Jiang P, Liang J, Song R, Zhang Y, Ren L, Zhang L, et al. Effect of octacalcium-phosphate-modified micro/nanostructured titania surfaces on osteoblast response. ACS applied materials & interfaces. 2015;7:14384-96.

35. Barrere F, Layrolle P, Van Blitterswijk C, De Groot K. Biomimetic calcium phosphate coatings on Ti6Al4V: a crystal growth study of octacalcium phosphate and inhibition by Mg^{2+} and HCO_3^-. Bone. 1999;25:107S-11S.

36. Hjørting-Hansen E, Andreasen J. Incomplete bone healing of experimental cavities in dog mandibles. British Journal of Oral Surgery. 1971;9:33-40.

37. Lin X, Chen J, Liao Y, Pathak JL, Li H, Liu Y. Biomimetic Calcium Phosphate Coating as a

Drug Delivery Vehicle for Bone Tissue Engineering: A Mini-Review. Coatings. 2020;10:1118.

38. Liu Y, Schouten C, Boerman O, Wu G, Jansen JA, Hunziker EB. The kinetics and mechanism of bone morphogenetic protein 2 release from calcium phosphate-based implant-coatings. Journal of Biomedical Materials Research Part A. 2018;106:2363-71.

39. Quinn J, McFadden R, Chan C-W, Carson L. Titanium for orthopedic applications: an overview of surface modification to improve biocompatibility and prevent bacterial biofilm formation. IScience. 2020;23:101745.

40. Du Y, Guo JL, Wang J, Mikos AG, Zhang S. Hierarchically designed bone scaffolds: From internal cues to external stimuli. Biomaterials. 2019;218:119334.

41. Thorén H, Snäll J, Hallermann W, Kormi E, Törnwall J. Policy of routine titanium miniplate removal after maxillofacial trauma. Journal of oral and maxillofacial surgery. 2008;66:1901-4.

42. Sullivan PK, Smith JF, Rozzelle AA. Cranio-orbital reconstruction: safety and image quality of metallic implants on CT and MRI scanning. Plastic and reconstructive surgery. 1994;94:589-96.

Part IV

Biodegradable WE43 scaffold in BTE

Article 5

Biocompatibility and osteogenic capacity of additively manufactured biodegradable porous WE43 scaffolds: an in vivo study in beagle dogs

Yifei Gu[1], Yiwen Liu[2], Reinhilde Jacobs[1], Lei Tian*[2], Yi Sun*[1], Holger Jahr*[3], Constantinus Politis[1]

[1] OMFS IMPATH research group, Department of Imaging & Pathology, Faculty of Medicine, KU Leuven and Department of Oral and Maxillofacial Surgery, University Hospitals Leuven, Leuven (3000), Belgium.

[2.] State Key Laboratory of Military Stomatology & National Clinical Research Center for Oral Diseases & Shaanxi Clinical Research Center for Oral Diseases, Department of Craniofacial Trauma and Orthognathic Surgery, School of Stomatology, FMMU, Xi'an (710000), China.

[3] Department of Orthopaedics, University Hospital RWTH Aachen, Aachen (52074), Germany.

5.1   Abstract

Degradable implants are a hot topic in BTE, and Mg is one of the most promising metal materials. In one of the Mg alloys, WE43, rare earth elements have been added to improve the corrosion resistance of Mg. There have been no studies performed on biodegradability, biocompatibility, and osteogenic ability of WE43 alloy in large animal models, whose bone metabolism is more similar to that of humans. The objective of this study was to investigate the biocompatibility, degradation rate and osteogenic ability of the WE43 alloy porous scaffold (4*6mm) fabricated by SLM technology in the femur and tibia defects of beagle dogs. The results of complete blood cell counting, blood biochemistry, blood trace element analysis, and multi-organ histological analysis demonstrated that WE43 alloy has a good biocompatibility. Micro-CT showed that the scaffold had undergone a greater volume degradation at week 4 (36%±19%), while the degradation at week 12 (41% ± 14%) was not significantly different from that at week 4, indicating the scaffold had entered a slow degradation stage between week 4 and week 12. In histological study, a degradation of the scaffold was observed at the same time as new bone was formed. At week 4, the new bone trabeculae grew into the bone defect and wrapped the scaffold fragments. At week 12, a large amount of mineralized bone had been distributed within the bone defect, forming a favorable support for it. WE43 has good biocompatibility and osteogenic ability, but a surface modification might be necessary to slow down its degradation rate for better application in future BTE.

Keywords: biodegradable metal; Mg alloy; 3D-printing; porous scaffold; WE43

5.2   Introduction

BTE has emerged as a promising technique for repairing bone defects, and porous scaffolds play a crucial role in BTE [1]. A porous scaffold is an artificial structure that supports 3D tissue formation and mimics bone ECM structure and function while promoting cell adhesion, proliferation, and differentiation for bone repair [2]. In recent years, advances in AM technology have enabled the fabrication of porous scaffolds with precise geometries and interconnected networks that promote blood and bone regeneration. By adjusting the design parameters of the scaffold, failures caused by stress shielding can be avoided [3].

To promote bone regeneration, the ideal porous scaffold should be biocompatible, have a fully interconnected porous structure, and degrade while bone regenerates [4]. Metal materials are essential in BTE due to their mechanical properties. Common bioinert metal materials such as Ti and its alloys, cobalt-chromium alloys, stainless steel, etc., do not degrade over time [1]. Infection can result from bacterial colonization of the undegradable scaffold surface, causing permanent physical irritation and chronic inflammation [5, 6]. In addition, metal scaffolds would interfere with radiological examinations, such as X-rays and magnetic resonance imaging in patients' follow-ups, requiring further surgery to remove them [7, 8]. The second surgery increases patient morbidity and surgical costs. Additionally, the biodegradable properties of the scaffold are crucial to ensuring tissue formation and degradation are occurring simultaneously, and maintain structural integrity and provide smooth load transfer between scaffolds and tissues. Therefore, researchers and clinicians are interested in developing biodegradable materials with biocompatibility, strength, radio visibility, and osseointegration properties.

Mg is an essential mineral for metabolism, with a daily intake of 300-400mg. Mg and its alloys are popular candidates for BTE because of their biodegradability [9]. The density and Young's modulus of Mg are similar to those of human cortical bone [10]. As a result, Mg implants are less prone to have the stress shielding risk [11]. Furthermore, approximately half of the total physiological Mg is stored in bone tissue, which plays a crucial role in human metabolism [12]. In addition, previous in vitro and in vivo studies have demonstrated that Mg ions can enhance the proliferation and osteogenic differentiation of stem cells [13], promote the adhesion of osteoblasts [14], promote the mineralization of ECM structure [15], and inhibit osteoclast differentiation and function [16], while promoting angiogenesis [17], etc. Thus, Mg and Mg alloys can be used as biodegradable BGS. However, their rapid decline in mechanical strength and unsatisfactory degradation rates prohibit their development in BTEs. Besides, the flammability of Mg makes it challenging to fabricate porous Mg by AM technology [18].

By virtue of their relatively high solubility, slight electrode potential differences, and passivation, rare earth elements greatly enhance Mg-based materials' oxidation and corrosion resistance. WE43 alloy, made up of 4 wt% yttrium and 3 wt% rare earth metal mixture of neodymium, cerium, and dysprosium, is the first Mg alloy to be used clinically (compression screws in orthopedic surgery) [19]. WE43 alloy has also been successfully implanted in clinical trials as a biodegradable scaffold for cardiovascular surgery [20, 21].

Y. Li et al. fabricated diamond cell structured WE43 scaffolds using AM techniques [4, 22]. The scaffolds displayed less than 25% cytotoxicity in vitro. After 4 weeks of degradation in the simulated body fluid, the WE43 scaffolds showed a 20% loss in volume and a 52% loss in mechanical strength. However, they still had a compressive strength within the range of trabecular bone [4, 22]. The potential of WE43 alloy as a customized porous scaffold in BTE has yet to be explored.

In addition, in principle, toxicologically concerned elements should be avoided or used in minimum doses to manufacture biodegradable materials. Given these reasons, we should evaluate the biocompatibility and stability of WE43 scaffolds in vivo, especially in large animal models that are more like humans [23].

By far, most research on WE43 alloy still uses solid metal bulks. Only a few studies have used AM techniques to fabricate porous WE43 alloy scaffolds, however, most of these studies only did in vitro tests. The behavior of porous WE43 scaffolds has yet to be characterized in vivo, especially in large animal models whose bone metabolism is much more similar to that of the humans. The application of WE43 scaffolds in BTE has attracted our attention, but our understanding of such scaffolds' biocompatibility, biodegradation, and osteogenic potential is limited.

The aim of the present study was to construct topologically ordered biodegradable WE43 scaffolds using SLM technique. The secondary objective was to evaluate the biocompatibility, biodegradation behavior, and osteogenic potential of the WE43 scaffolds in vivo using a beagle dog model.

5.3   Materials and methods

5.3.1 Fabrication of the WE43 scaffold

A porous cylindrical scaffold with diamond unit cell structures was designed. The scaffold has a diameter of 4mm and a height of 6mm. WE43 scaffolds have the following parameters: the Tb.Th of 400μm, the pore size of 600μm, and the porosity of 67%. A laboratory scaled SLM machine was used to manufacture the scaffolds [24]. The machine maintained an inert atmosphere by adding

argon (less than 10ppm of oxygen). The spherical WE43 granular powder (4 wt% yttrium and 3 wt% rare earth elements, Mg Elektron UK, Manchester, M27 8BF, UK) was gas atomized and sieved to a particle size range of 25-60μm.

In total, 15 scaffolds were printed, of which 12 were used for animal study and 3 for in vitro characterization. All scaffolds were chemically polished for 2 minutes in a solution containing 5% HCl, 5% HNO_3, and 90% C_2H_5OH before the study (**Figure 5.1**).

Figure 5.1. WE43 scaffold before (left) and after (right) the chemical polishing.

5.3.2 Micro-CT scan

Microtomography imaging (AX-2000 Microfocus Industrial CT) was used to analyze the porosity and original volume of the WE43 scaffolds. The maximum voltage of the micro-CT system was 120kV, and the maximum current was 100μA. Additional scanning parameters: integration time 0.6s; projection number 1440; resolution 9μm. The region of the scaffold was selected as the ROI. The images were processed using 3D image processing software (VG Studio Max 3.0, Volume Graphics, Heidelberg, Germany).

5.3.3 SEM scan

Following micro-CT, the scaffolds were embedded with epoxy resin (Epofix resin, Struers,

Copenhagen, Denmark). Then, a sander was used to remove the upper half of the scaffold, revealing the cross-section of the scaffold. The surface morphology of the scaffolds was observed using SEM (Philips XL-30, FEI company, The Netherlands).

5.3.4 Animal study

A review and approval of our research were completed by the Fourth Military Medical University Ethics Committee (No. kq-2022-078). Six healthy beagle dogs were kept in separate cages and fed a quantitative, regular diet and water every day. Animals were fed in a constant environment: temperature around 20°C; humidity between 40-70%; ventilation 10-20 times per hour.

After a two-week acclimatization period and a 12-hour fast, we preoperatively administered 8×10^6 units of penicillin potassium to prevent infection in the animals. We used intravenous injections of 3% pentobarbital sodium solution for general anesthesia on the animals. The beagle dogs were immobilized in a lateral recumbent position. After making an incision and carefully dissecting the tissue, a dental handpiece and bur were used to create two 6 mm diameter and 6 mm long bone defects in the distal epiphysis of the left femur and the proximal epiphysis of the left tibia (**Figure 5.2**). The entire procedure was rinsed with normal saline to cool down. The 6mm side of the scaffold was perpendicular to the bone surface when inserted. After the subcutaneous tissue and skin were sutured, the wound was cleaned with 75% alcohol and then tightly bandaged. An immediate postoperative CT scan demonstrated that the scaffold was successfully placed in the corresponding positions of the femur and tibia (**Figure 5.2**). Experimental animals were given anti-inflammatory drugs for five days following surgery. Animals were monitored daily for wound healing and general well-being.

After the surgery, three experimental animals were sacrificed by excessive anesthesia at weeks 4 and 12. The femur and tibia bones were dissected, and the bone segments including scaffolds were removed and preserved. The heart, liver, and kidney tissues were removed, immersed in 4% paraformaldehyde, and stored in a 4° refrigerator.
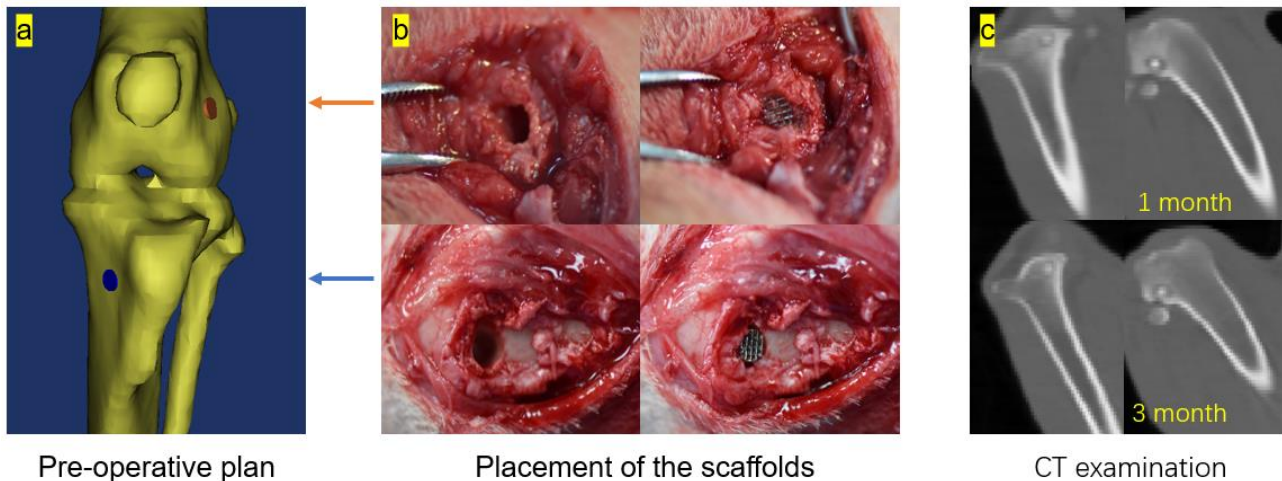
Figure 5.2. (a) preoperatively determined scaffold placement locations, i.e., the distal epiphysis of the femur and the proximal epiphysis of the tibia. (b) Scaffold placement during surgery. (c) Scaffolds were examined using CT before scarification to ensure they weren't dislocated.

5.3.5 Hematology analysis

Blood was collected from all animals at five time points to perform complete blood cell count and blood biochemistry tests: before surgery, week 1, week 4, week 8 and week 12 after the surgery. Blood was collected in tubes with EDTA as an anticoagulant and tubes without any additives. Blood collected without any additives was kept for 30 minutes and then centrifuged (4000rpm for 8 minutes) to separate serum. An automated blood cell analyzer (SYSMEX SE-9000, DKK-TOA, Japan) was used for counting RBCs, WBCs, and PLTs. A 7600P automatic biochemical analyzer (Hitachi, Japan) was used to analyze blood biochemistry. The indexes measured included AST, ALT, ALB, ALP, BU, and CR. Blood ion concentration analysis, including the determination of Zn, Mg, Fe, Ca, and Cu levels, was performed using the BH5300 Whole Blood Multi-Element Analyzer (Bohui Technology, China).

5.3.6 Micro-CT analysis

The collected scaffold-containing bone blocks were fixed in 4% paraformaldehyde for 48 hours, and the samples were scanned using the same microtomography imaging system (AX-2000 Microfocus Industrial CT) as in the in vitro experiments to determine new bone formation. The implantation area (6mm in diameter and 6mm in length) was selected as the ROI. The volume loss of the implants was assessed using the 3D image processing software (VG Studio Max 3.0, Volume Graphics, Heidelberg, Germany).

5.3.7 Histological examination

The collected heart, liver, and kidney tissue were fixed in 4% neutral buffered formalin for 48 hours. After dehydration in graded ethanol, they were cleared in xylene, embedded in paraffin, and cut into 5μm sections. Hematoxylin and eosin were used to stain these sections. Additionally, all bone segments containing scaffolds were cut into cubes of about 2*2*2cm. The fixation, dehydration, and embedding process were the same as above, and then the bone segments were cut into 5-10μm slices. The sections were dried in an oven at 60°, and an optical microscope (Axio-Imager M2, Carl Zeiss Microscopy, Jena, Germany) was used to observe the histomorphology of the organs and the formation of new bone.

5.3.8 Statistical analysis

Results are expressed as mean ± standard deviation. Data were analyzed using SPSS statistics software (SPSS 26.0, SPSS Inc., Chicago, USA). Statistical significance was assessed using a one-way ANOVA followed by Tukey's test. A p-value less than 0.05 was considered statistically significant.

5.4   Results

The WE43 scaffold was successfully printed. Micro-CT results showed that the scaffold's porosity was 75.3±0.7%, and the original volume of the scaffold was 18.57±0.59mm^3.

5.4.1 SEM scan

There was an even distribution of flake-shaped, white second-phase particles on the scaffold (**Figure 5.3,** yellow arrow). According to a previous study that used XRD to determine the scaffold phases (Y_2O_3 and Mg_3Nd), these particles may be yttrium oxide [4].
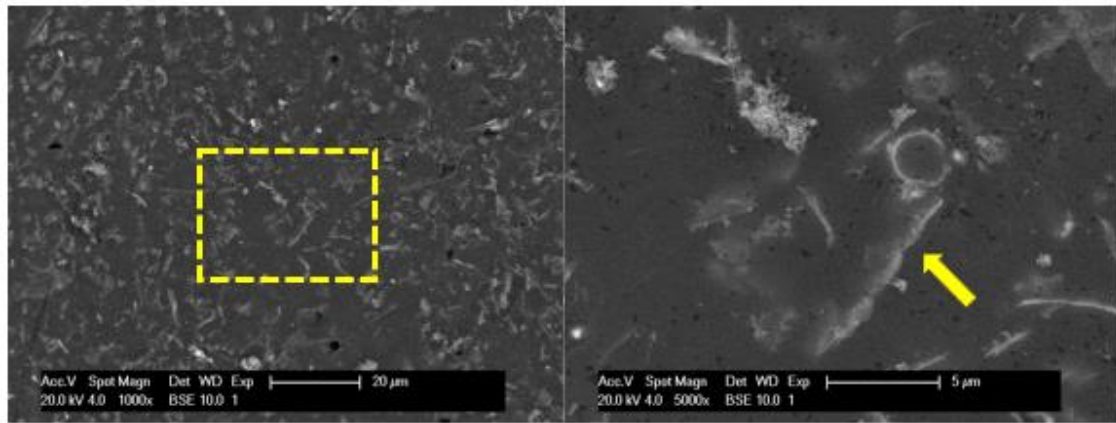
Figure 5.3. SEM results of the WE43 scaffold. The right image is a magnified version of the yellow box in the left image. The yellow arrow points to a white second-phase particle.

5.4.2 General status of the animals

In all animals, femoral and tibial defects were successfully prepared, and scaffolds were successfully inserted into the defects. Following surgery, the animals were able to stand and eat without difficulty. There were no signs of inflammation, healing disorders, allergic reactions, or other complications. By scarification, CT tests revealed that none of the scaffolds were dislodged.

5.4.3 Hematology analysis

Figure 5.4 shows the results of the hematological analysis. After complete blood cell counting, the WBC, RBC, and PLT levels were within the normal range in all animals, with no statistically significant differences before and after surgery ($p > 0.05$). The levels of ALT, AST, ALP, ALB, TP, CRE, and BU were not abnormal during the observation period, and all values fluctuated within the normal range. The differences between time points were not statistically significant ($p > 0.05$). The blood concentrations of Zn, Mg, Fe, Ca, and Cu was normal and showed no significant changes during the observation period compared to preoperative values ($p > 0.05$) (**Figure 5.5**). Thus, the degradation of the WE43 scaffold does not cause a substantial increase in blood Mg concentrations or interfere with the metabolism of Zn, Fe, Cu, or Ca. Overall, the analysis results showed that the use of the WE43 scaffold led to no abnormal changes in blood indexes, demonstrating the scaffold's ideal in vivo biosafety.
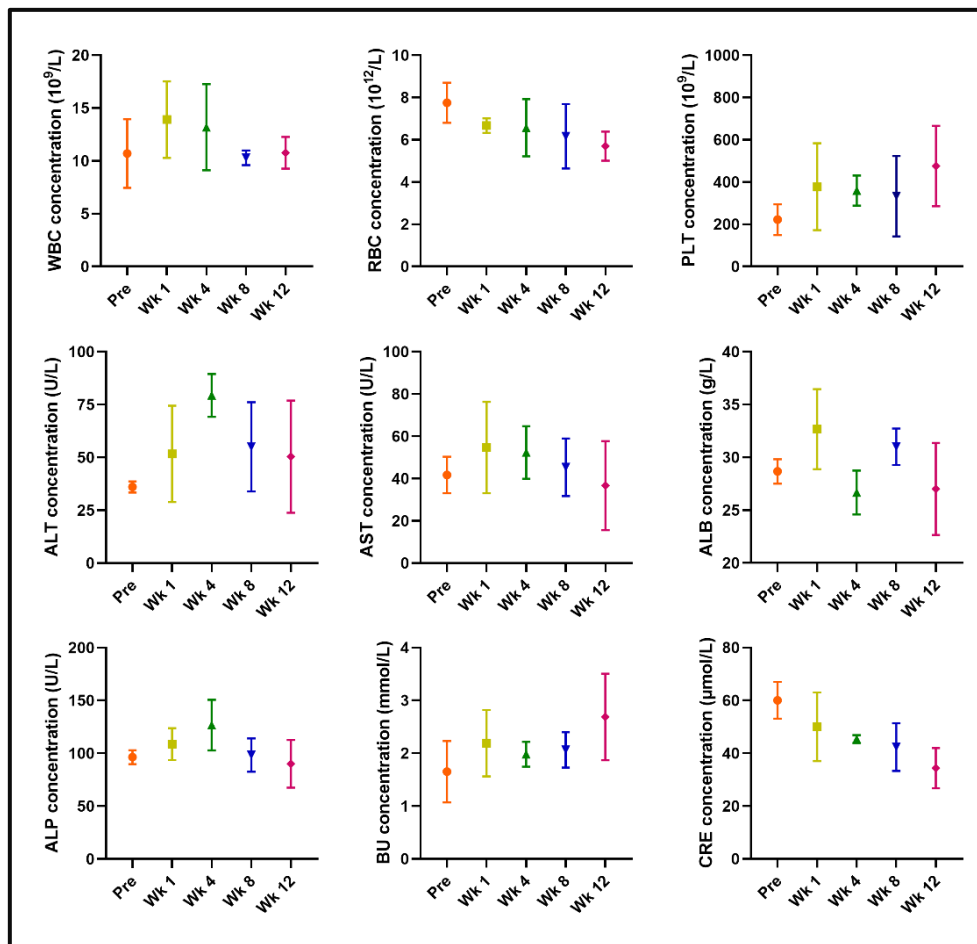
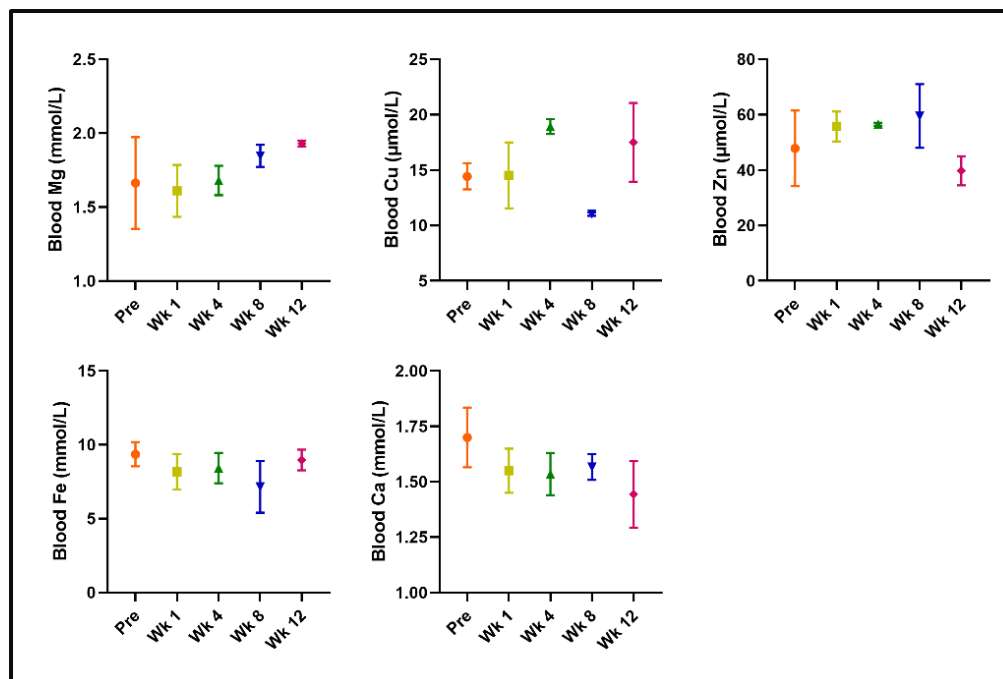**Figure 5.4.** Results of complete blood cell counting and blood biochemistry tests

Figure 5.5. Results of blood ion concentration analysis.

129

5.4.4 Micro-CT analysis

Micro-CT scans revealed that the scaffold gradually degraded with time. The scaffold underwent major morphological changes at week 4, including the appearance of a large absorption cavity and an obvious defect boundary. Metabolites accumulated within and on the scaffold (**Figure 5.6a**). At week 12, the resorption cavity decreased, and new trabeculae filled the defect. The volume of the WE43 scaffold was analyzed using VG-studio 3.0 software. After debugging, the material threshold was about 24,000, the bone threshold was about 20,000, and the degradation product threshold was lower than bone and infinitely close to zero (completely degraded materials cannot be visualized). **Table 5.1** shows the results of the Micro-CT calculation of scaffold degradation and osteogenesis. BV, BV/TV, and Tb.Th within the ROI were significantly higher in the week 12 group that those in the week 4 group. From week 4 to week 12, there was a decrease in degradation products and a slight decrease in residual scaffold volume, but there was no significant difference between the two groups. The scaffold decreased by 36%±0.19% at week 4 and 41%±14% at week 12, with no significant difference between the two groups found.
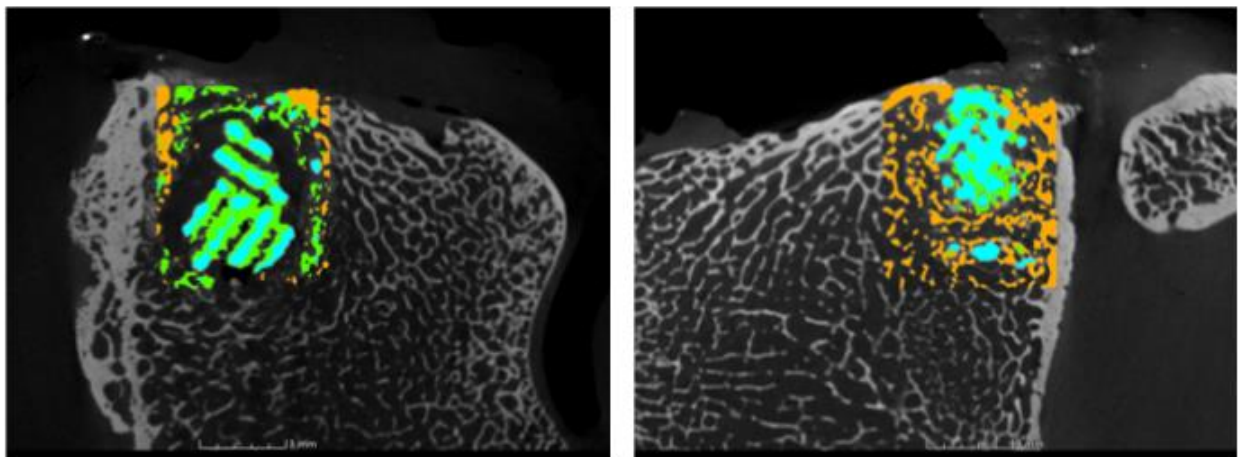
Figure 5.6. Micro-CT analysis results at week 4 (left) and week 12 (right). The yellow parts represent bone tissue; the green parts represent degradation products; and the blue parts represent scaffold residues.

Table 5.1: Micro-CT calculation results.

Micro-CT analysis parameters	4-week group	12-week group
BV (mm^3) *	20.99±6.41	40.01±16.53
BV/TV *	0.12±0.04	0.24±0.10
Tb.Th (mm) *	0.07±0.01	0.14±0.03
Tb.N (mm^{-1})	1.65±0.49	1.55±0.77
Tb.Sp (mm)	0.58±0.18	0.66±0.38
Degradation product volume (mm^3)	17.35±13.86	6.14±3.75
Degradation product volume/Tissue volume	0.10±0.08	0.04±0.02
Scaffold volume (mm^3)	11.88±3.57	11.00±2.60
Scaffold volume /Tissue volume	0.07±0.02	0.06±0.02

*indicates that there is a significant difference between the two groups.

5.4.5 Histological analysis

Parts of vital organs were harvested from both groups of animals, and the histological morphology of these organs was used to identify histological changes. **Figure 5.7** illustrates the morphology of the tissue section. No significant changes in tissue morphology, no infiltration of inflammatory cells, and no damage to tissue structure were observed for all samples. A lack of visible lesions suggests that the WE43 alloy does not cause systemic toxicity.
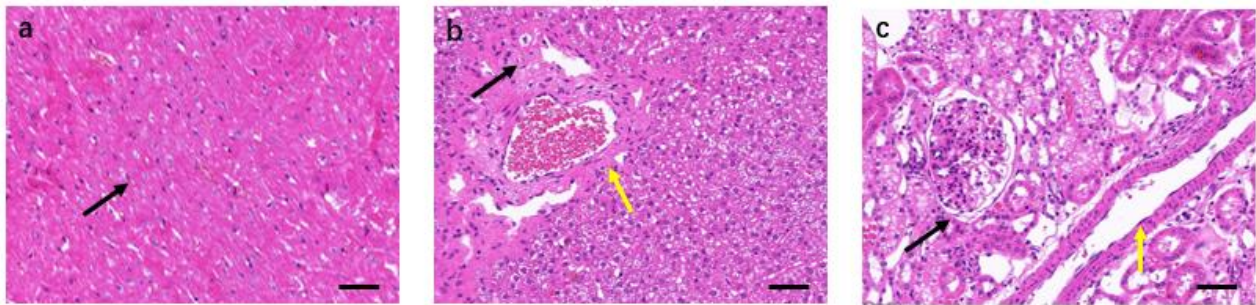
Figure 5.7. Histological results of the animal organs. (a) Section of heart tissue with a black arrow indicating cardiomyocytes. (b) A liver tissue section with black arrows representing hepatocytes and yellow arrows indicating a hepatic interlobular vein. (c) A section of kidney tissue with a black arrow indicating glomeruli and a yellow arrow indicating renal tubules. Scale bars = 50μm.

The histological results of the scaffold-containing bone blocks are shown in **Figure 5.8**. Based on the defect diameter (6 mm), a circular ROI was cut with the scaffold as the center. The mineralized bone is stained green, and the non-mineralized bone is stained orange/red. As a result of the thin nature of the sections, the scaffold and its metabolites appeared vaguely light green or light blue. By week 4, the porous structure of the scaffolds had been lost. There was a large amount of non-mineralized bone and a small amount of mineralized bone at the implant site. As can be seen from

131

the magnified image, the newborn non-mineralized bone wrapped scaffold fragments, and a few calcification foci have formed. At week 12, the implant site was surrounded by mostly the mineralized bone. There are still non-mineralized bone fragments wrapping the scaffold fragments and gradually calcifying.
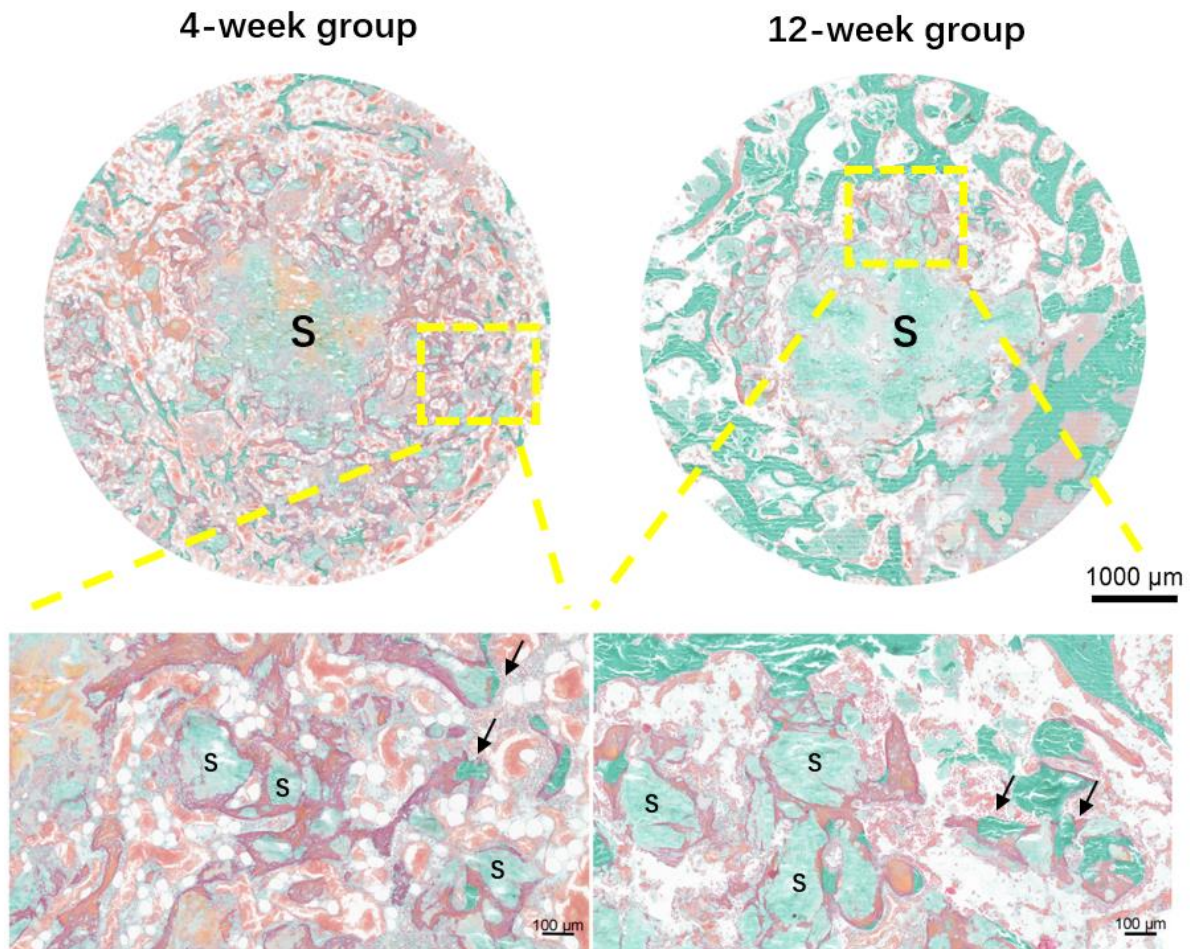

Figure 5.8. results of the histological analysis. The lower image is the magnified version of the yellow box in the upper image. Non-mineralized bone is stained orange/red, while the mineralized bone is stained green. The scaffold residue and fragments (S) appear indistinct light green/light blue. The black arrows indicate calcification foci in non-mineralized bone.

5.5   Discussion

The objective of this study was to investigate the biocompatibility, degradability, and osteogenic potential of biodegradable WE43 alloy scaffolds. We demonstrate that the alloy is non-toxic, biodegradable, and allows for the ingrowth of new bone, making it a potential clinical candidate for BTE.

Biocompatibility is an essential characteristic of medical implants. Mg is a crucial element for metabolism, requiring a daily intake of 300-400 mg. The ion release of Mg alloys during long-term

132

degradation may be harmful to humans. However, we demonstrate that we43 scaffolds are safe for in vivo use.

The blood trace element level is an effective method to monitor in vivo WE43 alloy degradation. All blood indexes in the current study fluctuated within the normal range. Although some showed specific trends, no statistically significant differences were found. The results indicated no severe blood cell abnormalities, liver or kidney dysfunction, or trace element disturbances during WE43 alloy implantation.

Hydrogen produced by corrosion of Mg alloys makes it difficult for cells to adhere to the surface of the implant material, reducing metabolism and slowing down tissue regeneration [25]. Moreover, hydrogen may accumulate around bone tissue, affecting osteoblast activity and the quality of new bone [26]. However, we did not observe subcutaneous emphysema or fistulas in animals, which indicates that the hydrogen may have been absorbed by the body fluids. Furthermore, micro-CT can show that a large absorption cavity has been generated when the scaffold is implanted for 4 weeks, and the hydrogen gas is difficult to detect. New bone tissue filled the resorption cavity during week 12 due to the slower degradation of the scaffold, and no apparent hydrogen accumulation was observed around it.

An excessive Mg intake may be toxic to the kidneys, liver, cardiovascular, neuro, and immune systems. However, we did not detect any lesions in the internal organs of beagle dogs during the degradation of the WE43 alloy scaffold, which agrees with the blood test results, suggesting that the WE43 alloy scaffold is biocompatible in vivo. Previous studies of small animal models have reached the same conclusion [23, 27].

Several factors affect the complex biodegradation environment in the body, including cells, pH, temperature, electrolyte flow, blood, and proteins. Therefore, the degradation rate of the WE43 alloy needs to be tested in vivo to reach conclusions.

After the WE43 alloy is implanted in the body, it causes a wound and a foreign body reaction, causing a hematoma and inducing an inflammatory response. The scaffold surface is covered with cells (macrophages, foreign body giant cells, neutrophils, osteoblasts, stem cells, etc.), body fluids, proteins, and inorganic ions. There is a fast degradation rate at this point. In the current study, it was also demonstrated that degradation rates before week 4 were significantly higher than those between week 4 and week 12, and the degree of degradation was not significantly different between week 4 and week 12. At the initial stage, the large absorption cavity around the WE43 alloy material may have allowed the material to be in full contact with the microenvironment. The degradation of the WE43 alloy was slowed after the initial fast degradation stage due to the

ingrowth of new bone trabeculae. This conclusion is similar to that of Lim et al. In the rabbit model, there was no significant difference between the absorption rates of WE43 alloy at 6 and 12 weeks [23]. Due to the 12-week observation period in the present study, it would be necessary to assess the in vivo degradation performance of the WE43 alloy in the future over a longer period of time.

Krause et al. implanted WE43 implants (2.5×25 mm) in rabbit tibias, with a volume loss of 9% at 3 months and 35% at 6 months [28]. During the current study, we observed fast absorption and loss of structural integrity in week 4 and week 12, which was caused by the porous structure. As the porous structure has a larger surface area in contact with bodily fluids, it is absorbed faster than a solid structure. Similarly, Schaller et al. constructed cannulated screws with a length of 6mm and a wall diameter of 0.3mm using WE43 alloy and implanted them into the mandible of a miniature pig model. With simultaneous degradation of the inner and outer surfaces, the screws degraded by 30-60% within two months [29]. At week 12, the residual fragments of the WE43 scaffold formed tight complexes with the newly formed trabecular bone, providing adequate support for the surrounding bone structure. The trabecular bone grows into the absorption cavity, preventing fractures and bone defects from collapsing. Using a surface modification coating can further reduce the degradation of WE43 alloy, reducing the rapid corrosion of Mg and extending the absorption time of WE43 implants [30-33]. The current results demonstrate simultaneous absorption of WE43 alloy and ingrowth of trabecular bone, which is an ideal bone repair effect.

Due to the excellent biocompatibility of porous WE43 shown in these experiments, we believe it could be used in clinical applications in the craniofacial region. However, it is difficult to determine the safety of WE43 in humans based on this study alone. Mg and Y are not harmful to human health in the WE43 alloy. Nd, however, can irritate the eyes, mucous membranes, and skin, and therefore the safety of WE43 alloy requires more long-term studies in animal models [34]. Compared to the WE43 compression screw that has received CE certification [35], the porous structure can reduce the WE43 volume in the human body to a greater extent, as long as there is sufficient mechanical strength. Future research should focus on surface modification techniques that help reduce the degradation rate of WE43 alloy.

The current study examined the in vivo degradation of the WE43 alloy during the first 12 weeks after implantation. Future studies should examine its complete degradation and how to maintain a uniform degradation rate through the later stages of implantation. It is also necessary to investigate the mechanism of WE43 alloy metabolism in vivo. Potential applications of WE43 alloy in vivo, such as subcutaneous, intramuscular, urethral, intestinal, and cardiac applications, should also be explored.

5.6   Conclusion

In the current study, we assessed the biocompatibility, degradability, and osteogenic potential of WE43 alloys to repair femoral and tibial defects in beagle dogs over a 4- and 12-weeks period. Tests on blood and vital organs have shown that WE43 alloy is well compatible in vivo. Micro-CT showed a 36% ± 19% decrease in scaffold volume at week 4, and a 41% ± 14% decrease at week 12. There is a tendency for degradation products to be replaced by new bone trabeculae over time, which provides sufficient support for the surrounding bone structure. In conclusion, this study shows that the WE43 alloy has good biocompatibility and can simultaneously degrade the scaffold and bone ingrowth, making it a promising candidate for osteosynthesis systems. Control of the degradation rate is needed in the future to assure adequate support for bone defects during the healing process.

5.7   References

1.   Qu H, Fu H, Han Z, Sun Y. Biomaterials for bone tissue engineering scaffolds: a review. RSC advances. 2019;9:26252-62.

2.   Roseti L, Parisi V, Petretta M, Cavallo C, Desando G, Bartolotti I, et al. Scaffolds for bone tissue engineering: state of the art and new perspectives. Materials Science and Engineering: C. 2017;78:1246-62.

3.   Kanwar S, Vijayavenkataraman S. Design of 3D printed scaffolds for bone tissue engineering: A review. Bioprinting. 2021;24:e00167.

4.   Li Y, Zhou J, Pavanram P, Leeflang M, Fockaert L, Pouran B, et al. Additively manufactured biodegradable porous magnesium. Acta biomaterialia. 2018;67:378-92.

5.   Jacobs JJ, Gilbert JL, Urban RM. Current concepts review-corrosion of metal orthopaedic implants. Journal of Bone and Joint Surgery. 1998;80:268-82.

6.   van Hengel IAJ, Riool M, Fratila-Apachitei LE, Witte-Bouma J, Farrell E, Zadpoor AA, et al. Selective laser melting porous metallic implants with immobilized silver nanoparticles kill and prevent biofilm formation by methicillin-resistant Staphylococcus aureus. Biomaterials. 2017;140:1-15.

7.   Thorén H, Snäll J, Hallermann W, Kormi E, Törnwall J. Policy of routine titanium miniplate removal after maxillofacial trauma. Journal of oral and maxillofacial surgery. 2008;66:1901-4.

8.   Sullivan PK, Smith JF, Rozzelle AA. Cranio-orbital reconstruction: safety and image quality of metallic implants on CT and MRI scanning. Plastic and reconstructive surgery. 1994;94:589-96.

9.   Lai Y, Li Y, Cao H, Long J, Wang X, Li L, et al. Osteogenic magnesium incorporated into

PLGA/TCP porous scaffold by 3D printing for repairing challenging bone defect. Biomaterials. 2019;197:207-19.

10. Zhou H, Liang B, Jiang H, Deng Z, Yu K. Magnesium-based biomaterials as emerging agents for bone repair and regeneration: From mechanism to application. Journal of Magnesium and Alloys. 2021;9:779-804.

11. Byun S-H, Lim H-K, Kim S-M, Lee S-M, Kim H-E, Lee J-H. The bioresorption and guided bone regeneration of absorbable hydroxyapatite-coated magnesium mesh. Journal of Craniofacial Surgery. 2017;28:518-23.

12. Staiger MP, Pietak AM, Huadmai J, Dias G. Magnesium and its alloys as orthopedic biomaterials: a review. Biomaterials. 2006;27:1728-34.

13. Zhang Y, Xu J, Ruan YC, Yu MK, O'Laughlin M, Wise H, et al. Implant-derived magnesium induces local neuronal production of CGRP to improve bone-fracture healing in rats. Nature medicine. 2016;22:1160-9.

14. Zreiqat H, Howlett C, Zannettino A, Evans P, Schulze-Tanzil G, Knabe C, et al. Mechanisms of magnesium-stimulated adhesion of osteoblastic cells to commonly used orthopaedic implants. Journal of Biomedical Materials Research. 2002;62:175-84.

15. Yoshizawa S, Brown A, Barchowsky A, Sfeir C. Magnesium ion stimulation of bone marrow stromal cells enhances osteogenic activity, simulating the effect of magnesium alloy degradation. Acta biomaterialia. 2014;10:2834-42.

16. Wu L, Feyerabend F, Schilling AF, Willumeit-Römer R, Luthringer BJ. Effects of extracellular magnesium extract on the proliferation and differentiation of human osteoblasts and osteoclasts in coculture. Acta biomaterialia. 2015;27:294-304.

17. Lin S, Yang G, Jiang F, Zhou M, Yin S, Tang Y, et al. A magnesium-enriched 3D culture system that mimics the bone development microenvironment for vascularized bone regeneration. Advanced Science. 2019;6:1900209.

18. Sezer N, Evis Z, Koc M. Additive manufacturing of biodegradable magnesium implants and scaffolds: Review of the recent advances and research trends. Journal of Magnesium and Alloys. 2021;9:392-415.

19. Torroni A, Witek L, Fahliogullari HP, Bortoli JP, Ibrahim A, Hacquebord J, et al. WE43 and WE43-T5 Mg alloys screws tested in-vitro cellular adhesion and differentiation assay and in-vivo histomorphologic analysis in an ovine model. Journal of Biomaterials Applications. 2021;35:901-11.

20. Schranz D, Zartner P, Michel-Behnke I, Akintürk H. Bioabsorbable metal stents for percutaneous treatment of critical recoarctation of the aorta in a newborn. Catheterization and

Cardiovascular Interventions. 2006;67:671-3.

21. McMahon CJ, Oslizlok P, Walsh KP. Early restenosis following biodegradable stent implantation in an aortopulmonary collateral of a patient with pulmonary atresia and hypoplastic pulmonary arteries. Catheterization and Cardiovascular Interventions. 2007;69:735-8.

22. Li Y, Jahr H, Zhang XY, Leeflang MA, Li W, Pouran B, et al. Biodegradation-affected fatigue behavior of additively manufactured porous magnesium. Additive Manufacturing. 2019;28:299-311.

23. Lim HK, Byun SH, Lee JY, Lee JW, Kim SM, Lee SM, et al. Radiological, histological, and hematological evaluation of hydroxyapatite-coated resorbable magnesium alloy screws placed in rabbit tibia. Journal of Biomedical Materials Research Part B: Applied Biomaterials. 2017;105:1636-44.

24. Witte F, Jauer L, Meiners W, Kronbach Z, Strohschein K, Schmidt T. Open-porous biodegradable magnesium scaffolds produced by selective laser melting for individualized bone replacement. Frontiers in Bioengineering. 2016;4:708.

25. Kim SM, Jo JH, Lee SM, Kang MH, Kim HE, Estrin Y, et al. Hydroxyapatite-coated magnesium implants with improved in vitro and in vivo biocorrosion, biocompatibility, and bone response. Journal of Biomedical Materials Research Part A. 2014;102:429-41.

26. Zhang N, Zhao D, Liu N, Wu Y, Yang J, Wang Y, et al. Assessment of the degradation rates and effectiveness of different coated Mg-Zn-Ca alloy scaffolds for in vivo repair of critical-size bone defects. Journal of Materials Science: Materials in Medicine. 2018;29:1-11.

27. Oshibe N, Marukawa E, Yoda T, Harada H. Degradation and interaction with bone of magnesium alloy WE43 implants: a long-term follow-up in vivo rat tibia study. Journal of Biomaterials Applications. 2019;33:1157-67.

28. Krause A, Von der Höh N, Bormann D, Krause C, Bach F-W, Windhagen H, et al. Degradation behaviour and mechanical properties of magnesium implants in rabbit tibiae. Journal of materials science. 2010;45:624-32.

29. Schaller B, Saulacic N, Beck S, Imwinkelried T, Goh BT, Nakahara K, et al. In vivo degradation of a new concept of magnesium-based rivet-screws in the minipig mandibular bone. Materials Science and Engineering: C. 2016;69:247-54.

30. Li Z, Gu X, Lou S, Zheng Y. The development of binary Mg-Ca alloys for use as biodegradable materials within bone. Biomaterials. 2008;29:1329-44.

31. Remennik S, Bartsch I, Willbold E, Witte F, Shechtman D. New, fast corroding high ductility Mg-Bi-Ca and Mg-Bi-Si alloys, with no clinically observable gas formation in bone implants. Materials Science and Engineering: B. 2011;176:1653-9.

32. Pietak A, Mahoney P, Dias GJ, Staiger MP. Bone-like matrix formation on magnesium and magnesium alloys. Journal of materials science: materials in medicine. 2008;19:407-15.

33. Gray-Munro JE, Seguin C, Strong M. Influence of surface modification on the in vitro corrosion rate of magnesium alloy AZ31. Journal of Biomedical Materials Research Part A. 2009;91:221-30.

34. Porru S, Placidi D, Quarta C, Sabbioni E, Pietra R, Fortaner S. The potencial role of rare earths in the pathogenesis of interstitial lung disease: a case report of movie projectionist as investigated by neutron activation analysis. Journal of trace elements in medicine and biology. 2001;14:232-6.

35. Kose O, Turan A, Unal M, Acar B, Guler F. Fixation of medial malleolar fractures with magnesium bioabsorbable headless compression screws: short-term clinical and radiological outcomes in eleven patients. Archives of orthopaedic and trauma surgery. 2018;138:1069-75.

General Discussion

Conclusions & future perspectives

6.1   Discussion

A variety of factors can cause maxillofacial bone defects, including congenital anomalies, trauma, tumor resection, periodontal disease, infection, etc. [1]. The oral and maxillofacial region contains various tissue types within a relatively small area. Restoration of oral and maxillofacial defects poses a great challenge to the surgeon due to the lack of suitable donor sites to obtain grafts that can accurately replicate missing tissue [2].

Implant materials commonly used in oral and maxillofacial bone reconstruction surgery have evolved from autografts to xenografts to allografts to xenografts. The autologous bone grafting technique to harvest grafts from various donor sites is considered the gold standard for repairing large-scaled bone defects due to its osteogenic potential and lack infection and antigenic reaction risks [3]. However, autografts have limitations, including graft resorption, secondary injury at the donor site, etc.   [4]. Due to these reasons, other bone graft biomaterials (i.e., xenografts or allografts) are increasingly used. However, these biomaterials have limitations: poor vascularization, limited mechanical properties, incomplete osseointegration with the surrounding natural bone, etc. As a result, these grafts often fail [5].

Due to these deficiencies, innovative techniques like BTE have been developed, which have great potential for achieving optimal bone healing under challenging cases while circumventing the disadvantages of traditional treatment. Porous scaffolds are the critical element in BTE because they manipulate cellular function. In addition to providing structural support, they direct the development of new organs and tissues [6, 7]. In the general introduction section, we describe the purpose, methods, and requirements of BTE. Furthermore, we discuss the biomaterials, design parameters, and manufacturing processes used in BTE.

This doctoral thesis presents a progressive BTE research idea starting from one fundamental question: Why is BTE research conducted? Autologous bone grafting remains the gold standard procedure for replacing or restoring large quantities of lost bone tissue [3]. Based on the results of the systematic review and meta-analysis in **article 1**, we derived a theoretical foundation for the study of BTE by showing that autologous bone grafting in mandibular reconstruction still has a high rate of complications, especially secondary injuries to the donor site. Due to the nerve damage caused during surgery, the most common complication after surgery is the chronic sensory disturbance at the donor site: the fibula or the iliac crest. It is believed that this chronic sensory disorder may lead to physical and mental illnesses that cannot be fully recovered [8]. Therefore, finding an alternative to autologous bone grafting that will reduce or even eliminate damage to the donor site is the primary goal of this doctoral research.

By focusing on this need, BTE stands out as a potential solution. The BTE approach is designed to take advantage of scaffolds, stem cells, and other innovative biological factors to create stable, reproducible bone formation strategies [9]. The **article 2** of this thesis explores one of the most commonly used scaffolding materials, Ti64, to assess the osteogenic potential of 3D-printed Ti64 scaffolds for repairing long bone defects. Furthermore, we summarize the ideal parameter ranges for designing scaffolds and potential influencing factors. Most of the many animal experiments in the database use long bones to create bone defect models. This is why we use long bones as an inclusion criterion since it will ensure that more articles are included. We found that pore size of approximately 500-600μm and a porosity of 60-70% are the most desirable parameters for designing Ti64 scaffolds. Despite this, the scaffold is complex in that the pore size and porosity are dependent on each other. The best combination of design parameters in a specific pore shape only comes from repeated debugging of the design file [10]. Moreover, although the findings show that diamond and rhombic dodecahedron are the most commonly used scaffold pore shapes, they are regular porous structures that cannot fully mimic the natural random structure of trabecular bone and can only facilitate limited bone ingrowth [11]. Additionally, the choice of this animal model limits the size of implants available due to the relatively small size of rabbit bones and lack of trabecular bone [12]. Therefore, there is still much room for improvement in the BTE practice using Ti64 scaffolds, like investigating more optimized pore shapes, randomizing the topology of scaffolds, supplementing in vivo data from large animal models, etc.

With the data we collected in **article 2**, we designed the Ti64 scaffold to conduct our animal experiments. A BMP-2 integrated biomimetic CaP coating was used to modify the surface of Ti64 scaffolds in this study to induce osteogenesis. First, we tested the osteogenic ability of the BMP-2 integrated biomimetic CaP coating subcutaneously in **article 3**. The biomimetic CaP coating only acts as a carrier for BMP-2, while BMP-2 is the crucial factor for osteogenesis [13]. CaP has also shown osteoconductive [14, 15] and osteoinductive [16] properties in other studies. However, its osteogenic ability alone is not ideal as a thin coating. When combined with BMP-2, this composite coating exhibited excellent ectopic osteogenesis properties. Nonetheless, some limitations were found in our study: for example, we tried to design the scaffolds with randomized pore sizes (438-82 μm). However, the coating did not penetrate all of the scaffolds, resulting in uneven thickness between the internal and external coating. Despite this, the osteogenic effect of the scaffold was not affected. The coating was therefore demonstrated to be osteoinductive in **article 3**.

Following this, we began to wonder: what effect will this coating have on actual maxillofacial bone defects if used clinically? Hence, the objective of **article 4** was to determine the osteogenic

capability of coatings and scaffolds on a fabricated bicortical mandibular defect in large animal models to simulate a clinical situation. This is due to the fact that mandibular bicortical defects are clinically significant [17]. With reference to previous research, we adjusted the pore size and porosity of the scaffold within an ideal range. The SEM revealed that the scaffold designed this time has the ability to be coated on the inside as well. Additionally, in the mechanical test, we printed a cube-shaped standard test piece according to the ASTM E9-89a standard. In this study, the osteogenic ability of the coating was demonstrated in a beagle dog model of mandibular bicortical bone defect, and we will further analyze and elucidate the new bone formation pattern once the hard tissue sectioning has been completed.

As the osteogenic ability of the coating has been double-certified in both ectopic sites and bone defects, in **article 5**, we have switched our focus from non-absorbable Ti-based scaffolds to degradable Mg alloy scaffolds in order to make this coating more widely used in BTE. The biodegradable metal scaffolds can enable bone formation simultaneously with metabolic processes, resulting in better bone healing [18]. In this study, we discovered that the constructed porous scaffolds degraded very quickly and completely collapsed by week 4. As a result, the degradation rate of the WE43 scaffold slowed between week 4 and week 12, and new mineralized bone surrounded the remnants and fragments of the scaffold, providing sufficient mechanical support for the bone defect. In addition, in this study, the ideal biocompatibility results needed to be analyzed to determine if they were due to the small size of the scaffolds. Since the rear earth elements tend to bind to various components of physiological fluids, it is difficult to quantify their toxic effects [19]. Further research is needed on the long-term effects of rare earth elements on biocompatibility. The main goal of future research on WE43 alloy will be to control its degradation rate. There are currently studies using phosphate plasma electrolytic oxidation coatings [20], CaP coatings [21], MAO/TiO2 composite coatings [22], and other methods to control the degradation rate of WE43 scaffolds. Can a biomimetic method be used to create a coating that can not only slow down the degradation rate of metal scaffolds but also release active BMP-2 to stimulate osteogenesis, thus ensuring synchronization between bone formation and scaffold metabolism? This is a question that needs further and comprehensive research.

6.2   Conclusions

According to the report of a systematic review and meta-analysis presented in **article 1**, we demonstrated that the use of VFF and VIF to repair bone defects in mandibular reconstruction leads to a number of complications, among which, sensory disturbances in the donor site were the

most frequent in both groups. While autogenous bone grafting is temporarily still the gold standard for large-scaled bone defect repair, its high incidence of complications will eventually be replaced by more scientific and practical bone repair methods. The **article 2** of this thesis summarizes the role of Ti64 scaffolds in long bone repair based on a systematic review and summarizes the most used scaffold design parameters (pore size 500-600μm, porosity 60-70%, dodecahedron and diamond pore shapes) as the basis for the BTE studies that follow. As mentioned in **article 3** of this thesis, we found that porous TI64 scaffolds were able to support the ectopic formation of new bone evenly distributed within the scaffolds when modified with BMP-2 integrated biomimetic CaP coatings. A cell-mediated release of BMP-2 was achieved by using the coating as a carrier. According to **article 4**, we have found that the BMP-2 integrated biomimetic CaP coating coated Ti scaffold significantly promoted bone regeneration 8 weeks after implantation in bicortical bone defects created in the mandibles of beagle dog models. As soon as the results of the hard tissue section are complete, the content of bone formation patterns will be further supplemented. The **article 5** of this thesis examines in detail the biocompatibility, degradability, as well as osteogenic capacity of SLM fabricated WE43 scaffolds for repairing femoral and tibial defects in beagle dogs over a period of 4 and 12 weeks. The analysis showed that the WE43 scaffold has good biocompatibility and osteogenic potential. It should be noted, though, that the excessive degradation speed of this material needs to be solved via some other surface modification method, such as coating, etc., if it wants to be widely used in BTE.

6.3　Future perspectives

- The majority of the research data in Part I are retrospective in nature. The need for more prospective studies is essential in order to identify complications after VIF and VFF more accurately.

- Although small animals are acceptable for demonstrating the general principles, replication in larger animal models is needed to translate the experimental findings to humans. A long-term follow-up is also needed to determine the precise osteogenic ability of Ti64 scaffolds. It is recommended to follow the ISO guidelines when designing experiments and to standardize parameters to quantify bone growth.

- To date, various studies have investigated the osteogenic potential of 3D-printed scaffolds. However, most of these studies are done in vitro or in vivo, using scaffolds with simple topologies with regular pore structures in the longitudinal direction and are not meant to mimic cancellous bone. There is a need for further in vivo studies to examine the growth of bone in a

3D porous scaffold with a topology that resembles native bone tissue.

- There is a serious issue regarding the sterilization of BMP-2 coated implants that have not been adequately addressed. There may be appropriate sterilization methods suitable for the industrial production of scaffolds in the future, and more studies need to verify these methods' safety and efficacy.

- Due to the interaction between degradation and the body, the biocompatibility of the WE43 scaffold is the most fundamental issue. Comparing rare earth elements with Mg, the mechanism and effect of rare earth elements on biocompatibility are not well understood. A long-term study of rare earth elements' effects on biocompatibility is needed.

- In vivo experiments confirmed that the degradation rate of WE43 porous scaffolds was considered to be too fast in the early stage for a bone remodeling process. Controlling the degradation rate of WE43 scaffolds requires investigations into surface treatments, such as coatings.

6.4 References

1. Sethi A, Kaus T, Cawood JI, Plaha H, Boscoe M, Sochor P. Onlay bone grafts from iliac crest: a retrospective analysis. International journal of oral and maxillofacial surgery. 2020;49:264-71.

2. Mobini S, Ayoub A. Bone Tissue Engineering in the Maxillofacial Region: The State-of-the-Art Practice and Future Prospects. Regeneration, Reconstruction, & Restoration.1(1):8.

3. Schmidt AH. Autologous bone graft: Is it still the gold standard? Injury. 2021;52:S18-S22.

4. Elnayef B, Porta C, Del Amo FS-L, Mordini L, Gargallo-Albiol J, Hernández-Alfaro F. The Fate of Lateral Ridge Augmentation: A Systematic Review and Meta-Analysis. International Journal of Oral & Maxillofacial Implants. 2018;9:33.

5. Zhang XY, Fang G, Zhou J. Additively Manufactured Scaffolds for Bone Tissue Engineering and the Prediction of their Mechanical Behavior: A Review. Materials. 2017;10:50.

6. Badylak SF, Taylor D, Uygun K. Whole-organ tissue engineering: decellularization and recellularization of three-dimensional matrix scaffolds. Annual review of biomedical engineering. 2011;13:27-53.

7. Bose S, Roy M, Bandyopadhyay A. Recent advances in bone tissue engineering scaffolds. Trends in biotechnology. 2012;30:546-54.

8. Kalk WWI, Raghoebar GM, Jansma J, Boering G. Morbidity from iliac crest bone harvesting. Journal of Oral and Maxillofacial Surgery. 1996;54:1424-9.

9. Black CR, Goriainov V, Gibbs D, Kanczler J, Tare RS, Oreffo RO. Bone tissue engineering. Current molecular biology reports. 2015;1:132-40.

10. Chen Z, Yan X, Yin S, Liu L, Liu X, Zhao G, et al. Influence of the pore size and porosity of selective laser melted Ti6Al4V ELI porous scaffold on cell proliferation, osteogenesis and bone ingrowth. Materials science & engineering C, Materials for biological applications. 2020;106:110289.

11. Tanzer M, Chuang PJ, Ngo CG, Song L, TenHuisen KS. Characterization of bone ingrowth and interface mechanics of a new porous 3D printed biomaterial: an animal study. The Bone & Joint Journal. 2019;101:62-7.

12. Xiu P, Jia ZJ, Lv J, Yin C, Cai H, Song CL, et al. Hierarchical Micropore/Nanorod Apatite Hybrids In-Situ Grown from 3-D Printed Macroporous Ti6Al4V Implants with Improved Bioactivity and Osseointegration. Journal of Materials Science & Technology. 2017;33:179-86.

13. Gu Y, Wei L, Zhang Z, Van Dessel J, Driesen RB, Lambrichts I, et al. BMP-2 incorporated biomimetic CaP coating functionalized 3D printed Ti6Al4V scaffold induces ectopic bone formation in a dog model. Materials & Design. 2022;215:110443.

14. Jarcho M. Calcium phosphate ceramics as hard tissue prosthetics. Clinical Orthopaedics and Related Research. 1981;157:259-78.

15. Hing KA. Bioceramic bone graft substitutes: influence of porosity and chemistry. International journal of applied ceramic technology. 2005;2:184-99.

16. LeGeros RZ. Properties of osteoconductive biomaterials: calcium phosphates. Clinical Orthopaedics and Related Research. 2002;395:81-98.

17. Chen T-L, Lu H-J, Liu G-q, Tang D-H, Zhang X-h, Pan Z-L, et al. Effect of autologous platelet-rich plasma in combination with bovine porous bone mineral and bio-guide membrane on bone regeneration in mandible bicortical bony defects. Journal of Craniofacial Surgery. 2014;25:215-23.

18. Li Y, Zhou J, Pavanram P, Leeflang M, Fockaert L, Pouran B, et al. Additively manufactured biodegradable porous magnesium. Acta biomaterialia. 2018;67:378-92.

19. Liu J, Liu B, Min S, Yin B, Peng B, Yu Z, et al. Biodegradable magnesium alloy WE43 porous scaffolds fabricated by laser powder bed fusion for orthopedic applications: Process optimization, in vitro and in vivo investigation. Bioactive materials. 2022;16:301-19.

20. Arrabal R, Matykina E, Viejo F, Skeldon P, Thompson GE. Corrosion resistance of WE43 and AZ91D magnesium alloys with phosphate PEO coatings. Corrosion Science. 2008;50:1744-52.

21. Rahman M, Li Y, Wen C. Realization and characterization of double-layer Ca-P coating on WE43 Mg alloy for biomedical applications. Surface and Coatings Technology. 2020;398:126091.

22. Zhang S, Guo W, Liu N, Xia C, Wang H, Liang C. In situ preparation of MAO/TiO2 composite coating on WE43 alloy for anti-corrosion protection. Vacuum. 2022;197:110835.

Summary

Maxillofacial bone defects can be caused by congenital deformities, trauma, tumor resections, or any combination of these factors. This can lead to aesthetic and functional issues, such as facial incoordination, asymmetry, and difficulty swallowing. In most cases, autologous bone grafting is the gold standard for the treatment of such bone defects. However, autologous bone transplantation has certain drawbacks, such as complications at the donor site and a limited supply. Furthermore, allogeneic or xenograft bone grafts can also be used, but there are also concerns regarding the spread of disease with these methods. For this reason, the prospect of using bone tissue engineering (BTE) to reconstruct maxillofacial hard tissue defects is of interest to reconstructive surgeons. As the success of this approach depends on providing mechanically supported porous 3D scaffolds and a suitable environment for bone tissue regeneration, the design and fabrication of porous scaffolds with biocompatibility, desired structure, mechanical properties and resorbability is a crucial factor for the success of the BTE approach.

This doctoral thesis aims to fabricate metal scaffolds that are suitable for BTE and evaluate the scaffolds' osteogenic ability in animal models. The thesis begins with a general introduction of the objectives, the methods, and the requirements and methods of scaffold design and fabrication in BTE. To rationalize the study of BTE, in **article 1** of this thesis, we compared early and late morbidity at the donor and recipient sites in patients who underwent mandibular reconstructions with autologous bone reconstructions. According to the results, the early morbidity rate in the VFF group ranged from 3% to 12%, and the late morbidity rate in the VFF group ranged from 5% to 67%. In the VIF group, early morbidity ranged from 3% to 16%, and late morbidity ranged from 6% to 43% at the donor site. The most common complication in both groups was chronic sensory impairment at the donor site. Because of this, we should use BTE for bone reconstruction surgery to reduce the damage to the donor area caused by the surgery.

Through **article 2** of this thesis, we summarize the osteogenic potential of 3D-printed porous Ti64 scaffolds to repair long bone defects in animal models and investigate the influencing factors that may affect their osteogenic capacity. Our research found that pore size of approximately 500-600μm and a porosity of 60-70% are ideal parameters for designing Ti64 scaffolds, where both dodecahedral and diamond pores promote optimal osteogenesis. Ti64 scaffolds may serve as a promising medium to provide sufficient mechanical support and a stable environment for bone growth in long bone defects. However, since it lacks osteoinductivity, surface modification

technologies are required to enhance its bone defect repairability.

Using the results of **article 2**, we have designed and fabricated 3D-printed porous Ti64 scaffolds. In addition, we have also surface-modified the Ti64 scaffolds using a BMP-2 integrated biomimetic CaP coating. We studied the effect of the coated scaffold on increasing ectopic osteogenesis in the beagle dog model in **article 3** of this thesis. This study shows that the BMP-2 integrated biomimetic CaP coating formed a micro/nano surface structure on the Ti6Al4V scaffold, which improved the biocompatibility of the product. Ectopic bone formation in vivo is mediated by BMP-2. Next, we manufactured the 3D-printed Ti scaffold and coated it with the same coating. In **article 4** of this thesis, we implanted the scaffold in a mandibular bicortical bone defect of a beagle dog to study the osteogenic effects of the scaffold. The micro-CT results showed that the coated Ti scaffold significantly promoted bone regeneration 8 weeks after being implanted into a mandibular bicortical bone defect. Thus, we demonstrate in Part III that BMP-2 integrated biomimetic CaP coating offers a promising approach to modifying porous Ti scaffold surfaces for repairing clinical bone defects through in vivo testing of ectopic and bone defects.

Scaffolds should be biocompatible, exhibit a fully interconnected porous structure to allow bone ingrowth, and degrade as the bone regenerates. We investigated the biocompatibility, osteogenic capacity and metabolic rate of 3D-printed porous WE43 alloy scaffolds in a beagle dog bone defect model in **article 5** of this thesis. Results demonstrate that the WE43 alloy scaffold has good in vivo biocompatibility. Compared to the original scaffold volume, scaffolds were reduced by 36%±0.19% at week 4 and 41%±14% at week 12, with no significant difference between the two groups. At 12 weeks, hard tissue sections revealed that a large amount of mineralized bone grew around the remnant of the scaffold, demonstrating the synchronization of scaffold metabolism and osteogenesis. In this study, WE43 alloy is shown to have good biocompatibility and osteogenic ability, making it a promising candidate for osteosynthesis systems. To further optimize the application of the WE43 scaffold in BTE, it needs to be surface modified to slow down the absorption rate.

This thesis demonstrates that autologous bone grafts, such as vascularized fibular flap (VIF) and vascularized iliac flap (VFF) have complications that cannot be ignored. BTE is a potentially effective treatment for maxillofacial bone defects. In BTE, both the BMP-2 integrated biomimetic CaP-coated Ti-based porous scaffold and the biodegradable WE43 porous scaffold exhibited good osteogenic properties. Translating lab-made methods into clinically relevant products will require a joint effort of clinicians and engineers.

Samenvatting

Maxillofaciale botdefecten kunnen worden veroorzaakt door aangeboren misvormingen, trauma, tumorresecties, of een combinatie van deze factoren. Dit kan leiden tot esthetische en functionele problemen, ter hoogte van het aangezicht, alsook tot asymmetrie, spraak- en slikproblemen. In de meeste gevallen is autologe bottransplantatie de gouden standaard voor de behandeling van dergelijke botdefecten. Autologe bottransplantatie heeft echter bepaalde nadelen, zoals complicaties op de donorplaats en een beperkt weefselaanbod. Verder kunnen ook allogene of xenograft bottransplantaten worden gebruikt, maar ook bij deze methoden bestaat er problemen zoals overdracht van ziektekiemen of vreemd lichaamreacties. Daarom is het vooruitzicht van het gebruik van botweefsel engineering (BTE) voor de reconstructie van hardweefseldefecten in het maxillofaciale gebied interessant voor reconstructieve maxillofaciale chirurgie. Aangezien het succes van deze benadering afhangt van de levering van mechanisch ondersteunde poreuze 3D scaffolds en een geschikte omgeving voor botweefselregeneratie, is het ontwerp en de fabricage van poreuze implantaten tot een biocompatiebele, patient-specifieke structuur met goede mechanische eigenschappen en afbreekbaarheid een cruciale factor voor het succes van de BTE benadering.

Deze doctoraatsthesis heeft als doel metalen implantaten te fabriceren die geschikt zijn voor BTE en hun osteogeen vermogen te evalueren in diermodellen. Het proefschrift begint met een algemene inleiding over de doelstellingen, de methodes, en de vereisten en methodes van het ontwerp en fabricage in BTE. Om de studie van BTE te rationaliseren, vergeleken we in **artikel 1** van dit proefschrift de vroege en late morbiditeit op de donor- en ontvangerplaats bij patiënten die mandibulaire reconstructies ondergingen met autologe botreconstructies. Volgens de resultaten varieerde de vroege morbiditeit in de VIF-groep van 3% tot 12%, en de late morbiditeit in de VIF-groep varieerde van 5% tot 67%. In de VIF-groep varieerde de vroege morbiditeit van 3% tot 16%, en de late morbiditeit van 6% tot 43% op de donorplaats. De meest voorkomende complicatie in beide groepen was chronische gevoelsstoornissen op de donorplaats. Daarom moeten wij BTE gebruiken voor botreconstructieve chirurgie om de schade aan het donorgebied als gevolg van de operatie te beperken.

In **artikel 2** van dit proefschrift vatten we het osteogeen potentieel samen van 3D-geprinte poreuze Ti64 scaffolds voor het herstel van lange botdefecten in diermodellen en onderzoeken we de

beïnvloedende factoren die hun osteogeen vermogen kunnen beïnvloeden. Uit ons onderzoek is gebleken dat een poriegrootte van ongeveer 500-600µm en een porositeit van 60-70% ideale parameters zijn voor het ontwerpen van Ti64 scaffolds, waarbij zowel dodecahedrale als diamanten poriën een optimale osteogenese bevorderen. Ti64 scaffolds kunnen dienen als een veelbelovend medium om voldoende mechanische ondersteuning en een stabiele omgeving te bieden voor botgroei in lange botdefecten. Aangezien het echter osteo-inductiviteit mist, zijn oppervlaktemodificatietechnologieën nodig om de herstelbaarheid van botdefecten te verbeteren. Met behulp van de resultaten van **artikel 2** hebben we 3D-geprinte poreuze Ti64 scaffolds ontworpen en vervaardigd. Daarnaast hebben we ook de Ti64 scaffolds gemodificeerd met behulp van een BMP-2 geïntegreerde biomimetische CaP coating. We hebben het effect van de gecoate scaffold op de toename van ectopische osteogenese in het beagle hondenmodel bestudeerd in **artikel 3** van dit proefschrift. Deze studie toont aan dat de BMP-2 geïntegreerde biomimetische CaP coating een micro/nano oppervlakte structuur vormde op de Ti6Al4V scaffold, wat de biocompatibiliteit van het product verbeterde. Ectopische botvorming in vivo wordt gemedieerd door BMP-2.

Vervolgens hebben we de 3D-geprinte Ti scaffold vervaardigd en gecoat met dezelfde coating. In **artikel 4** van dit proefschrift hebben we de scaffold geïmplanteerd in een mandibulair bicorticaal botdefect van een beagle hond om de osteogene effecten van de scaffold te bestuderen. De micro-CT resultaten toonden aan dat de gecoate Ti scaffold significant de botregeneratie bevorderde 8 weken na implantatie in een mandibulair bicorticaal botdefect. Aldus tonen we in deel III aan dat BMP-2 geïntegreerde biomimetische CaP coating een veelbelovende benadering biedt voor het modificeren van poreuze Ti scaffoldoppervlakken voor het herstellen van klinische botdefecten door *in vivo* testen van ectopische en botdefecten.

Scaffolds moeten biocompatibel zijn, een volledig onderling verbonden poreuze structuur vertonen om botingroei mogelijk te maken, en degraderen naarmate het bot regenereert. In **artikel 5** van dit proefschrift hebben we de biocompatibiliteit, osteogene capaciteit en metabolische snelheid onderzocht van 3D-geprinte poreuze WE43-legering scaffolds in een beagle hond botdefect model. Resultaten tonen aan dat de WE43-legering scaffold een goede *in vivo* biocompatibiliteit heeft. Vergeleken met het oorspronkelijke scaffoldvolume waren de scaffolds 36%±0,19% kleiner bij week 4 en 41%±14% bij week 12, zonder significant verschil tussen de twee groepen. Bij 12 weken hard weefsel secties bleek dat een grote hoeveelheid gemineraliseerd bot groeide rond de scaffold, waardoor synchronisatie van scaffold metabolisme en osteogeneses kon aangetoond. In deze studie is aangetoond dat de WE43-legering een goede biocompatibiliteit en osteogeen

vermogen heeft, waardoor het een veelbelovende kandidaat is voor osteosynthesesystemen. Om de toepassing van de WE43 scaffold in BTE verder te optimaliseren, moet het oppervlak worden gewijzigd om de absorptiesnelheid te vertragen.

Dit proefschrift toont aan dat autologe bottransplantaten, zoals gevasculariseerde fibulaire flap (VIF) en gevasculariseerde iliacale flap (VFF), complicaties hebben die niet kunnen worden genegeerd. BTE is een potentieel effectieve behandeling voor maxillofaciale botdefecten. Bij BTE vertoonden zowel de BMP-2 geïntegreerde biomimetische CaP-gecoate Ti-gebaseerde poreuze scaffold als de biologisch afbreekbare WE43 poreuze scaffold goede osteogene eigenschappen. De vertaling van in het laboratorium gemaakte methoden naar klinisch relevante producten zal een gezamenlijke inspanning van clinici en ingenieurs vereisen.

Scientific Acknowledgements

Personal Contribution

The author, Yifei Gu, conceived the projects, collected data and managed the animal studies, and wrote the research publications with the scientific support of her promoters and other co-authors. Accordingly, Yifei Gu is the first author of all the thesis chapters and corresponding research papers.

Conflict of Interest

The authors declare no conflicts of interest concerning the publications of this work.

Curriculum Vitae

YIFEI GU (顾旖菲)

Birthday: 1992.4.17

Gender: female

Nationality: Chinese

Address: Herestraat 49

State/County: 3000 Leuven, Belgium

E-mail: guyifeiscu@gmail.com

EDUCATION

Katholieke Universiteit Leuven

Ph.D. candidate

2018-2022

Sichuan University

Bachelor and Master's degrees

2010-2018

Researched on the surface modification of 3D-printed porous titanium alloy scaffolds under the guidance of **Prof. Constantinus Politis**, **Prof. Reinhilde Jacobs** and **Dr. Sun Yi** from KU Leuven.

Attended the School of Dentistry for an eight-year undergraduate and postgraduate program, focusing in oral implantology.

EXPERIENCE

West China

Stomatological Hospital

2015-2018

West China

Stomatological Hospital

2013-2015

Clinical postgraduate and trainee of resident doctor

Conducted a three-year clinical practice in the oral implantology department to learn the basic operation of oral implantology.

Trainee

Received medical practice in various departments to learn the basic operation techniques of stomatology.

CERTIFICATEDS&AWARDS

- Qualification and practicing certificates for dentists in China
- Certificate of standardized training for residents in China
- First prize of China College Students English Competition
- First prize of English skill competition in Sichuan University
- Scholarship for Bachelor and Master students in Sichuan University
- Outstanding student award in College of Stomatology, Sichuan University

ENGLISH SKILLS

- TOFEL: 109 points
- CET-6: 604 points
- Certificate of interpretation, level 3 (CATTI)

CONFERENCES

- Oral presentation in the Annual Conference of Oral Implantology, China
- Oral presentation in the International Academy of Stomatology, West China.

PUBLICATIONS

- **Gu Y**, Ma H, Shujaat S, Orhan K, Coucke W, Amoli MS, Bila M, Politis C, Jacobs R. Donor- and recipient-site morbidity of vascularized fibular and iliac flaps for mandibular reconstruction: A systematic review and meta-analysis. Journal of Plastic, Reconstructive & Aesthetic Surgery. 2021 Jul 1;74(7):1470-9.

- **Gu Y**, Sun Y, Shujaat S, Braem A, Politis C, Jacobs R. 3D-printed porous Ti6Al4V scaffolds for long bone repair in animal models: a systematic review. Journal of Orthopaedic Surgery and Research. 2022 Dec;17(1):1-7.

- **Gu Y**, Wei L, Zhang Z, Van Dessel J, Driesen RB, Lambrichts I, Jacobs R, Tian L, Sun Y, Liu Y, Politis C. BMP-2 incorporated biomimetic CaP coating functionalized 3D printed Ti6Al4V scaffold induces ectopic bone formation in a dog model. Materials & Design. 2022 Feb 2:110443.

- **Gu Y**, Van Dessel J, Politis C, Sun Y. 3D printing and 3D printed scaffolds. Computer-Aided Oral and Maxillofacial Surgery. 2021:183-200.

- **Gu Y**, Sun Y, Jacobs R, Politis C. Accuracy and reliability of a newly developed 3D tool for maxilla positioning measurement. International journal of oral and maxillofacial surgery (under review).

- Jacobs R, **Gu Y**, Quirynen M, De Mars G, Dekeyser C, van Steenberghe D, Vrombaut D, Shujaat S, Naert I. A 20-year split-mouth comparative study of two screw-shaped titanium implant systems. International Journal of Oral Implantology. 2021 Nov 1;14(4):421-30.

- Shi Q, Yang S, Sun Y, **Gu Y**, Mercelis B, Zhong S, Van Meerbeek B, Politis C. In-situ formation of Ti-Mo biomaterials by selective laser melting of Ti/Mo and Ti/Mo2C powder mixtures: A comparative study on microstructure, mechanical and wear performance, and thermal mechanisms. Journal of Materials Science & Technology. 2022 Jan 20;115:81-96.

- Ma H, Van Dessel J, Shujaat S, Bila M, **Gu Y**, Sun Y, Politis C, Jacobs R. Long-term functional outcomes of vascularized fibular and iliac flap for mandibular reconstruction: A systematic review and meta-analysis. Journal of Plastic, Reconstructive & Aesthetic Surgery. 2021 Feb 1;74(2):247-58.

- Zhong S, Shi Q, Sun Y, Yang S, Van Dessel J, **Gu Y**, Chen X, Lübbers HT, Politis C. Biomechanical comparison of locking and non-locking patient-specific mandibular reconstruction plate using finite element analysis. Journal of the Mechanical Behavior of Biomedical Materials. 2021 Dec 1;124:104849.

- Shi Q, Sun Y, Yang S, Van Dessel J, Lübbers HT, Zhong S, **Gu Y**, Bila M, Dormaar T, Schoenaers J, Politis C. Failure analysis of an in-vivo fractured patient-specific Ti6Al4V mandible reconstruction plate fabricated by selective laser melting. Engineering Failure Analysis. 2021 Jun 1;124:105353